Soft Bending Actuator for Body-Powered Application

Sivakumar Kandasamy

Supervisor

Assoc. Prof. Kean C. Aw

Co-Supervisor

Assoc. Prof. Andrew McDaid

A thesis submitted in partial fulfilment of the requirements for the degree of Doctor of Philosophy in Mechanical Engineering, The University of Auckland, 2022.

Abstract

Soft actuators are inherently compliant, highly dexterous, and lightweight alternatives to traditional electromechanical actuators in many robotic applications, especially human-interactive robots. This research aims to develop a soft robotic actuator that leverages body movements to mimic the function of human fingers to perform gripping and grasping tasks. Unlike the predominantly used chamber-based actuation techniques, this study involves braiding fibres along the axis at two different angles on each half of the cylindrical actuator. This angle difference allows the actuator to bend in one direction when pressurized by a pneumatic or hydraulic source. Furthermore, winding the fibres continuously along the axis increases bending by limiting radial expansion.

As a first step, the bending concept based on variable stiffness has been validated using numerical and finite element analyses. Secondly, manufacturing a fibre-based soft actuator using materials of low Young's moduli with a split fibre-reinforcement (SFR) technique was studied, followed by altering the fibre braiding pattern using the continuous fibre-reinforcement (CFR) method. The third study investigated the effect of Young's modulus on the bending and force output of the actuator. Additionally, a comparison was made between pneumatic and hydraulic-powered actuators. As a final step, the shoulder movements of the body were studied and utilized to power a set of actuators capable of performing gripping and grasping tasks. The low modulus materials and the continuous fibre winding technique allowed us to develop a portable, standalone, cost-effective body-powered prosthetic device.

Acknowledgements

This thesis was possible because of many people's continuous support and guidance. Firstly, I would like to express my deep sense of gratitude to my supervisor, **A/Prof. Kean C. Aw,** who has been moral support and encouragement throughout my research. I will always be thankful to him for his guidance and constructive ideas, which constantly motivated me to achieve better research outputs.

I want to express my sincere thanks to **A/Prof. Andrew McDaid** for all his contributions of time and ideas. I am also thankful to him for allowing me to collaborate with the IRTG Soft Tissue Robotics research group from the University of Stuttgart, which helped me widen my knowledge and learning.

I would also like to express my deepest gratitude and appreciation to **Prof. Krishnan Jayaraman**, who provided me with critical advice and volunteered his valuable time to complete this thesis successfully.

Besides my supervisor and advisor, I would like to thank the lab technicians for assisting me in purchasing research materials and allowing me to utilize the lab facilities more effectively. I thank my colleagues Narrendar Ravichandran, Kumar Jena, and Keemi Lim for devoting their time and providing valuable suggestions and support.

I want to express my sincere gratitude to my parents. As a farmer, my father sacrificed many things to bring me to such a position, and my mom's constant love and care helped me overcome hurdles during my most challenging times.

Lastly, I would like to thank my wife, **Dr. Mei Ying Teo,** and my daughter **Thendral Teo** for lifting my spirits simply with a smile and making every day worth living.

Table of Contents

List of tables

List of figures

List of abbreviations

CFR	Continuous fibre reinforced
DEA	Dielectric elastomeric actuators
FEA	Finite element analysis
PAM	Pneumatic artificial muscle
PDMS	Polydimethylsiloxane
SFA	Soft fluidic actuators
SFR	Split fibre reinforced
TPU	Thermoplastic polyurethane

Chapter 1

Introduction

1.1 Biorobotics

Over the past decade, interdisciplinary approaches have resulted in significant advances in robotics [1]. Bioinspired robotics is a subfield in robotics that emphasizes replicating extraordinary capabilities found in natural organisms [2]. Robots of this type have been extensively used in healthcare, social administration, and field investigation as an essential and inseparable part of modern technology [3]. Fabrication of these robots is mainly based on a modular design concept using electric motors, printed circuit boards, semi-rigid synthetic compounds, and carbon-based composites to establish sensing, control, and actuation strategies (**Figure 1.1**) [4].

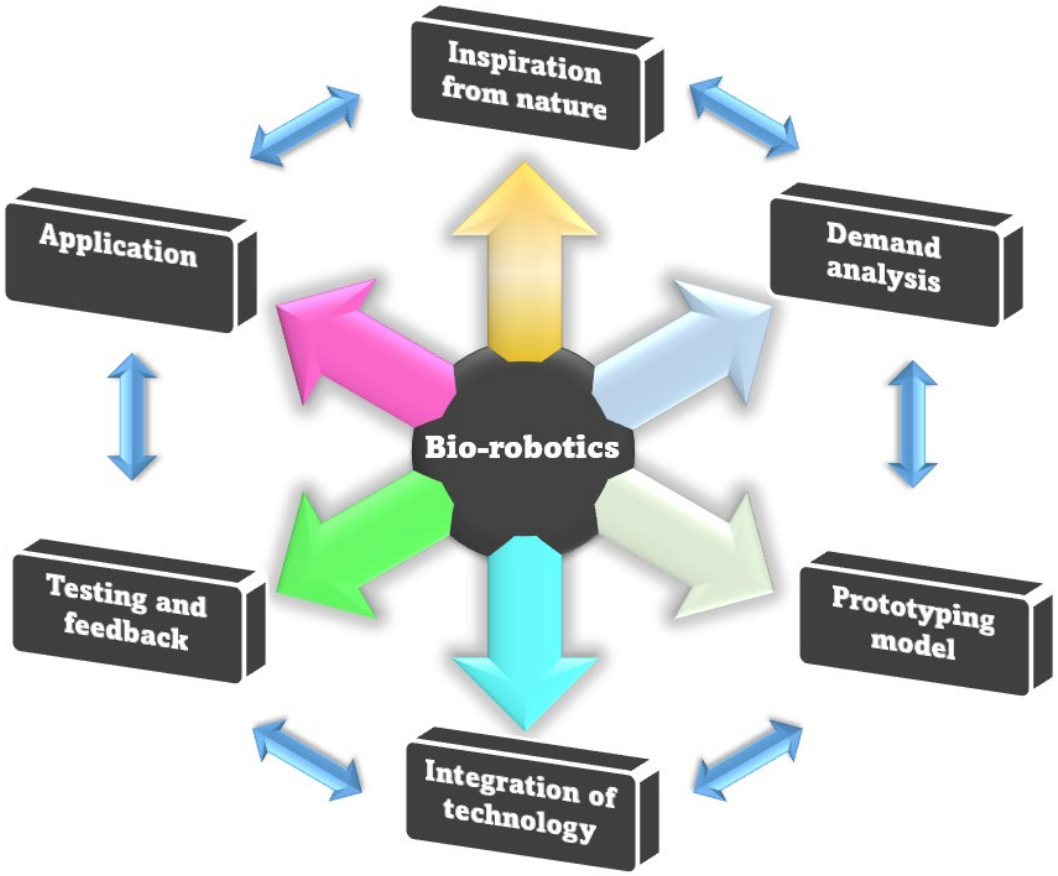

Figure 1.1 Outline of the process of making a biorobot from inspiration to application.

While these developments are promising, there are still many challenges to overcome, including the flexibility, biocompatibility, and adaptability of materials used in these robotic applications. Recent researchers have focused on utilizing more compliant and flexible materials to help these robots interact safely with humans [5]. When a human body is considered, muscles make up 42% of its mass, while bones make up 11%. The integration of soft materials in human-centric robotics can therefore be the next step in bio-inspired robotics technology. In recent years, bio-inspired soft robots have enabled similar automated tasks to be performed without rigid counterparts. For soft robotic applications, the materials used must guarantee the human system's functionality and acceptability upon installation [6]. When choosing materials for soft actuators, it is important to consider whether the actuators' application involves external or internal interactions with the human body. [7].

1.2 Soft actuators

There are many challenges associated with soft robotics. Actuation is one of the biggest challenges and designing flexible actuation systems that can generate output forces comparable to the ones exerted by the muscles in the human body [8]. Humans can change their body posture depending on the extension, expansion, twisting, and bending of muscles. Numerous research has been conducted on generating actuation mechanisms using soft materials [9]–[11]. The most common ones are dielectric elastomeric actuators (DEAs') [12] and fluidic actuators that operate on hydraulic and pneumatic power sources [13]. The dielectric elastomeric actuators are made of soft materials that actuate through electrostatic forces – an important development in the quest for artificial muscles. Despite its relatively high-performance metric (high strain/stress and mass-specific power), this technique has few limitations. (i) Most designs that use DEAs require a rigid frame that pre-strains the elastomer. Some design works have been done without rigid frames;

however, they resulted in a very low stress, and their fabrication process is highly complicated. (ii) The reliability of the compliant electrodes used in these designs needs improvement. (iii) The technique requires high voltages, which is undesirable for many applications [14].

Fluidic actuators, on the other hand, use fluids like compressed air to power the actuator [15]. This technique has provided robust actuation systems for soft materials since the 1950s [16]. Compressed air or fluids can be used to create deformation in these actuators to directly replicate motions found in body parts by inflating the network of chambers and creating motion in tethered robots [17]. Fibre-reinforced actuators are another type of actuator that can produce a variety of motions like bending and twisting by restricting the radial bulging by winding fibres on a soft material core. Depending on the braiding pattern, the actuator's movements can be customized to suit the application [18].

Materials play a significant role in the performance characteristics of the actuator. The materials used to make these actuators vary from elastomer-based products like Ecoflex™ [19], Dragon skin, and PDMS to 3D-printed materials like Polylactic Acid [20], Acrylonitrile Butadiene Styrene and fabric-based materials like TPU (Thermoplastic polyurethane) [21] as shown in **Figure 1.2**.

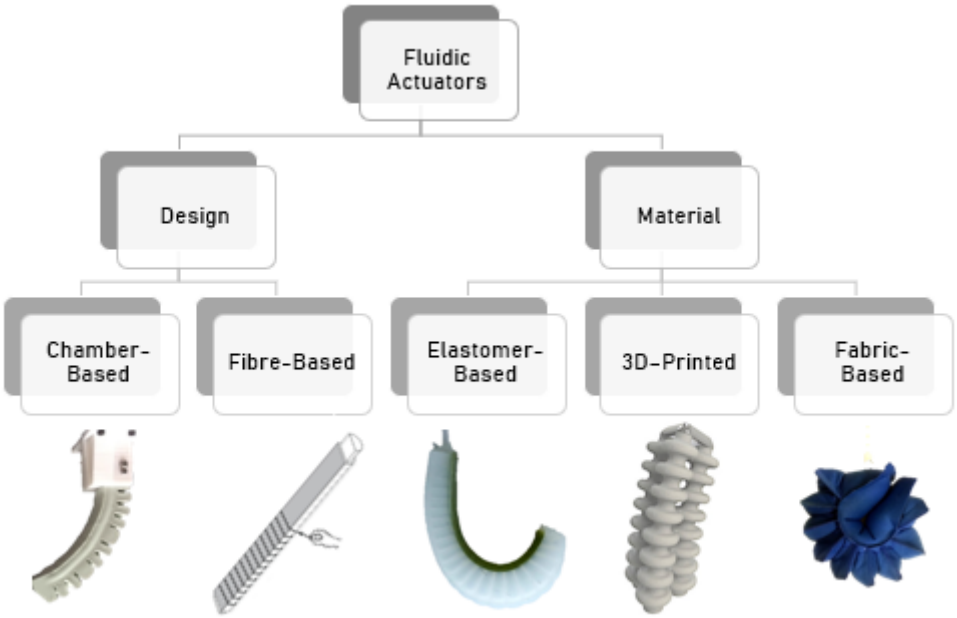

Figure 1.2 Classification of fluidic actuators based on design and material.

1.3 Motivation

In elastomeric actuators, chamber-based designs are geometrically complex, and adding chambers will increase the actuator's weight. Reducing the size of these chambers to make a low-powered less mass actuator requires the actuator walls to be made thin, which makes them prone to bulging. Therefore, improving efficiency can be done at the design level. Wang et al. and other researchers successfully manufactured a non-chamber-based actuator. However, it involves utilizing materials with high Young's moduli, dirty manufacturing processes, and embedding an inextensible strip layer to induce bending [22]; hence there is a requirement of an external compressor to generate sufficient pressure, negating the suitability of using body movement to power these actuators. These drawbacks have affected their usage in different applications. Therefore, this work aims to develop an actuator of simple design, powered by the wearer's body movement, and easy to fabricate that can be utilized in body-powered prosthetic applications.

1.4 Objectives

This research aims to utilize body movements to power a soft elastomer-based prosthetic device to perform gripping and grasping tasks. A detailed literature study has been conducted to analyse the parameters that can be modified to make this application possible. The research objectives have been summarised as follows.

Task 1. Create an actuator that operates at a low pressure.

Task 2. Design and evaluate the characteristics of split and continuous fibre winding techniques and different braiding combinations.

Task 3. Characterise and evaluate the actuator response with soft materials of different Young's moduli.

Task 4. Utilization of body power to operate soft bending actuators for gripping applications.

1.5 Outline of the thesis

This thesis is organized as follows:

Chapter 2 provides the background and literature on the soft materials used in making soft robots, actuation, and design techniques responsible for bending, twisting, and other types of motion found in soft actuators. It also discusses the application of soft actuators in wearable robotics and body-powered prosthesis.

Chapter 3 explains the design concepts based on which this work has been based on. It also validates using numerical analysis that the actuator's bending is possible with a pressure input.

Chapter 4 explains the simulation of the actuator model using a finite element analysis tool to support the concept of bending based on stiffness difference.

Chapter 5 demonstrates two fabrication methods, i.e., split-fibre and continuous-fibre-reinforcement techniques. It also discusses these fabrication methods' results, advantages, and disadvantages.

Chapter 6 discusses the effect of the material's Young's modulus on bending and the force output of the actuator by utilizing three different elastomeric materials. It also explains the impact of compressible fluids on generating pressure inside these actuators.

Chapter 7 demonstrates the implementation of a body-powered prosthesis on an actual human.

Chapter 8 summarises all the main findings of this thesis and suggests the potential future work for this research.

Chapter 2

Literature review

To begin with, an overview of soft materials used in the construction of soft robots has been discussed. As a second step, the design and powering techniques that are responsible for bending and other types of motion in various soft actuators have been discussed. Last section of this review discusses the applications of these soft actuators for wearable robotics and body-powered prosthetics applications.

2.1 Actuator

2.1.1 Categorized by materials

Materials used in biologically inspired soft robotic systems should be elastic or flexible to perform multiple functions naturally found in living organisms. In human-machine interaction applications, soft materials also provide comfort and safety [23]. The ability of soft materials to integrate with other functional mechanisms or robots without altering their mechanical properties allows for high customizability options in robot design, depending on the application [24]. As a result, material selection plays a vital role in the quality of the soft robot. Generally, soft robots are made from one of the material categories: silicone elastomers, polymer composites, and fabrics [25].

2.1.1.1 Silicone elastomers

Elastomers made with silicone are composed of reactive, straight-chained molecules and cross-linking agents to provide excellent mechanical properties. Several advantages make silicone elastomers one of the most widely used soft robotic materials, including their high flexibility, biocompatibility, tear strength, stretchability, compliance, and elastic resilience [26]. Due to their elastic response over a wide range of strains and the fact that they have a stress-strain relationship derived from a strain energy density, these elastomers are considered hyper-elastic [27]. Young's modulus is an effective tool for comparing

stiffnesses, and most elastomers used in soft robotic actuators possess moduli between 0.1 to 10 MPa, as summarized in **Table 2.1**.

Table 2.1 Young's moduli of silicone elastomers

Material Name	**Young's modulus (E) MPa**	
Ecoflex™ 00-10	0.038	[28]
Ecoflex™ 00-30	0.066	[29]
Ecoflex™ 00-50	0.089	[28]
Dragon skin	0.226	[29]
Elastosil-M4630	1.18	[30]
Sylgard 186	1.2	[31]
Sylgard 184	2.4	[31]
PDMS	2.6	[28]
Smooth Sil™ 940	3.8	[32]

Soft robotics utilize polysiloxanes like PDMS due to their high strain limit, low hysteresis, and low modulus during loading and unloading cycles. A variety of elastomers like Ecoflex™ 00-30 from Smooth-On and Sylgard 184 are prevalent because they are transparent, inert, and mechanically robust [33]. Engineers typically consider properties like strain limit, modulus, and manufacturing processability when choosing an elastomer. However, creep, stress relaxation, and other forms of inelastic deformation can result in energy loss and hysteresis during the consecutive loading and unloading of these materials [34]. Soft robots use elastomers for a variety of purposes. In addition to housing the electrical circuit for soft sensors, it can also serve as a fluidic pressure channel for actuators. Fluidic pressure deforms these elastomers, enabling them to produce a variety of movements under controlled conditions. One such model utilizing fibres to control a

soft silicone material's motion is demonstrated in **Figure 2.1** [18]. With the help of elastomers integrated with conductive materials like Carbon nanotube and graphene, the soft robots can be made to sense mechanical deformation [31].

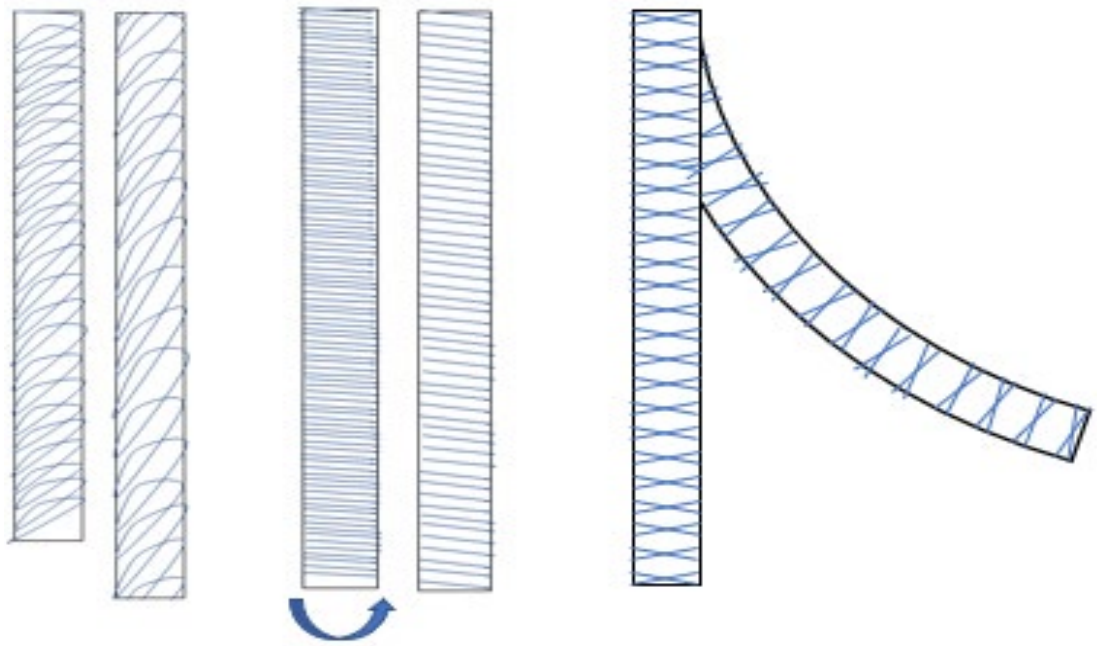

Figure 2.1 Demonstration of motions using soft silicone elastomers. (a) Extension (b) Twisting (c) Bending [18].

2.1.1.2 Polymer composites

Polymer composite materials result from combining two or more materials of different natures. This is done to obtain a product with a quality superior to the originals. In other words, the idea is to create a resource that meets the needs that pure polymers do not. In selecting soft materials for robotic applications, tensile strength, Young's modulus, and dynamic modulus are the mechanical properties most often considered [35].

Since the soft robot finger is mainly designed to have flexion, extension, abduction, and adduction movements, the material's flexural strength is another essential mechanical property that must be considered in the selection. The bending strength of the chosen

material will decide the degree of rotation or bend of the soft finger [36]. These properties may be achieved from synthetic polymer matrices mixed up with naturally occurring mineral fillers such as silica, mica, glass fibres, or carbon fibres as summarized in **Table 2.2**. The use of filler in the polymer matrix may make the composite an anisotropic non-linear material like human skin [37].

Table 2.2 Polymer composites in soft robots

Material-1	**Material-2**	**Application**	
Smooth Sil™ 950	Kevlar fibre	Soft bending actuators	[38]
Polyvinyl alcohol	Iron Oxide	Magpol actuators	[39]
PDMS	Carbon nanotube	Robotic skin	[40]
Sylgard-184	Gallium & Indium	Stretchable capacitor	[41]
Hydrogel	Sodium Chloride	Ionic skin	[42]
Ecoflex™ 0030	Liquid metal	Stretchable electronics	[43]

2.1.1.3 Fabric materials

Textile-based pneumatic actuators have become increasingly popular for wearable applications due to the high strength-to-weight ratio of these actuators and the range of actuation modalities [44]. A spandex and nylon fabric-based soft actuator, along with neoprene, is used for ankle-foot orthosis to assist in inversion-eversion ankle support and gait rehabilitation [45]. A soft ankle-foot Exo-sock is used to passively assist bed-ridden patients affected by deep vein thrombosis, preventing blood clots and serving as an alternative to mechanical prophylaxis [46]. A lightweight pneumatic exoskeleton for total knee arthroplasty patients was developed using a fabric pneumatic actuator to assist the patient's knee movements during rehabilitation [47]. Thermoplastic polyurethane (TPU) fabric materials were used to fabricate a foldable pneumatic bending actuator [48]. A fully fabric-based pneumatically

driven bidirectional glove was made by sealing TPU fabrics, providing both active flexion and extension. In comparison with fabric-embedded elastomeric gloves [49], fully fabric-based gloves are much lighter and can achieve a larger range of motion and higher force output at lower pressures (**Figure 2.2**).

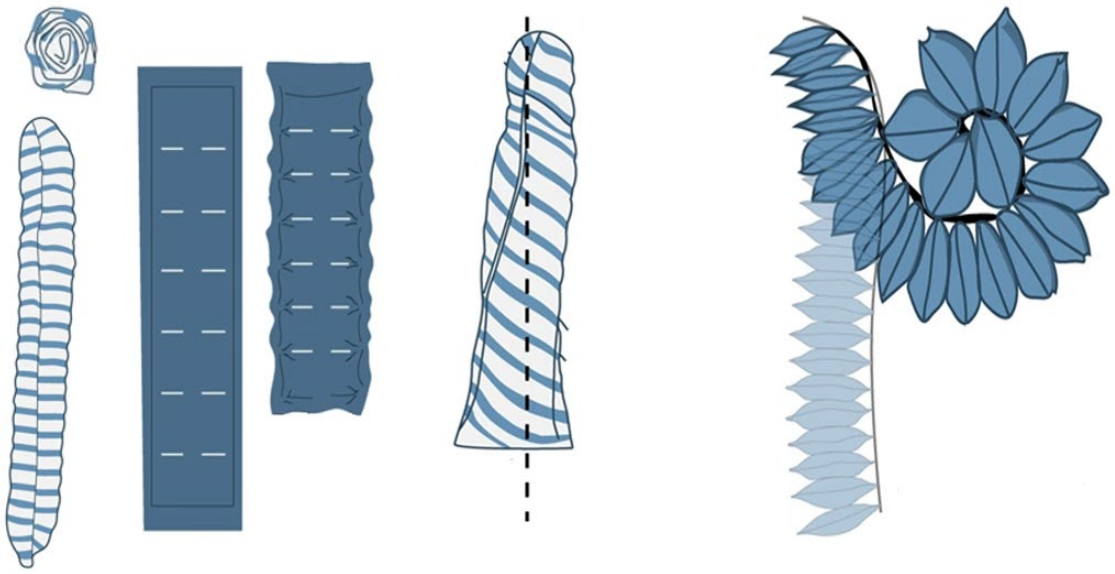

Figure 2.2 Demonstration of motions from fabric actuators (a) Extension (b) Contraction (c) Twisting (d) Bending [21].

The use of the extension fabric actuators can activate a faster pneumatic discharge to assist in boosting the speed to achieve bidirectional motions (**Figure 2.3**) [21][50]. Another wearable suit was made by sewing multiple soft, thin pneumatic muscles into a flexible fabric, which provided high power density, high force, good flexibility, and lightweight nature [51]. However, they may not be sufficient for medical rehabilitation programs due to their limited force. Additionally, fatigue tests on fabric-based actuators and efficacy evaluation in impaired patients need to be conducted.

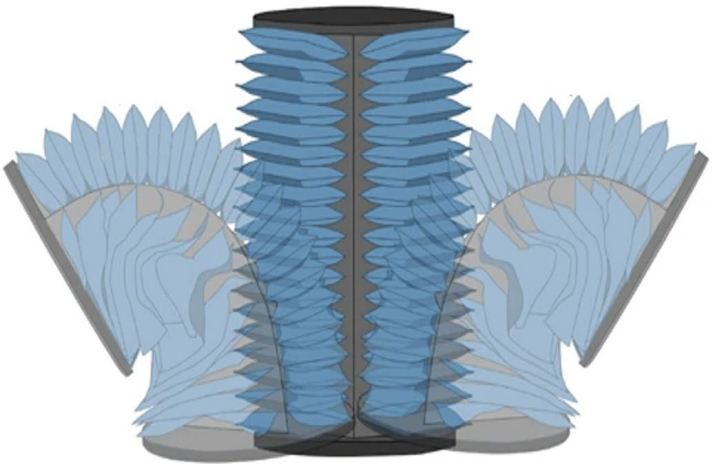

Figure 2.3 A bidirectional bending soft actuator made of thermoplastic polyurethane [21].

2.1.2 Categorized by actuation motion

It is possible to categorize soft actuators into electroactive polymers and soft fluidic actuators based on the source responsible for the actuation.

2.1.2.1 Electroactive polymers

Electroactive polymers are polymer materials that respond to electrical stimulation by undergoing significant changes in dimension or shape [52]. Dielectric elastomeric actuators (DEAs) are one of the popular electro-active polymers used in soft robotic actuators. It consists of a thin elastomer membrane between two compliant electrodes. The elastomer deforms when a voltage is applied, leading to mechanical actuation, as shown in **Figure 2.4** [53].

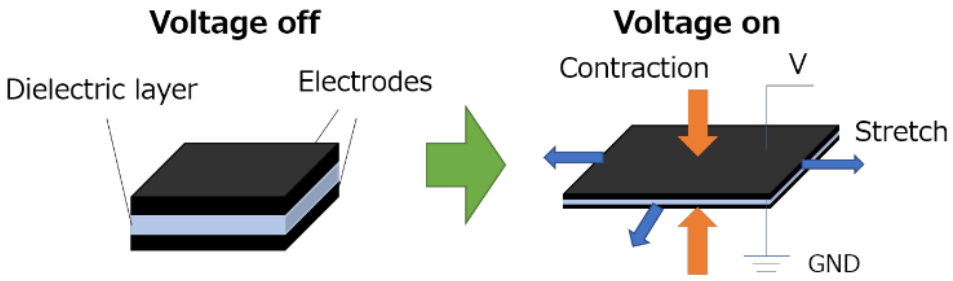

Figure 2.4 Mechanical deformation of dielectric elastomers upon electrical actuation [53].

By stacking multiple electrodes and elastomers, the performance output of the DEAs can be significantly improved [54]. The main performance advantages of DEAs can be highlighted by large deformation [55], high energy density, fast responses [56], lightweight, and low cost [56]. The sensing capabilities of DEAs [57], [58] and the ability to configure customized shapes make them ideal actuators for soft robotics [59]. One of the simplest examples is the annular type diaphragms that were used in early DEA development. When the potential energy of these systems is minimized with respect to the thickness of the film, it results in a highly nonlinear relationship between bidirectional stretch and power supplied [34], [60]. In addition, such couplings often exhibit instability at a critical point, where the film wrinkles or creases suddenly when the supply exceeds a critical value. There is also the possibility that the elastomer may fail at these high voltages due to a dielectric breakdown, depending on how strong the applied electric field is on the elastomer. The failure of DEAs due to this phenomenon is sometimes difficult to prevent because they only undergo significant deformation when voltages are close to these critical values [61]. Furthermore, the use of DEAs in combination with fluidic actuators has been developed to improve both the work density and load capacity. Despite their ability to be integrated with mobile electronics, DEAs may still be too bulky to be compatible with miniaturized soft robotic systems due to their high voltage circuitry requirements [62].

Ionic electroactive polymers are another type of electroactive polymer in which actuation is caused by the displacement of ions inside the polymer, as shown in **Figure 2.5** [63]. For actuation, only a small voltage is required, but for the actuator to maintain its position, higher electrical power and energy are needed [64]. A few examples of ionic electroactive polymers are conductive polymers [65], ionic polymer-metal composites [66], and gels that react to electro actuation [67]. One example is bucky gel actuators, consisting of a polymer-supported polyelectrolyte layer made of an ionic liquid gel sandwiched between

two single-wall carbon nanotube electrode layers [68]. Another type of ionic electroactive polymers includes electrorheological fluids, which change their viscosity with the applied electric field. This fluid is mostly made of a suspension of polymers in a low dielectric-constant liquid [69]. When a large electric field is applied, the suspension's viscosity increases. A shock absorber, engine mount, and acoustic damper could all benefit from these fluids [70].

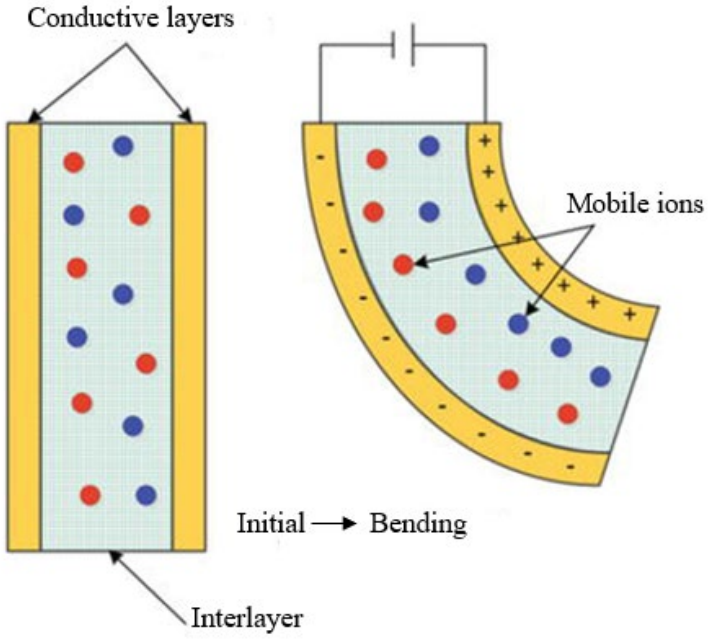

Figure 2.5 Universal architecture and mechanism of ionic polymer actuators [63].

2.1.2.2 Soft fluidic actuation (SFAs)

Soft fluidic actuators utilize pneumatic or hydraulic fluids to power them. In the demonstration shown in **Figure 2.6**, multiple modules are inflated to cause bending when pressurized with fluids. Soft actuators made of silicone [71], fabrics [72], polymer composites [73], [74], and flexible fibreglass [75] are of particular interest in manufacturing soft fluidic actuators. These actuators can be rapidly fabricated in a multi-step moulding process, and with new design concepts, fabrication approaches, and the

availability of varieties in soft materials, they can be used to achieve combinations of contraction, extension, bending, and twisting using pressurized fluids. Applications like heart assist devices and soft robotic gloves for rehabilitation can be considered as a ground to define the movements and force requirements expected of these actuators.

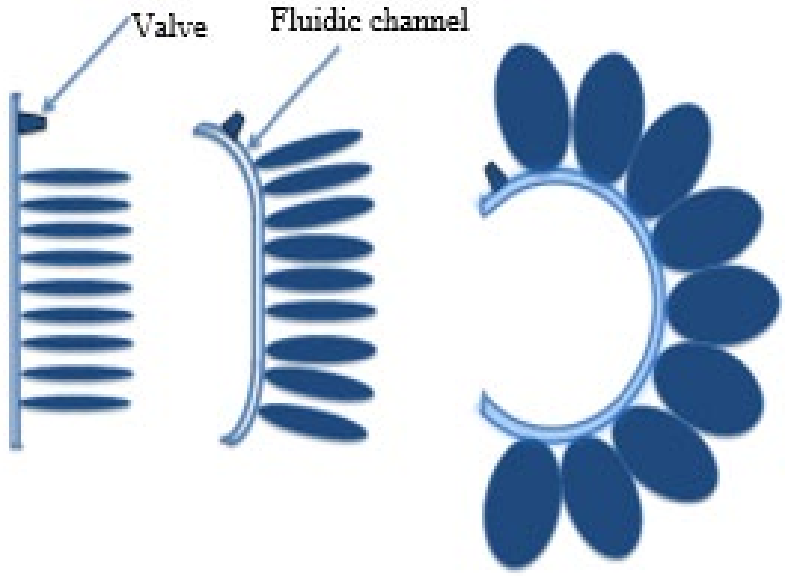

Figure 2.6 Bending of fabric-based soft actuator upon fluidic actuation.

A pneumatic artificial muscle (PAM) was one of the first soft robots that used compressed air for actuation [76]. Essentially, these actuators consist of elastomer shells that are lined with braided textiles that would contract when filled with compressed air. The use of pressurized air produced by combustion and fuel decomposition has recently been investigated as a way to drive soft pneumatic actuators [77]. One approach that has been taken is to use platinum as a catalyst to activate the disintegration of hydrogen peroxide or to promote the combustion of butane and oxygen [78]. Gas pressures of 50 kPa can be generated by such reactions. This is sufficient for actuator motion. A robot powered by combustion can jump, and it requires functionally graded materials with varying degrees

of mechanical compliance so that internal stresses can be equally distributed during impact landings [8].

Water is also used as a propellant in soft fluidic actuators, as water can carry a greater load and allows a quicker response from the actuator. Water is treated as being incompressible when considered with the surrounding elastomer, which means that slight displacements to the boundaries between the fluid and the surrounding elastomer can lead to rapid changes in both fluidic pressures as well as actuator stiffness [79]. **Figure 2.7a** shows a traditional schematic for controlling a bidirectional fluidic actuator requiring high and low pressures. This method employed two five-way valves, a high-pressure accumulator, a digital pressure, and a vacuum gauge, which was mapped to position through electrical control. **Figure 2.7b** shows an integrated positive displacement pump schematic showing the need for just one stepper-motor-driven peristaltic pump to drive the entire system. Alternatively, there have been recent developments in the development of underwater soft actuators based on hydrogels, which allow for the flow of water into a fluidic medium [80]. Hydrogel's density and transparency are similar to seawater, making the actuators optically and acoustically transparent. It might be possible to engineer underwater soft robots that do not interfere with the natural behaviour of marine organisms [81].

Several techniques can be used in conjunction with soft fluidic actuators (SFAs) to improve their performance in terms of constructability, variable stiffness, and operational range criteria. The SFAs along with shape memory polymers, are integrated to improve the bending point, shape configuration, and variable stiffness [82]. SFAs combined with Gecko adhesion provide higher-strength grasps at lower pressures [83]. SFAs integrated with dielectric elastomers (DEAs) are targeted toward improving the handling of soft and delicate targets [84]. It also helps in the reduction of the size of SFAs [85]. SFAs used along with tendons can be controlled by a servo motor for precise control of the actuator

bending [86]. In addition, improving control tendons helps to miniaturize the size of SFAs as well [87].

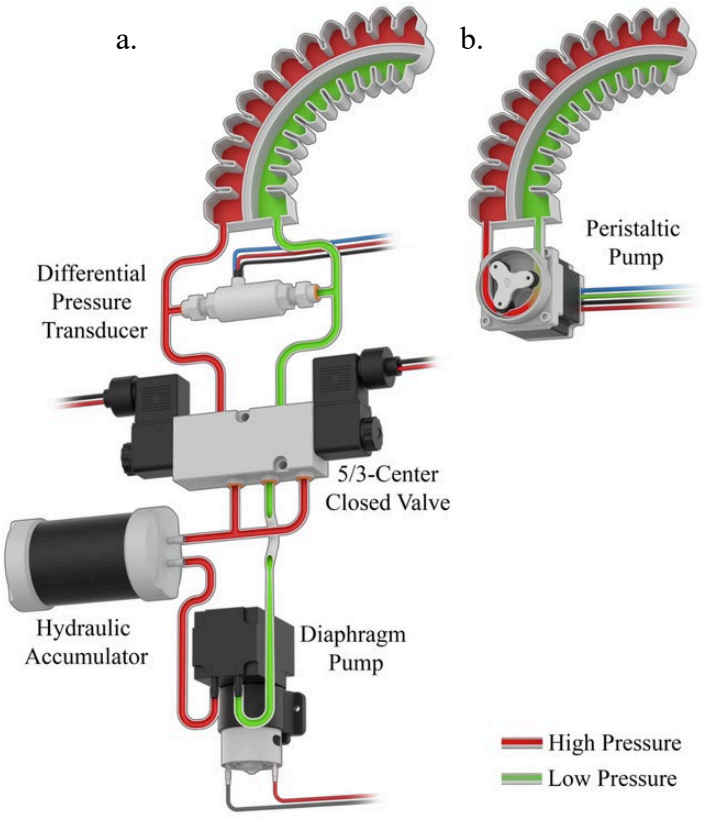

Figure 2.7 Traditional schematic of a controlled bidirectional fluidic actuator. (a) Conventional soft robotic hardware (b) Peristaltic fluidic engine [88]

A combination of SFA and rigid robot paves the way for improving the flexibility of determining bending point, modifying the shape configuration and variable stiffness. It also increases the capability of actuators to perform multiple functions [24], [89], [90]. SFAs with electro-adhesion are used for delicate gripping tasks on flat or irregularly shaped objects [91]. SFAs with layer jamming mechanisms provide variable stiffness in the actuator due to the change in friction between layers [92], [93]. Soft pressurized fluidic actuators, along with soft vacuumed fluidic actuators provide variable stiffness [94], [95], increased actuation [96], and linear motion capabilities [95].

It is important to note that fluids perform similar functions in soft actuators as they do in traditional pneumatic and hydraulic machinery. However, there are a wide variety of parameters that influences the performance of a soft robotic system, including thrust performance and hysteresis [97].

2.1.3 Categorized by design

Based on the design factor that is responsible for bending in a soft actuator, the actuators can be classified into bellow actuators and fibre-reinforced actuators.

2.1.3.1 Bellow actuators

Bellow-based actuators consist of a parallel arrangement of chambers that are connected internally via a channel [98]. Generally, each chamber has two thin walls that are perpendicular to this channel and expands upon pressure. A thicker base of the actuator restricts this expansion leading to a seamless bending of the actuator as shown in **Figure 2.8** [99], [100]. Inflating these actuators non-collinearly can produce coupled twisting and bending motions when actuated [101]. This coupled motion enables the actuators to be more flexible and dexterous, making them a suitable candidate for a wide variety of applications, such as flexible manipulators, biologically inspired robots, and medical devices [102].

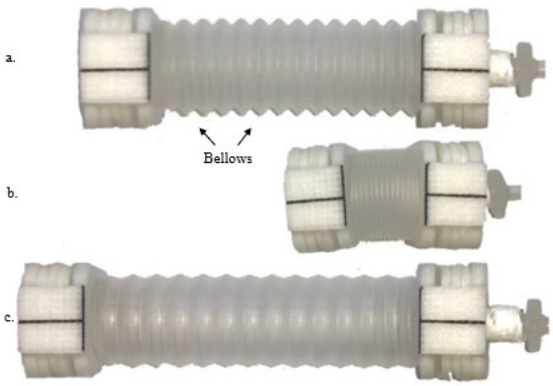

Figure 2.8 Bellow actuators (a) Origin state, (b) compression state, and (c) inflation state of the bellow actuator [103]

Multicore actuator design is useful for assisting joints in a single degree of freedom and has been widely used in the flexion of finger and elbow joints [104]. A soft wearable robotic device used chambers to make muscle-like structures to generate bidirectional active knee motions. Each muscle had four muscle cells creating a maximum force of 38N and contraction of 18mm. With different combinations of actuations, the device was able to create active motions for knee extension and flexion [105]. Inspired by the fore flippers of seals, a supernumerary soft robotic (SSR) flipper was designed to replicate their strength, dexterity, as well as flat-shape foldability using origami and kirigami techniques. A range of experiments using the fabricated prototype showed excellent object adaptability, grasping capability, and versatility [106].

2.1.3.2 Single-core actuators

In recent years, many research groups have developed soft actuators with single cores due to their simpler design technique. The design concept involves an elastomer bladder surrounded by inextensible reinforcements (e.g., skeleton-like structures) [107]. When inflated, the bladder expands in all directions. Inextensible fibres constrain the bladder from expanding radially, allowing only axial expansion [108]. Inflated bladders undergo a particular type of motion due to the arrangement of reinforcements as shown in **Figure 2.9** [73].

A combination of bending, extension, and twisting can be achieved by selecting the appropriate placement [109]. Several different behaviour types can be achieved along a single actuator. For example, when the actuator is inflated, one segment will bend, another segment will extend in the axial direction, and one segment will twist and bend [18]. Pre-programming complex behaviours like this are one of the primary advantages of soft robotics over traditional rigid robotics.

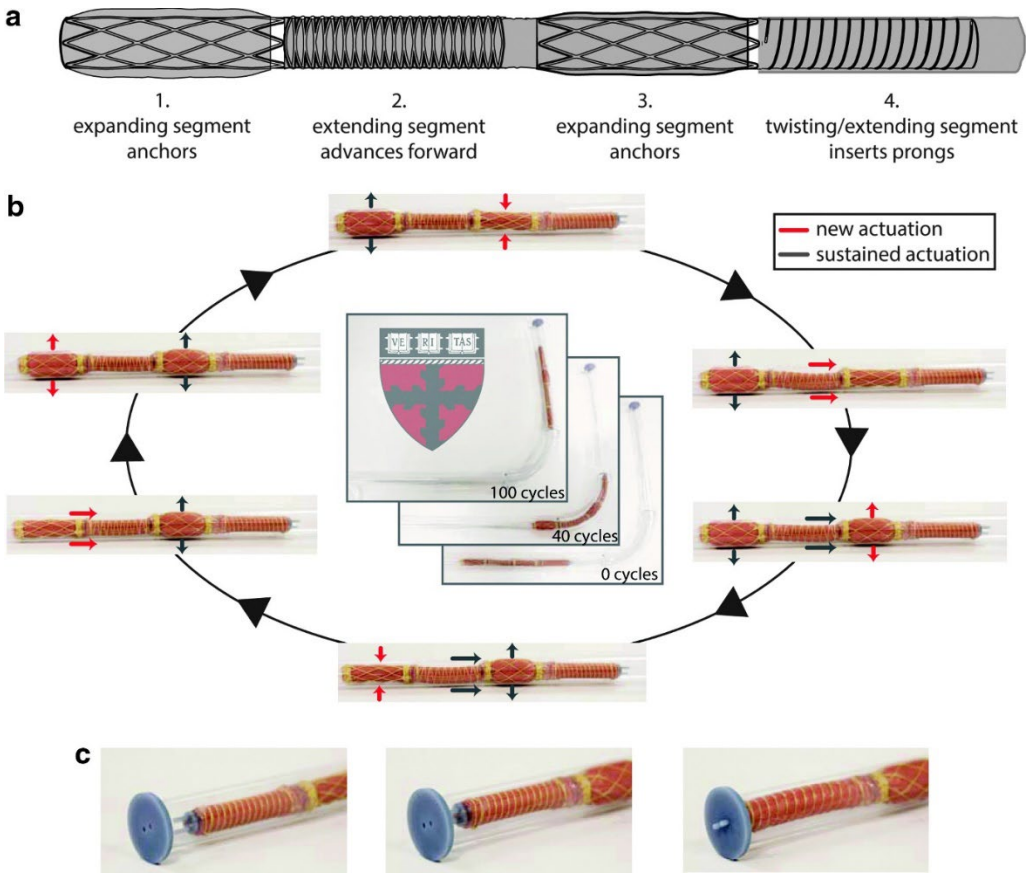

Figure 2.9 Actuator performing an orientation-specific task. (a) Four actuator segments are combined in series to achieve forward locomotion and perform an orientation-specific task. (b) Segments 1, 2, and 3 are actuated in sequence to move the device through a bent tube. (c) As the device approaches the end of the tube, the prongs are not aligned with the holes. Segment 4 is then actuated, extending and twisting the prongs into the holes [73].

The importance of reinforcing a system is to alter the overall material strength to achieve customized movements [110]. By doing so, the stiffness can be increased in areas where deformation isn't needed to achieve the task. Soft fluidic actuators are particularly vulnerable to this problem, as an increase in internal pressure may result in the extrusion of their walls and ultimately rupture [111]. Also, it is possible to change the strain-limiting reinforcement fibre braiding angle of the core to study the different behaviour of the soft

actuators [74]. Due to a difference in expansion between one side and the other of the actuator, when inflated, the actuator bends [22]. The reinforcements can be added at any point during the moulding process. To avoid friction and hysteresis, they must, however, be properly bound to the soft structure [112]. Alternatively, reinforcements can be achieved by over-moulding or glueing [113], [114] later in the process. There are also ways to generate complex behaviours using internal skeletons [115], fabric jackets, or plastic exoskeletons [116]. In these hybrid designs, the soft core of the product is ideal for soft interactions, and rigid sections of the product provide larger force generation.

In the process of optimizing soft actuator flexibility, different materials can be combined to provide different mechanical properties. Using heterogeneous materials together provides the anisotropy necessary for enabling soft mobility with limited transverse deformation [117]. Despite similar chemical compositions, materials can have contrasting mechanical properties. For example, [118] suggests the use of a PDMS rubber, which has a Shore hardness of 50 A, in combination with a relatively soft Siloxane rubber as the actuator body. In this way, a pneumatically actuated bending grasper was created based on the contrast between stiffnesses.

Embedding papers or fabric in the fluidic structure would be another option [112], [114]. Layers of these materials are very stiff when stretched, but they can also bend very easily, which makes them an ideal reinforcement for bending actuators. Alternatively, if the structure is to be extended linearly, inextensible threads may be wound around the structure, exhibiting very low radial expansion [119]. A combination of strain-limiting paper and winding fibre around the actuator can also result in interesting designs that combine twisting and bending [120].

Fibre-reinforced actuators have advantages and disadvantages over bellow actuators. For example, the reinforced actuators are more robust and can be used to achieve a greater spectrum of movements. In addition, these actuators have only one seam at the top where it attaches to the base, while bellow actuators have a seam throughout the axis. As a result, there is less risk of failure in reinforced actuators. However, reinforcing fibres in elastomers and moulding is both resource and time-consuming, whereas the bellow actuators can be cast and assembled in a shorter amount of time using moulds. Therefore, the actuator chosen should be based on the application, available time, and access to resources.

2.2 Applications

2.2.1 Soft Actuator in wearable applications

Soft actuators have become an important part of wearable robotic applications due to their mechanical flexibility, lightweight, and portability [121]. A paradigm shift has occurred from rigid exoskeletons with isolated compliant actuation methods to soft, garment-like wearables that feel very light on the human body. Recently, a significant increase in the number of robotic devices made from soft, compliant materials in research and commercial products [122]. Lightweight, low-cost garment-like devices eradicate the need for heavy, bulky, and rigid components in favour of materials with inherent softness and compliance [2]. In addition to their flexibility, soft robotics offer unmatched versatility and adaptability, resulting in systems that are very easy to use and that can conform to their surroundings and their users for greater comfort and ease of use.

2.2.1.1 Shoulder assistive devices

The shoulder joint, as one of the most important upper body joints, plays an important role in the assistive device due to the advantages of smoothness and high flexibility for movement [123]. Significant research was conducted in developing a compliant soft

wearable shoulder assist device that closely mimics the functionality and comfort found in the human body [124]. However, the high flexibility of shoulder joints makes it difficult for use as conventional assistive wearable devices made of solid counterparts. The initial approach of using the shoulder joints requires the user to be in a stable position for the utilization of device. **Figure 2.10** demonstrates a wearable, soft robotic shoulder assist device for shoulder overuse syndrome (SOS) patients, utilizing pneumatic artificial muscles (PAMs) to assist the biological muscles during the push phase of the wheelchair stroke cycle [125].

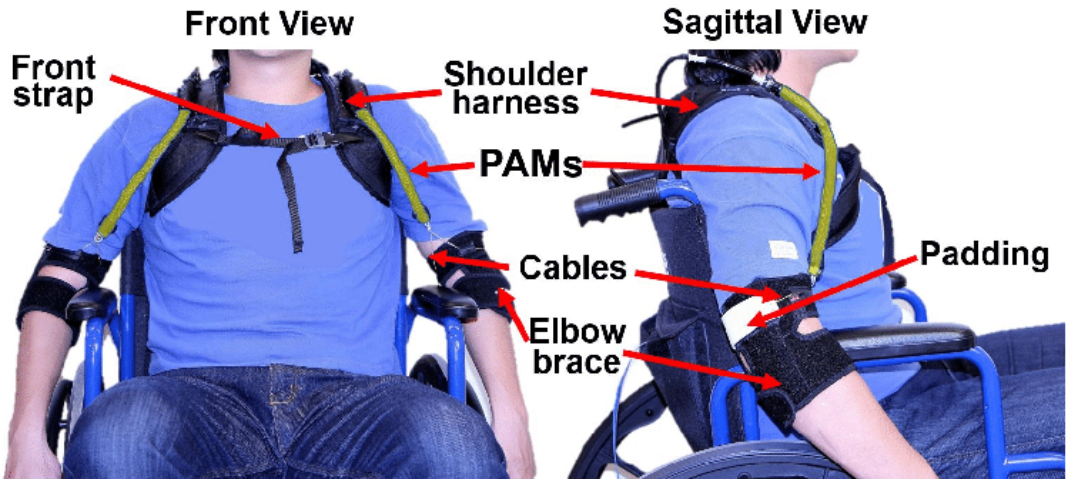

Figure 2.10 The soft robotic shoulder assist prototype device worn by a user shown in front and sagittal views [125].

McKibben actuators were one of the early stages of soft actuators utilized to form assistive devices for the shoulders. They were simpler and easy to wear due to their lightweight [126]. However, when powered, these actuators tend to slip from the initial position and cause discomfort to the user while translating the generated force into an accountable application. Further developments in the McKibben actuators have been made to improve the ability, in terms to shift the balancing posture for shoulder flexion and extension

movements [51]. Cable-driven mechanisms that utilize tendons to assist movements were another choice for shoulder assistance wearables due to their compactness and identical behaviour. They overcome the problems present in McKibben actuators in terms of limited tensile force and allow easy placement options on the shoulder, paving the way for an increased degree of freedom [127]. The development of fabric-based soft actuators [128] has proven to generate enough force to lift the arm with smoother movements in pediatric wearable assistive devices [129].

2.2.1.2 Soft actuators in trunk assistance

The posture of the trunk plays a major role in preventing injury with people who constantly work sitting for a long time and also with people who frequently lift heavy materials as part of their work in industries. Also, people who injured parts of their trunk in accidents or other causes need assistance in lifting themselves in order to move places. A passive, assistive device has been developed to support the trunk of patients with Duchenne muscular dystrophy [130].

Figure 2.11 shows a mechanical design in which a spring is configured in series to Bowden cable transmissions [131]. The spring is compressed during a lowering task, and this energy is released to assist in a lifting task. Another passive exoskeleton used for torso twist assistance helps eliminate Musculo skeletal disorders in nursing people [132]. Pretensioned soft bands and pads help protect the extra pressure exerted on the muscles and also prevent injuries [133]. The development of a trunk support trainer provides active support to the trunk and generates reasonable force for assistance [134].

Figure 2.11 System architecture of a lifting assist device (LAD) prototype [131].

2.2.1.3 Elbow protection and rehabilitation devices

Elbow injuries are one of the common injuries that can occur in the human body. Leaning on a hard surface using your elbow can cause bursitis and tendinitis due to repetitive strain or injuries to tendons that attach muscle to bone. Therefore, elbow assistance is an important factor in preventing injury and provides rehab assistance for elbow-injured patients. **Figure 2.12** shows an untethered elbow Exo-suit designed to assist elbow flexion [135].

Figure 2.12 Untethered elbow Exo-suit .1. Load cell 2. IMU sensors 3. Load cell amplifier 4. Actuation stage 5. Embedded controller and motor drive stage 6. Controller battery pack 7. Motor drive battery pack [135].

McKibben actuators were used to design elbow rehab devices, but they suffer the same problem as shoulder assist devices in terms of converting the force generated to the motion of the elbow joint without causing discomfort. By using cable-driven systems, the upper arm can be flexed and extended in a way that mimics the biological function of the muscles [136]. With cables attached to the forearm and routed to the shoulder, the cables can help to flex and extend the elbow joint. Chamber-based soft actuators were designed to implement flexion assistance in elbow joints by creating a rotational torque [137], [138].

2.2.1.4 Wearable wrist protectors

A fall or slip will first induce our brain to use our hand or wrist to reduce the damage occurring to the front of the torso or head. It was reported that wearable wrist guards

reduced the impact of landings by half and effectively prevented fractures by stabilizing the wrist against bending moments [139].

An active wrist protector uses a pre-inflated airbag that transfers the pressure from one compartment to another based on the fall detection input [140]. With the discovery of lightweight, stronger materials, passive wrist protectors are now commercially available that use cushion-like bands on the wrist to absorb impact during landings [141]. **Figure 2.13** shows a wrist-protecting device that can absorb the impact during a fall, pass it over the wrist area, and transmit it to the forearm [142].

Figure 2.13 Wrist protector [142].

Hand-assistive devices to rehabilitate patients with disabilities are becoming a popular area of research. These devices are designed with the focus of executing repetitive flexion and extension motions to prevent the formation of blood clots in stroke patients and also assist them in performing daily activities. Rehabilitation is necessary for patients post-surgery to restore hand functionality [143]. **Table 2.3** provides the list of end-effector devices used in hand rehabilitation [144]. These devices generally are not portable due to the need for pneumatic or electrical power sources based on the type of actuator and are mostly used in a clinical or medical environment. These devices typically have sensors to give therapists

feedback on a patient's progress and to determine his or her degree of impairment. These devices are mostly active devices with a relatively high output force projected to the patient’s fingers depending on the training or rehabilitation given by the therapist as well as to overcome stiff joints [145]. Currently, haptic exoskeletons are being developed as a safety measure for healthy individuals with the intent of giving haptic feedback as part of virtual or teleoperation applications. In this virtual environment, the individual can interact with objects and feel them through the exoskeleton [146]. Augmentation [1], [147] type of hand exoskeletons serve the purpose of increasing the user's power. Besides their military use, these exoskeletons are also used in space programs to assist in motions that are hard to execute using the thick suits of astronauts [148].

Table 2.3 End effector devices for hand rehabilitation [144]

Name	DOF	Features	Movement	Output force	Remarks
Rutgers Master II	4	Active finger rehabilitation	Extension and flexion of four fingers (without little finger)	16.4 N	ROM is limited (internal mechanism)
Reha-Digit	4	Passive finger rehabilitation	Extension and flexion of four fingers (without thumb)	Not specified	Ambidextrous, not significant gains of ADL
Amadeo	5	Passive finger rehabilitation	Extension and flexion of the five fingers	Not specified	Improvements in joint, grasping and pinching power. Not suitable for spasticity
Haptic Knob	2	Active hand rehabilitation	Opening and closing movements (pronation and supination of the forearm)	1.5 N m	Suitable for wrist and forearm recovery
HandCARE	5	Active hand rehabilitation	Opening and closing hand movements extension/flexion of the five fingers	15 N	Compact robot easy to use and setup
BiManu Track	1	Active hand rehabilitation	Forearm pronation/supination, wrist flexion/extension	5 N m	It works under the principle of bilateral training
ReachMAN	2	Active hand rehabilitation	Forearm pronation/supination, palmar grasp	10 N	–
GENTLE/G	3	Additional hand module	Extension and flexion of four fingers and thumb extension/flexion	18 N	Connected to a Haptic Master robot
Hand Robot Alpha-Prototype II	1	Additional hand module	Extension and flexion of the five fingers	120 N	Connected to MIT-MANUS

2.2.1.5 Hip assistive devices

Wearable devices in the lower body generally aim to assist in the adjustment of gait posture while walking or provide rehab therapy in restoring functions. Heavier devices will result in unnatural gait adaptations, and safety concerns as any added weight will increase the inertia of the limb, increasing the risk of trip and fall when walking [149].

The hip is a critical joint that supports the body's posture and assists in standing and balancing tasks by allowing the transmission of force from the ground to the torso. However, it requires more force outputs since it involves balancing the whole torso. Cable-driven actuators can provide such a level of force outputs [150], [151]. A PVC gel-based soft elastomeric actuator was made to provide hip joint support during walking [152]. In addition to providing hip protection and support while walking, soft wearable hip devices are used in stationary sit-to-stand tests [153] and corrective gait therapies [154]. **Figure 2.14** shows a wearable Hip-assist Robot with an assist-as-needed algorithm for stroke patients with gait disorder. This robot was designed to deliver active-assistance torque to both the hip or hip joint of the paretic side for extension and flexion [155].

Figure 2.14 Gait Enhancing and motivating System-Hip (GEMS-H) [155].

2.2.1.6 Knee flexion and extension devices

Like elbows, soft actuators help to flex and extend the knees in the lower body and provide stability, as shown in **Figure 2.15**. A cable-driven system was used to assist the knee [156], while other researchers used soft, flexible actuators for knee assistance [47]. Rehabilitation treatments for ligament injuries have been developed with soft knee braces [157], [158].

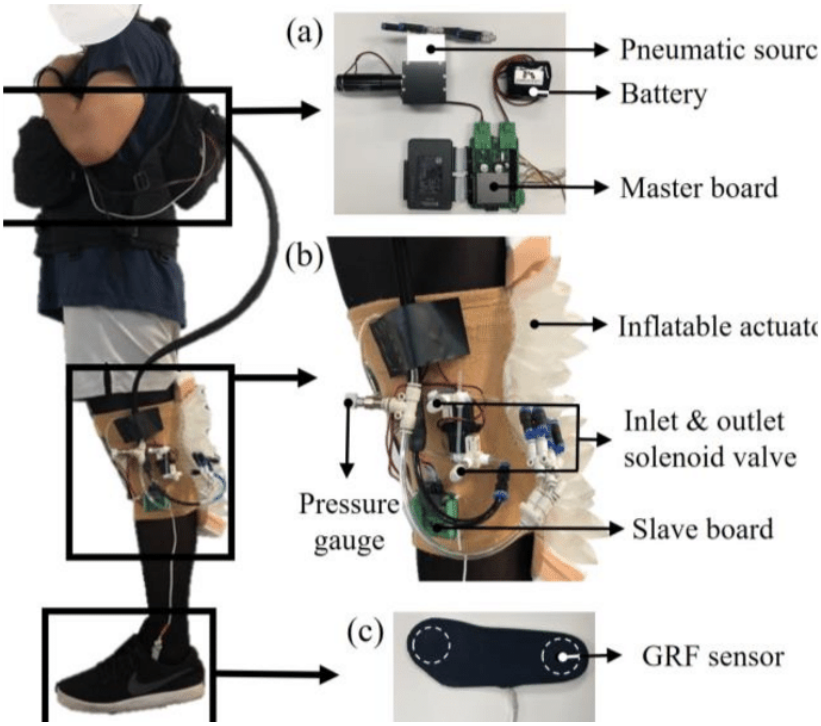

Figure 2.15 Wearable knee suit with a soft actuator to assist the human knee while walking [159].

2.2.1.7 Wearable actuator for ankle joint

When soft actuators are chosen to assist the ankle, joint extra care has to be considered since it will be closely involved with the walking movements of the human body. Heavier devices or devices that cause discomfort while wearing are more prone to cause accidents due to the high inertia present at the foot [160]. In addition to assisting soldiers, cable-driven ankle actuators can also help post-stroke patients regain their walking ability. The

most notable ankle assistive devices include McKibben actuators that are connected to a rigid orthosis [161], Fabric-reinforced assist devices [46]. Users' body weight may be used to distribute pressure through different chambers depending on where they apply their body weight, improving stability and preventing trips and falls [162]. **Figure 2.16** shows the use of a soft actuator as a robotic sock device, worn on the sock to guide plantarflexion when pressurized and deflated to pull the ankle into dorsiflexion.

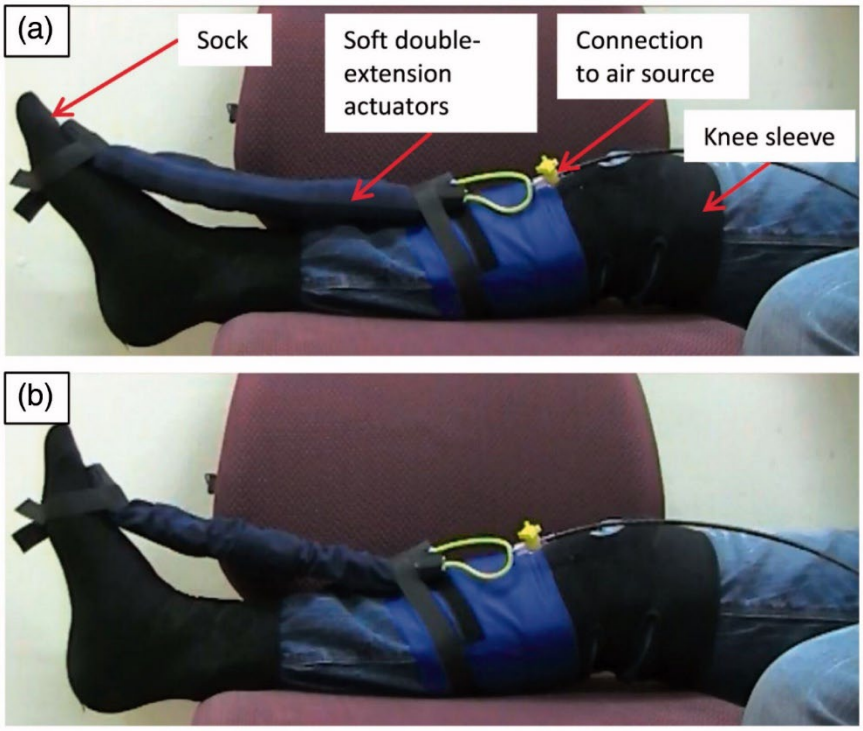

Figure 2.16 Soft robotic sock for assisted ankle rehabilitation [46].

2.2.2 Body-powered wearable applications

Recent experimental efforts have greatly demonstrated soft actuators and their use in wearable applications. It is a long process to make a wearable device from a compact and comfortable setup to bending and force output generation capability in performing an application using these devices. But powering this setup is the most important task, where lightweight, compact wearable devices can easily add more than double their weight due

to the power and control sources involved in them. These things make them non-portable and prone to safety risks involving electricity or compressed air safety risks. Hence alternate powering methods have to be researched to make them more effective in usage. By eliminating the external powering sources, they will be able to provide additional advantages in terms of reduction in production and maintenance costs as well.

This can be done by utilizing naturally available motions found in the human body. Body-powered robots are comparatively less utilized than externally powered robots. This is because, either the force generated by body movements is insufficient to actuate the actuators or the device is bulky and difficult to wear. Cable-driven setup using shoulder flexion has been combined with amplified power using gears and additional locking mechanisms used to hold the cable in a fixed position until further movements, as shown in **Figure 2.17** [163]. Also, EMG signals from wearable sensors can be used to establish control in body-powered prostheses [164].

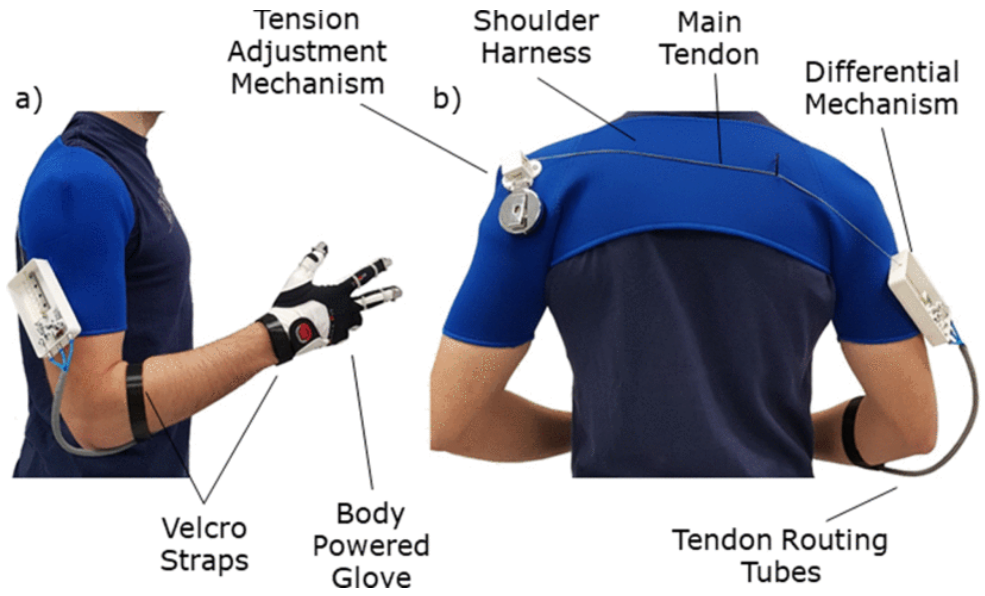

Figure 2.17 Body-powered soft Exo-glove. Reprinted with permission from [163].

Another cable-driven elbow brace was used to power the hand hook, which opens with left shoulder flexion and scapular abduction and closes with left shoulder extension and scapular adduction **Figure 2.18** [164]. Cable-driven actuators that are body-powered need time and assistance for installation. It has to be fixed by a technician since people with disability or hand-impaired functions find it difficult to install the setup on their own.

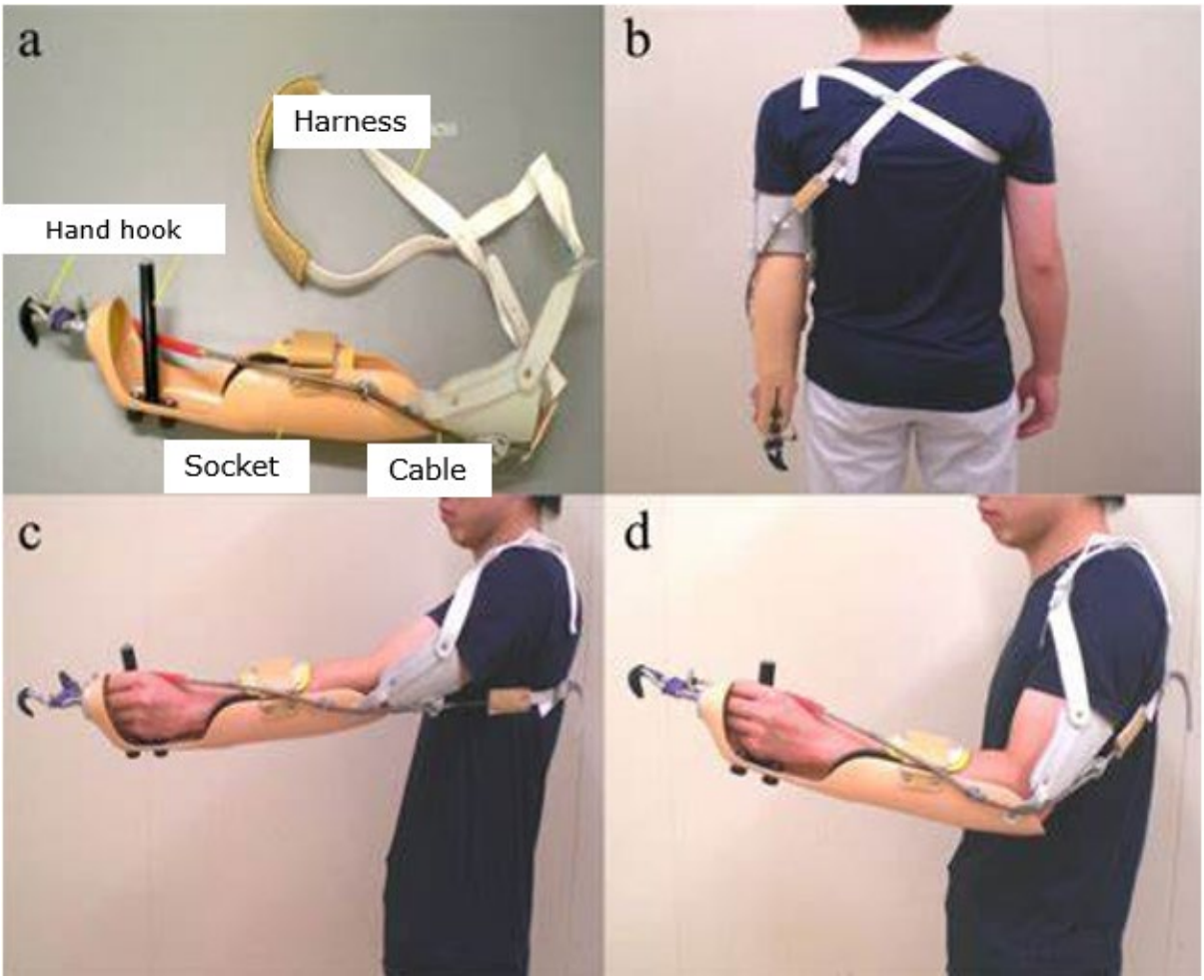

Figure 2.18 Body-powered prosthetic simulator [164].

2.2.3 Other applications of soft actuator

In addition to wearable applications, soft actuators are used in a variety of other fields. In robotics, soft actuators enable robots to perform complex and versatile movements, such as gripping, grasping, crawling, and manipulating objects with varying shapes and sizes [165]. Soft actuators are utilized in human-machine interaction scenarios to create intuitive and

natural interfaces. For example, soft actuators embedded in haptic feedback systems can provide realistic tactile sensations, enhancing virtual reality experiences or remote teleoperation of robotic systems [166]. Soft actuators have applications in bioengineering and biomechanics research. They are used to develop artificial muscles and tissues for experimental purposes, such as studying muscle function, modeling physiological systems, or creating devices for medical simulations. Soft actuators can replicate the natural movements and forces observed in biological systems, allowing for more accurate and realistic studies [167]. Soft actuators are employed in industrial automation processes where the interaction between robots and humans or delicate objects is required. Soft grippers and manipulators can handle fragile items without causing damage, reducing the need for complex and expensive sensing systems. They can also adapt to objects of varying shapes, simplifying the grasping process [168]. Soft actuators are incorporated into textiles to create fabrics that respond to environmental stimuli or user input. These responsive textiles can adjust their porosity, stiffness, or shape, enabling applications like adaptive clothing, breathable materials, and smart textiles with enhanced functionality [169]. Soft actuators offer possibilities for artistic expression and interactive installations. They are used to create kinetic sculptures, interactive installations, or soft toys that respond to touch or external stimuli. Soft actuators add a level of organic movement and responsiveness to these creations [170]. These are just a few examples of the many potential applications of soft actuators. As the field continues to advance, we can expect to see even more innovative uses for this versatile technology.

2.3 Challenges and limitations

As observed from the literature, the critical areas to be addressed in utilizing a soft bending actuator in wearable/prosthesis applications include

- Making soft bending actuators that are lightweight and can operate at low pressure,

- Development of user-friendly devices that can be self-operated by the user in an ideal environment.
- Standalone and portable device with the ability to make effective use of body movements in usable wearable/prosthesis applications by improving the powering system.

2.4 Summary

As outlined in this review, soft actuators are highly dependent on the type of materials, design, and actuation strategies used in making them for use in wearable and prosthetic applications. Wearable robotic technologies benefit from soft robotics by integrating and adapting the developments in material science, sensing, and control technologies, making them lighter, less expensive, and more comfortable to wear. Roboticists have been challenged to rethink wearable assistive devices since this field is rapidly growing and is providing new pathways offering wearable suits that feel like clothes embedded with superpowers. One much-needed area for growth across most wearable robots is their power source used for actuation. In general, to perform pneumatic actuation, a pressurized fluid source such as a pump or compressor source has to be used, which restricts the mobility of the user while operating the wearable device. Therefore, developing a standalone, portable, lightweight, easily wearable, and body-powered exoskeleton will substantially lead to a better user experience.

Chapter 3

Concept introduction

This chapter introduces the concept of bending actuators using two materials with different stiffness and analyses the bending angle using mathematical modelling.

3.1 Bending actuator concept

As aforementioned in the literature review, when two different materials with different mechanical properties are combined into the same structure, it would cause the hollow cylindrical shaped actuator to bend towards its more rigid side upon internal prezzurization [74], [171]–[173]. Two materials, M_1 and M_2, each with Young's modulus E_1 and E_2, respectively (where $E_1 < E_2$), form a cylindrical actuator with closed ends, as shown in **Figure 3.1.**

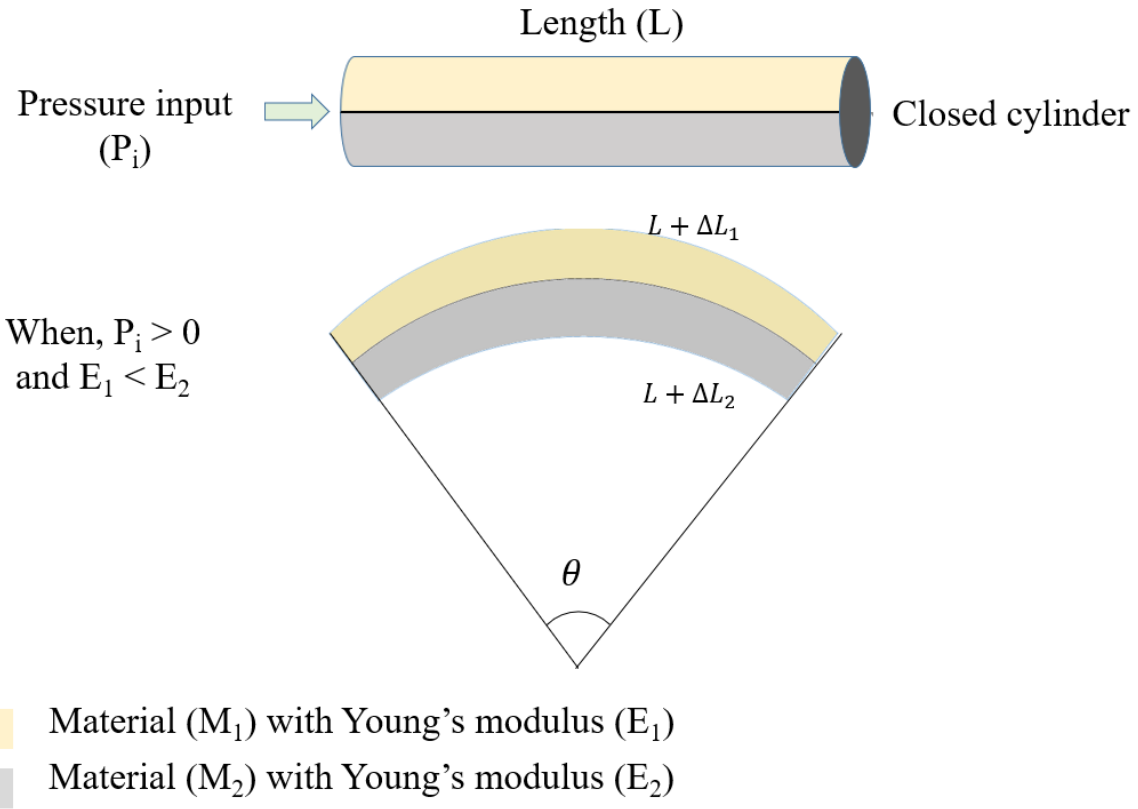

Figure 3.1 Schematic of bending in a variable stiffness cylinder.

By increasing input pressure (P_i) from zero, two materials M_1 and M_2, with Young's modulus values E_1 and E_2, exhibit changes in length ΔL_1 and ΔL_2 respectively leading to a bending of the cylinder. This is based on the assumption that P_i will not cause any radial strain but only axial strain. Due to the difference in Young's moduli, the top half made from material M_1 will elongate more than the bottom half made from material M_2. The bending angle of the cylinder can be measured using the θ indicated in **Figure 3.1**.

To explain this concept of bending actuators based on two stiffness materials, we establish a mathematical model. Firstly, the actuator was assumed as a thick-walled cylinder as it has a different inner and outer diameter with a thickness. It is loaded by internal pressure P_i and external pressure P_o, r_i, and r_o are the inner and outer radius of the cylinders, respectively, as shown in the cross-sectional view of the cylinder in **Figure 3.2**.

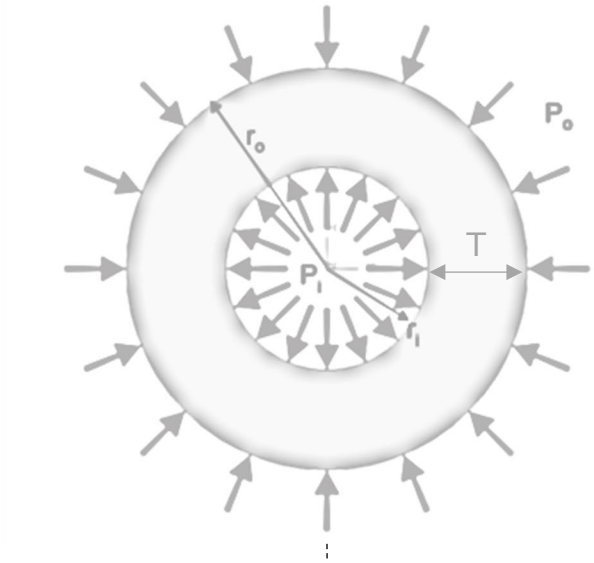

Figure 3.2 Cross-sectional view of a thick-walled cylinder.

As stated above, the two different stiffness material on two half of the cylindrical actuator undergoes a different change in length when pressurized internally. The less stiff material undergoes a larger change in length, while the stiffer material restricts its motion due to

the coupling between them. This, in turn, results in the bending of the actuator if the radial strain can be restricted.

To determine the bending angle of the actuator, we need to determine the change in length on both halves of the actuator. Change in length (Δ_L) can be represented in terms of axial strain and initial length of the actuator using the following equation

$$\Delta_L = \varepsilon_z * L \tag{3.1}$$

the axial strain (ε_z) can be calculated using the following equation

$$\text{Axial strain } (\varepsilon_z) = \frac{\sigma_z}{E} - \frac{\nu}{E}(\sigma_r + \sigma_\theta) \tag{3.2}$$

Here ν is the Poisson's ratio, and E is Young's modulus of the material.

σ_θ, σ_r and σ_z are tangential, radial, and axial stresses, respectively. In general, these stresses act upon the elements within a thick-walled cylinder when pressurized. They can be expressed as shown in the equation below.

$$\text{Tangential stress } (\sigma_\theta) = \frac{P_i r_i^2}{r_0^2 - r_i^2}\left(1 + \frac{r_0^2}{r^2}\right) \tag{3.3}$$

$$\text{Radial stress } (\sigma_r) = \frac{P_i r_i^2}{r_0^2 - r_i^2}\left(1 - \frac{r_0^2}{r^2}\right) \tag{3.4}$$

$$\text{Axial stress } (\sigma_z) = \frac{P_i r_i^2}{r_0^2 - r_i^2} \tag{3.5}$$

Here P_i is the pressure acting inside the cylinder, r_i and r_o are the inner and outer radius of the cylinders respectively.

Substituting equations (3.3), (3.4) and (3.5) in (3.2), the axial strain for a thick-walled closed cylinder can be narrowed down to the following equation,

$$(\varepsilon_z) = \frac{(1-2\nu)}{E} \times \frac{P_i r_i^2}{r_0^2 - r_i^2} \tag{3.6}$$

By substituting equation (3.6) in (3.1), it forms the equation as shown below,

$$\Delta_L = \frac{(1-2\nu)}{E} \times \frac{P_i r_i^2}{r_0^2 - r_i^2} \times L \tag{3.7}$$

For simplification, it is assumed that the bending angle on both sides of the actuators is the same in all cases, as they both increase in proportion with increasing pressure. (See **Figure 3.3**). Hence resulting bending angle can be calculated as follows,

$$\theta = \frac{(L+\Delta L_2)}{r_2} = \frac{(L+\Delta L_1)}{r_1} \tag{3.8}$$

For an actuator of diameter 20 mm, the radius r_2 can be calculated as shown below,

$$r_2 = r_1 + 10 \tag{3.9}$$

Assume $S_1 = (L + \Delta L_1)$ and $S_2 = (L + \Delta L_2)$ equation 3.8 becomes (3.10)

$$\theta = \frac{s_2}{r_1 + 10} = \frac{s_1}{r_1} \tag{3.11}$$

Rearranging equation (3.11), The radius r_1 can be calculated using the following equation

$$r_1 = \frac{10 * s_1}{(s_2 - s_1)} \tag{3.12}$$

On substituting equation (3.12) in (3.11)

$$\theta = \frac{s_1}{\frac{10 * s_1}{(s_2 - s_1)}} \tag{3.13}$$

$$\theta = \frac{(s_2 - s_1)}{10} \tag{3.14}$$

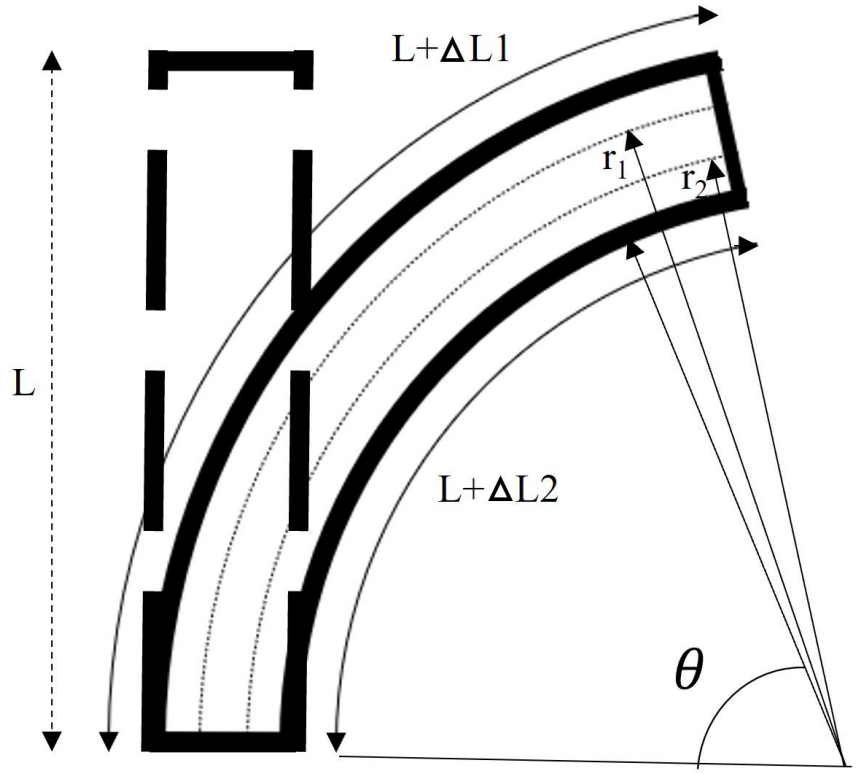

Figure 3.3 Bending angle ($\boldsymbol{\theta}$) calculation in a bending actuator.

With a known initial length of the actuator (L) and the change in length (Δ_L), calculated from equation (3.7), S_1 and S_2 from equation (3.10) can be calculated. These S_1 and S_2 can be used to determine θ in equation (3.14).

3.2 Fibre-reinforcement concept

Fibre winding is reported as an effective approach to reinforce soft elastic material and restrict the radial strain, endowing it with attributes such as fast response, high endurance, and excellent stability. In a research work by Wang et al., they have demonstrated that embedding fibres in an elastomeric material can alter the mechanical properties of the material. These properties can be programmed by varying the angle between fibre braids. It was experimentally verified in this work by testing samples made of two fibre-reinforced

elastomers braided at angles 10° and 80°, respectively. The angles were calculated from the axis of the actuator, as shown in **Figure 3.4**.

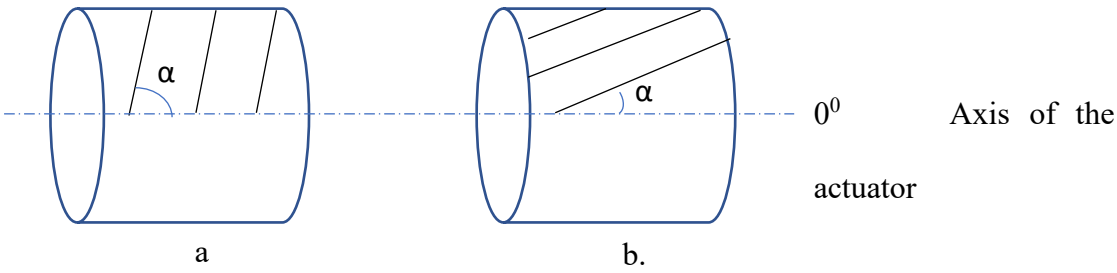

Figure 3.4 The braiding angle (α) measured from the flat projection of the cylindrical actuator. (a) 80° braiding from the axis of the actuator (b) 10° braiding from the axis of the actuator.

In order to determine the Young's modulus of the elastomeric materials reinforced with fibre braid, samples were prepared to be measured using an Universal Testing Machine (Instron 5567). Firstly, an acrylic sheet of a length of 525 mm and a width of 25 mm was used as the base. Secondly, a rectangular frame of 2 mm thick with an inner hollow rectangle of 500 mm x 20 mm dimension was cut. Thirdly, holes with a 1 mm diameter hole were drilled at a 2 mm spacing, and a 1mm nail was inserted into each hole. As shown in **Figure 3.5**, fibre braids were made at angles 10^0 and 80^0 using the nails as guides. The mould was then filled with the elastomeric material to form a fibre-reinforced sample, which was then cut into three samples for testing.

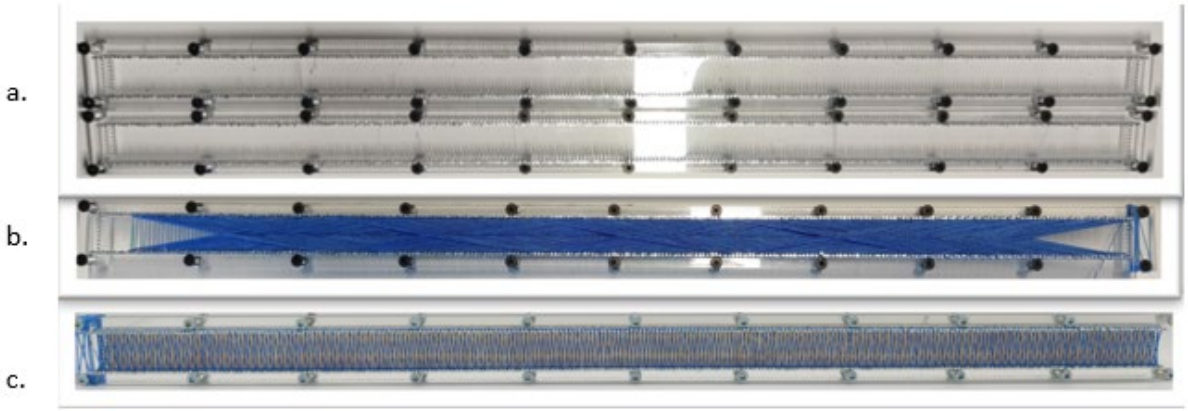

Figure 3.5 Sample preparation (a) Mould for braiding (b) braided sample 10^0 (c) braided sample 80^0.

In this research, three different materials were examined, Ecoflex™ 00-30, Ecoflex™ 00-50, and Smooth Sil™ 940, and were tested using an Instron machine with a 30 kN load cell, as shown in **Figure 3.6**.

Figure 3.6 Samples of 10° and 80° fibre braided Ecoflex 00-30 with Universal Testing Machine set-up.

A summary of the material properties obtained from the Universal Testing Machine machine is shown in **Table 3.1**. Young's modulus is shown to increase in the order of Ecoflex™ 00-30, Ecoflex™ 00-50, and Smooth Sil™ 940. Furthermore, samples with 10° braided angles have a higher modulus than samples with 80° braided angles. Note: Young's moduli of the pristine Ecoflex were obtained as per ASTM D638 standard and more details will be presented in Chapter 6.

Table 3.1 Material properties of Ecoflex™ 00-30, Ecoflex™ 00-50, and Smooth Sil™ 940.

Material	**Braiding angle (α)**	**Young's modulus (E) MPa**
Ecoflex™ 00-30	**-**	0.15
Ecoflex™ 00-50	**-**	0.21
Smooth Sil™ 940	**-**	0.90
Ecoflex™ 00-30	80°	0.08
Ecoflex™ 00-30	10°	4.46
Ecoflex™ 00-50	80°	0.14
Ecoflex™ 00-50	10°	5.60
Smooth Sil™ 940	80°	1.29
Smooth Sil™ 940	10°	42.75

The Ecoflex™ 00-30, Ecoflex™ 00-50, and Smooth Sil™ 940 materials used in to study their behaviour were assumed to be an isotropic materials. To calculate the ΔL from equation (3.7) Young's modulus and Poisson's ratio of the fibre-reinforced elastomeric materials are required. In this experiment, it was assumed that Poisson's ratio was insignificant and ignored. Substituting Young's modulus (E) values for Ecoflex™ 00-30, Ecoflex™ 00-50, and Smooth Sil™ 940 samples from **Table 3.1**, the change in length ΔL can be calculated.

This bending angle (θ) for all three fibre-braided Ecoflex™ 00-30, Ecoflex™ 00-50, and Smooth Sil™ 940 actuators were calculated using equation (3.13) and plotted against each other as shown in **Figure 3.7**. According to the numerical model, the bending angle of the actuator is directly proportional to the pressure input. Also, the actuator made of low-stiffness material tends to bend more compared to the ones possessing high stiffness as the pressure increase.

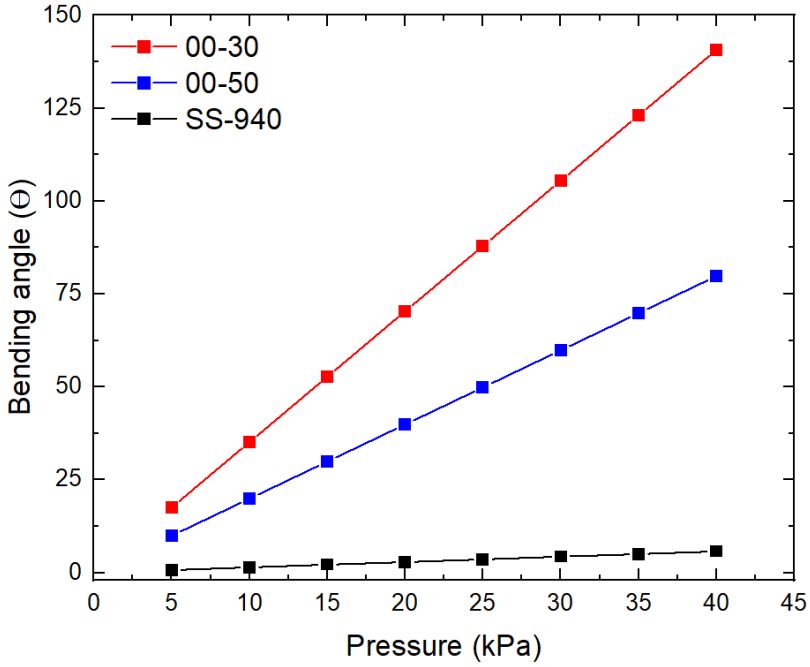

Figure 3.7 Numerical model results illustrating the relationship between the pressure and bending angle ($\boldsymbol{\theta}$) for Ecoflex™ 00-30, Ecoflex™ 00-50, and Smooth Sil™ 940 actuators calculated using samples braided with 10° and 80° combination.

Finally, a variable stiffness cylindrical actuator was proposed. **Figure 3.8** illustrates how fibres can be reinforced inside elastomeric materials at two different angles and combined to alter their stiffness for bending motion. The fibres around the actuator can act to eliminate the radial strain, and also prevent it from bulging.

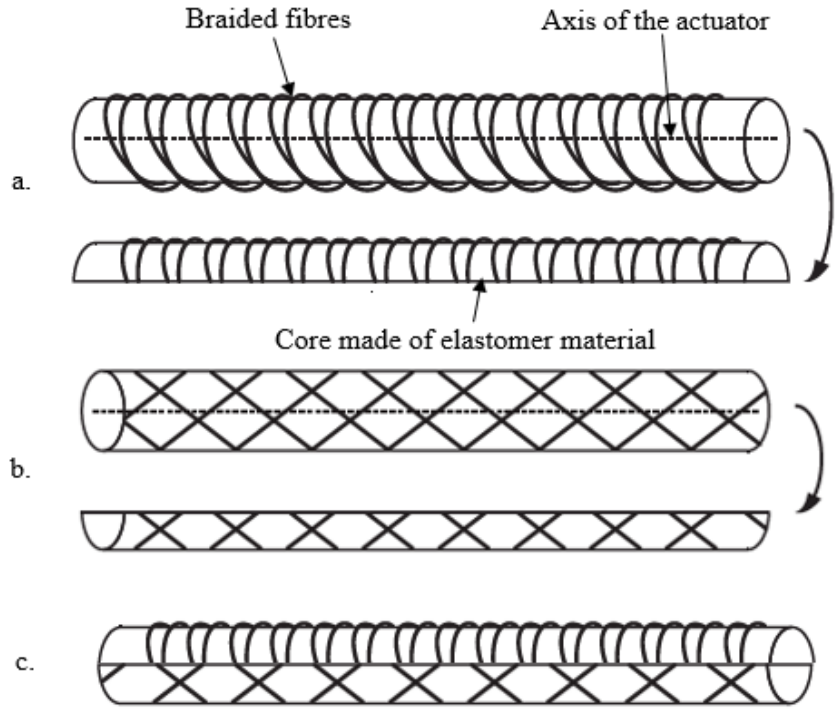

Figure 3.8 Schematic of a fibre braided elastomeric actuator. (a) Fibre braided at 80º (b) Fibre braided at 10º (c) Actuator with 10º/80º braiding combination.

3.3 Limitations of the model

The numerical model was developed based on a number of assumptions, including the assumption that the actuator is a thick-walled cylinder and ignore any radial strain and to maintain the same bending angle on both sides of the actuators. Also from previous studies [174], Ecoflex^{TM} 00-30, Ecoflex^{TM} 00-50, and Smooth Sil^{TM} 940 were considered as isotropic materials and the Poisson's ratio was assumed to be insignificant. Due to these assumptions, there is a possibility that the bending results may not be as accurate as those calculated using experiments. In the future, a comprehensive numerical analysis can be conducted to eliminate these limitations and improve the accuracy of the output results.

3.4 Summary

This chapter demonstrated a mathematical model that explains the possibility of bending in a closed cylinder made from two variable stiffness materials. Also, it explained a process

in which fibres braided at different angles could be used to program the stiffness of the material. These stiffness values were experimentally tested and applied to the mathematical model to calculate the bending undergone by a cylinder.

This concept of design looks promising as actuators can be made using a simple single-core design, involving exclusively fibres and elastomers to create a bending. It also avoids the usage of any external strain-limiting layers as used in literature to create bending [74]. Instead, the bending can be produced purely based on the stiffness difference between the two halves of the actuator. However, the adapted design from Wang et al. focussed only on using high-stiffness materials involving dirty fabrication processes and requiring high-temperature speciality ovens. Therefore, it is essential to use low Young's modulus materials in making actuators, as they can undergo larger deformation at lower pressures. This provides the possibility of utilization in the intended body-powered prostheses application where small movements available from the body are to be used in powering these actuators into performing useful tasks.

From the literature, it is also evident that it will be hard to implement the design with materials with a low stiffness range as breakage along the interface between the two materials will occur. The next few chapters will focus on the use of low-stiffness material in the construction of the actuators and improving the design to avoid breakage along the materials interface.

Chapter 4

Simulation of the actuator

4.1 Introduction

To model the behaviour of the actuators, 3D FEM models were constructed and analysed with ABAQUS/Standard (Simulia, Dassault Systems). This FEM model is to support the possibility of bending in fibre-reinforced soft elastomeric actuators, where the winding angle of the fibres results in the stiffness of the overall material. Additionally, FEM results are used to analyse if experimental results follow the same trend as the simulation model.

4.2 Finite element method

Finite element analysis (FEA) is a computerized method that can be used to predict the behaviour of soft-bending actuators to a pressure load. The FEA simulation software, such as ABAQUS®, provides a straight way to visualize the outcome of change in the parameter. It is widely used as an intuitive tool to model the proposed design. In this method, the actuator is modelled as a closed cylinder with two sections in order to apply two different stiffness on either side of the cylinder, as shown in **Figure 4.1**.

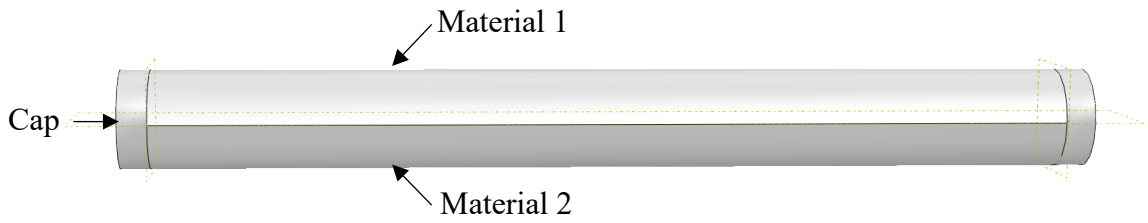

Figure 4.1 Closed cylinder with two sections for application of two different materials.

The main body's materials are modelled as mechanically elastic materials as elastomeric materials (non-linear) are used. Some other factors, such as external loading, the number and type of meshed elements, mechanical properties of materials, and boundary conditions, are all

pre-set in software before a simulation is performed. Notably, non-linear material modelling plays an important role in characterizing/modelling the proposed soft-bending actuator. Since the kinetics of this actuator is largely dependent on the elastic energy stored in soft material, the non-linearity of the material makes it challenging to build a working model to understand the behaviour of the proposed actuator.

4.2.1 Actuator model

When different modulus materials are used on each half of the actuator, significant bending can be achieved as a function of pressure. However, it is challenging to model the variable angle fibre-reinforcements and embed them in the elastomeric material to simulate the bending response. Hence, for a simplified model, Young's modulus of the composite samples made of fibres reinforced at 10° and 80° Ecoflex™ determined from chapter 3 **Table 3.1** were used to model the actuator to facilitate the bending performance.

The modelling starts by forming a hollow tube of 20 mm outer diameter and 10 mm hollow inner core as a 3D deformable solid extrusion. Two caps of 5 mm thickness were created and assembled to sit on both ends of the hollow tube. The inlet for pressurized air was not taken into account in the model, as the pressure was applied to all the internal walls of the chamber. The cylinder was partitioned into two halves along the axis to apply different materials to the top and bottom of the actuator, as shown in **Figure 4.1**. The main body of the actuator was chosen as an elastic material. Two surfaces, distinguished as inner and outer surfaces, were created. As a result, the actuator can be loaded with pressure on its internal surface. The load was set as a uniform pressure component that is distributed evenly on the inner surface of the tube, as shown in **Figure 4.2**.

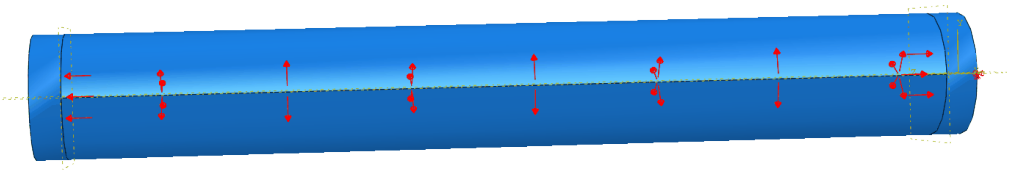

Figure 4.2 Uniform pressure load on the inner surface of the tube.

One end of the actuator was fixed using the boundary condition to visualize the bending on the other end of the actuator model, as shown in **Figure 4.3**.

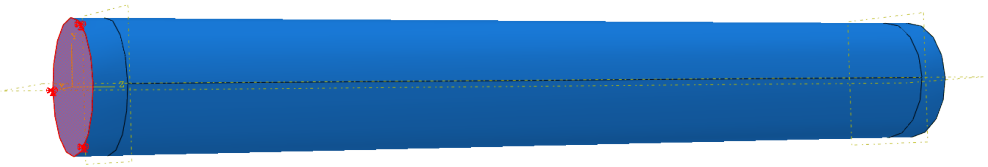

Figure 4.3 Boundary fixed on one end of the actuator.

Following the load and boundary condition, the actuator was meshed to observe the structural changes later during execution, as shown in **Figure 4.4**.

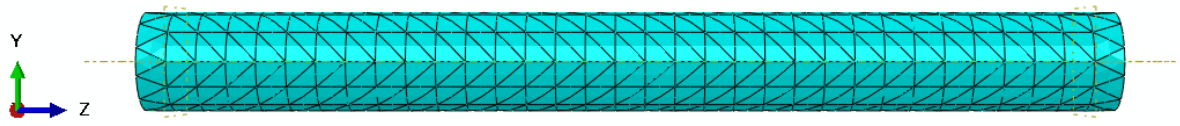

Figure 4.4 Meshed actuator model.

The model was submitted for successful compilation, and the results were observed. The bending of the actuator model is shown in **Figure 4.5**.

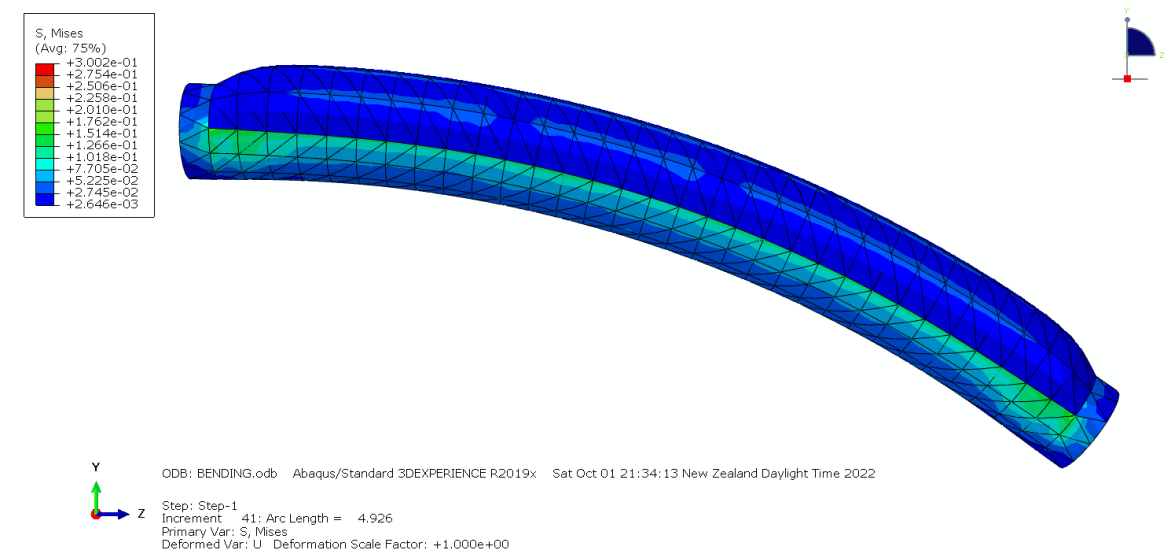

Figure 4.5 FEA actuator model's bending upon an increase in pressure load.

4.3 Results and discussion

The bending angle of the actuator model was determined for a proportional increment in input pressure load. These bending results from the FEA model were compared against the results from the numerical model calculated in chapter 3 and are plotted against pressure, as shown in **Figure 4.6.** Numerical results show higher bending angles than FEA model results as pressure is increased. This might be because some radial expansion (radial strain) seen in simulation results **(Figure 4.5**) was not taken into account in the numerical modelling of the actuator.

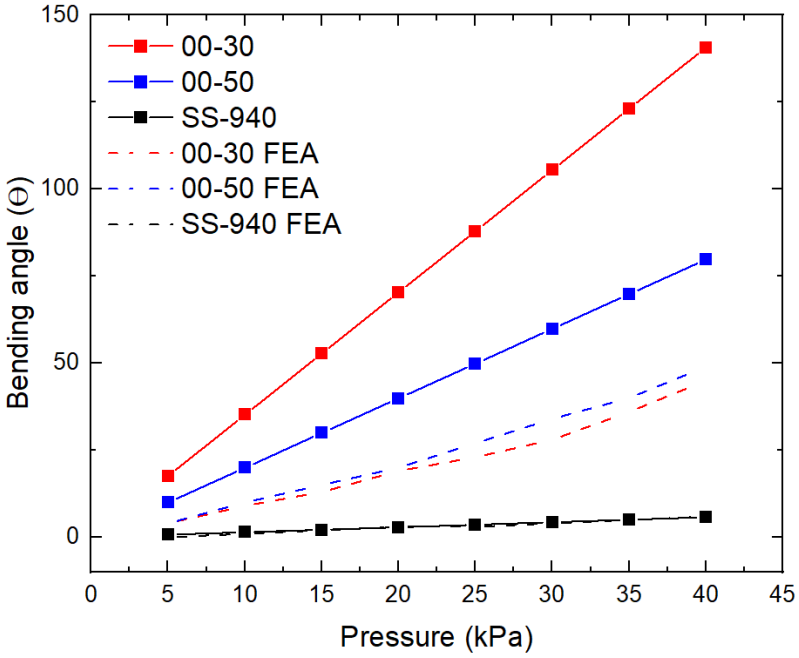

Figure 4.6 Bending angle vs pressure of FEA and numerical model for Ecoflex™ 00-30, Ecoflex™ 00-50, and Smooth Sil™ 940 actuators.

4.4 Conclusions

Soft fluidic actuators can generate complex 3D outputs at a very low mechanical cost with simple control inputs. To date, the development of such actuators has largely been an empirical process. FEA and numerical models have been used by the robotics research community for deterministically designing soft robotic systems and evaluating their performance prior to their manufacture. These FEA models provide the ability to simulate the function of the actuators and highlight local stress/strain concentrations where the pressure interacts with the elastomer and undergoes mechanical deformations. Results of the developed soft bending actuator FEA model were compared against the numerically calculated results. The findings from the modelling work were also evaluated through experimental characterizations in chapter 6, which provided a better understanding of the individual parameters that affect the performance of these soft actuators. Despite the fact that numerical and simulation results do not match, they

do prove that using materials of different stiffness with different fibre-braiding angles on different halves of the actuator can result in bending motion. Further, the stiffness of the material does affect the amount of bending. The effects of simplifying and making assumptions in addressing the numerical and simulation analysis of the actuator have been discussed in chapter 6, comparing them with experimental data.

Chapter 5

Design and fabrication

5.1 Overview

Fibre-based actuators take advantage of the fibres reinforced into a soft material matrix to create a strain gradient on the elastomeric layers to generate twisting and bending motions [18], [73], [175], [176]. Such motions can be controlled based on the fibre braiding pattern [177]. Restricting the lateral bulging by increasing the density of the fibre reinforcement has also been used to demonstrate actuators capable of undergoing linear extension under applied pressure [73]. Table 1 summarizes the most recent advances in soft pneumatic bending actuator designs (@ 80 kPa)

Table 2.1 Blocking force for some recent soft pneumatic actuators

Structure	Force (N) @80kPa
Chamber-based	0.25 [17]
Fibre-reinforced	1 [178]
	1.2 [75]
	0.5* [74]

Among these actuator designs, the research work by Wang et al., [74, 75] (marked by * in Table. 1) has demonstrated good performances but utilizing neoprene rubber for making the actuator involves vulcanization of this rubber in temperatures as high as 190°C demanding an extremely complex actuator fabrication process and a high-temperature oven. Also, these actuators operate at pressures of a few hundred kilopascals, which limits their utility in body-powered prostheses applications.

Towards addressing the drawbacks of Wang et al., [165]–[167], this chapter studies the utilization of low Young's modulus materials to facilitate bending and force generation at low pressures.

5.2 Experimental section

5.2.1 Materials

This chapter explores different fabrication techniques, and at this stage, Ecoflex™ 00-30 (Smooth-On, Macungie, PA18062)) was used because the aim is to use low Young's modulus material to reduce the actuation pressure to facilitate bending using minimum body movements. The fibre-reinforcement for the actuator was a nylon-based fibre (Kast King Superpower, Garden City, NY, 11530), as shown in **Figure 5.1**.

Figure 5.1 Braided line from Kastking.

5.2.2 Methods

This part of the chapter explains the series of steps involved in making a soft pneumatic actuator. The actuator walls are made thicker to enhance the strength and restrict bulging as much as possible. The cross-sectional dimension of the actuator is shown in **Figure 5.2.**

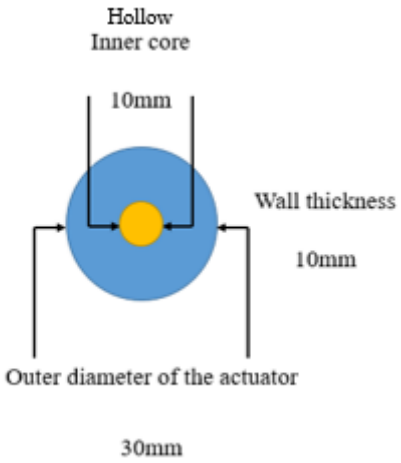

Figure 5.2 Cross-sectional dimension of the actuator.

The length of the actuator is 180 mm. Two acrylic pipes of diameter 20 mm and 30 mm were chosen to make the first layer and final layer of the actuator, respectively. These pipes were cut along the axis into two halves and taped around for easy removal of the sample, as shown in **Figure 5.3**.

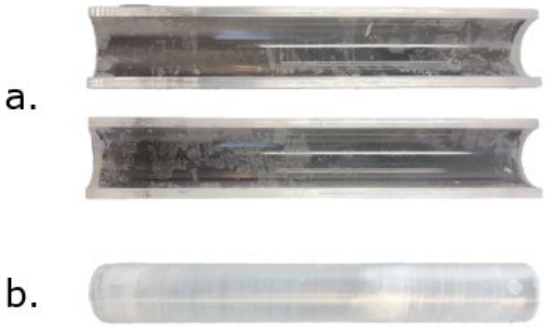

Figure 5.3 Acrylic mould (a) acrylic mould cut along the axis into two halves (b) taped around to bind the two halves together.

The fabrication of the actuator begins by using a 20 mm acrylic mould to create a single elastomeric chamber by mixing part A and part B of the Ecoflex™ 00-30 in a 1:1 weight ratio.

The liquid Ecoflex™ 00-30 was degassed in a vacuum desiccator for 10 min to remove air bubbles completely, as shown in **Figure 5.4**.

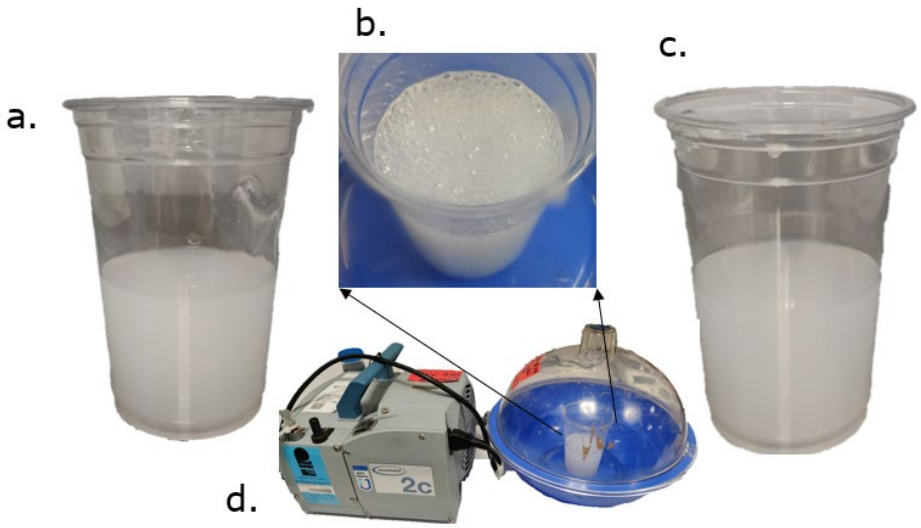

Figure 5.4 Bubble removal using vacuum desiccator (a) Mixed Ecoflex™ 00-30 Part A and Part B (b) Bubbles in the mixed solution (c) After bubbles removal (d) Vacuum pump and vacuum desiccator.

The Ecoflex™ 00-30 mixture was then poured into a cylindrical mould. All the mould and experimental set-up were assembled using appropriate 3D printed parts based on the requirement, designed using Creo Parametric software, and printed using Prusa i3 MK3S+ printer as shown in **Figure 5.5.**

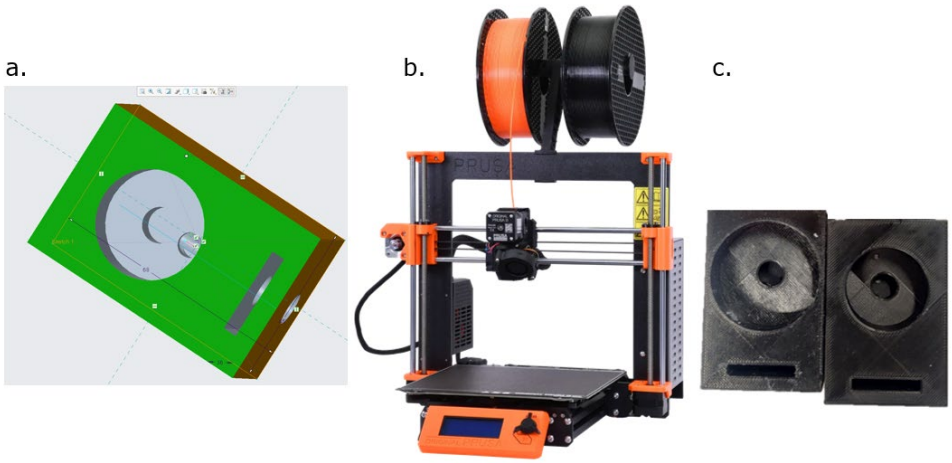

Figure 5.5 3D part designed in Creo and printed using Prusa i3 MKS3+ printer. (a) Parts drawn using Creo (b) Prusa i3 MKS3+ printer (c) 3D printed parts.

To make the cylindrical elastomeric chamber hollow, a steel rod of 10 mm diameter was concentrically inserted, forming the central core of the actuator mould. It was then cured at 50 ºC for 2 hours in a vacuum oven, as shown in **Figure 5.6**. This completes the first layer for the actuator.

Figure 5.6 Vacuum oven.

.

5.2.3 Split fibre-reinforced (SFR) bimorph bending actuator

As part of the SFR fabrication technique, fibres are braided around the first layer of elastomer to create two samples, one with a 10° angle and another with a 60° or 70° angle. Each sample was cut in half along its length, and the two different halves, one with 10° and the other with 60° or 70°, were moulded together to create a variable stiffness SFR actuator. An automatic winding process was created for accurate braiding of these angles, as shown in the following section.

5.2.3.1 Automatic fibre winding machine

To improve the precision of winding, the braiding process was automated with a custom-built precision winding machine equipped with two stepper motors, as shown in **Figure 5.7**.

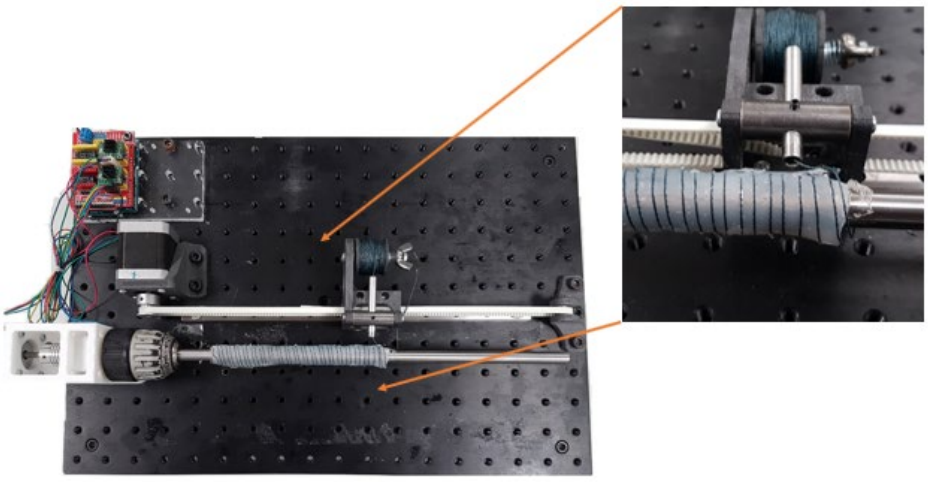

Figure 5.7 Automatic fibre winding machine with an exploded view of the spool supply.

One stepper motor drives the spindle about the axis of the elastomeric actuator, and the other motor moves the spool along the length of the spindle that feeds the fibre for braiding. The variation in the angle of the fibre braids was achieved by varying the spool feeder stepper motor's speed. This automated fibre braiding rig was connected to a PC via a MyRIO

controller, and a GUI programmed in LabVIEW™ (National Instruments Corp., Austin, Texas, USA). The input and motor control parameters programmed are shown in **Figure 5.8**.

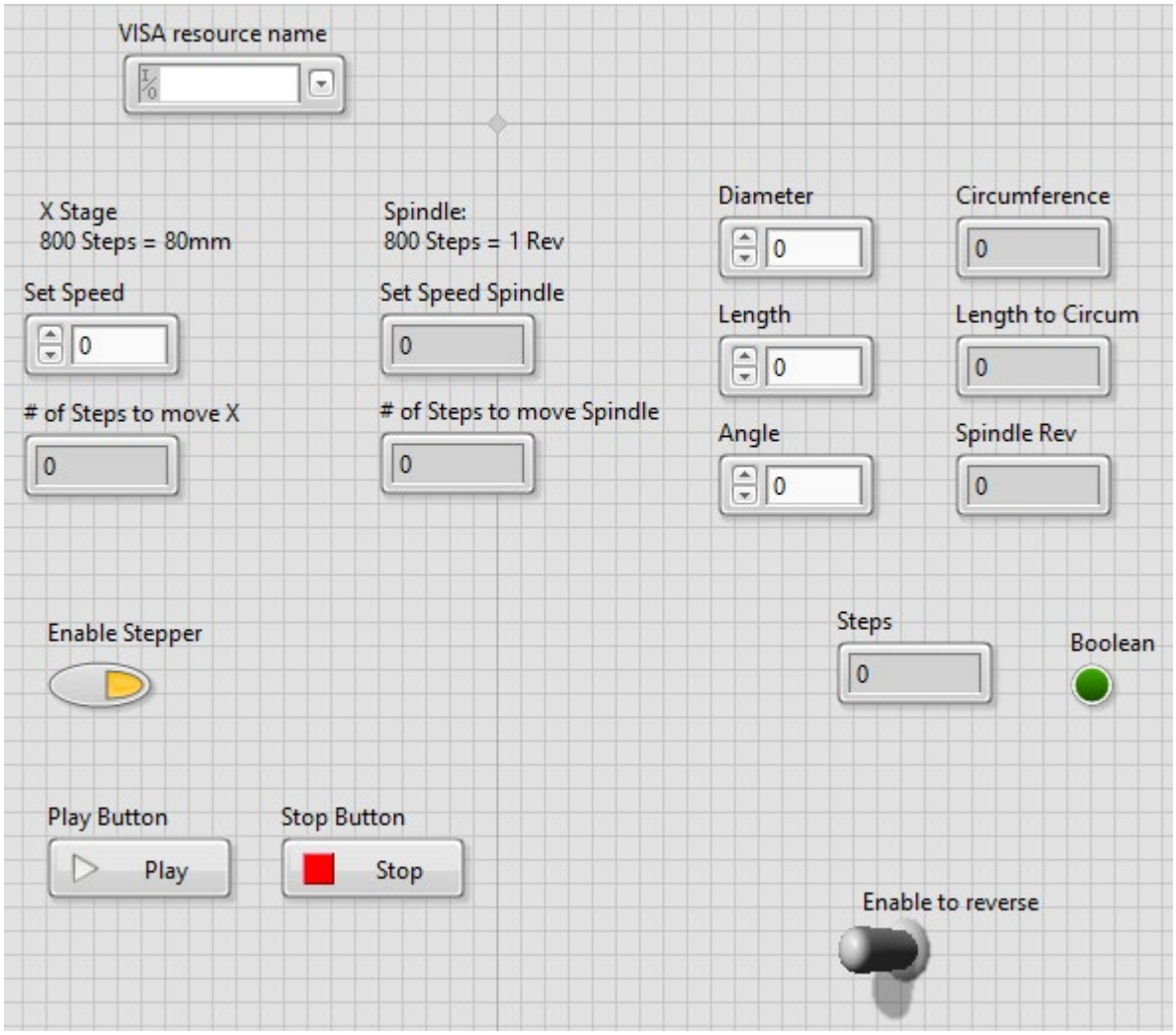

Figure 5.8 Stepper motor control for automatic fibre braiding machine

The step-by-step fabrication procedure is explained and shown in **Figure 5.9**.

Figure 5.9 Fabrication procedure of SFR actuator. (a) Steel rod (b) Fibres wound at 70°(c) Fibres wound at 10° (d) SFR actuator after winding.

Two fibre braiding angle combinations 10°/60° and 10°/70°, were chosen due to the good performance as demonstrated by previous literature [74], [171], [173]. However, this time softer material Ecoflex™ 00-30 is used instead of vulcanized rubber. After curing the first elastomer layer, reinforcing fibres were braided in a helical pattern at a precise angle. The pitch of the wound fibre was created by moving the fibre-feeding spool along the axis in the forward and reverse directions.

To keep these fibre layers in place, a thin layer of Ecoflex™ 00-30 was deposited over the fibre-reinforcement layer, thus at the same time ensuring the fibre angles remain intact even during bending actuation under the applied pressure. The fully cured fibre-reinforced elastomeric actuator was carefully removed from the actuator mould. Next, each of the fibres reinforced elastomeric bladders were cut along the length into two halves. One half with the 10^{0} fibre angle and the other half with 60^{0} or 70° fibre angle were placed around the cylindrical

steel rod with their edges aligned precisely, as shown in **Figure 5.10.** A final layer of Ecoflex™ 00-30 was coated using a mould of 30 mm diameter to form the resultant SFR actuator.

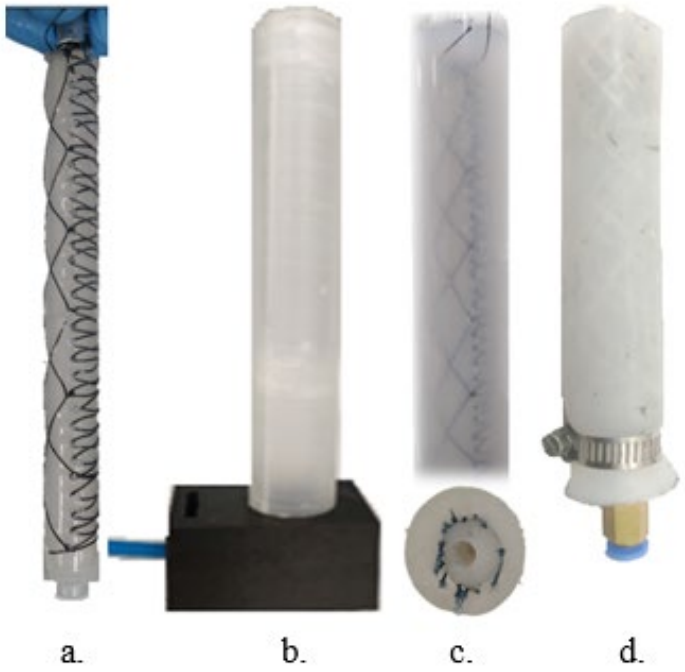

Figure 5.10 Demonstrates the coating of the final layer of Ecoflex™ 00-30 to finish SFR actuator. (a) SFR actuator before the final layer of Ecoflex™ 00-30 (b) 30 mm mould (c) Cross-sectional view of the actuator (d) SFR actuator after final layer of Ecoflex™ 00-30.

5.2.3.2 Testing set-up

All experiments on the fabricated actuators were performed with the actuator clamped vertically with the blind end at the bottom. This ensured that there was no bending bias due to the gravity effect. A compressed air source was used to power these actuators. A control system regulated the pressure to ensure the safety of the actuators. As a first step, a solenoid valve (SMC - VDW10EA, RS Components, NSW, Australia) was chosen to operate as an on-off switch. As a compact, direct-operated, 2/3 port solenoid valve, it can regulate water, air, and vacuum. Powered by a 24V supply, it can operate up to 0.9 MPa. A differential pressure sensor

MPX 5500DP from NXP Semiconductors was connected to the actuator's inlet tube to monitor the pressure inside the actuator chamber. The combination of a pressure sensor and solenoid valve provides the possibility of maintaining the desired pressure (**Figure 5.11**).

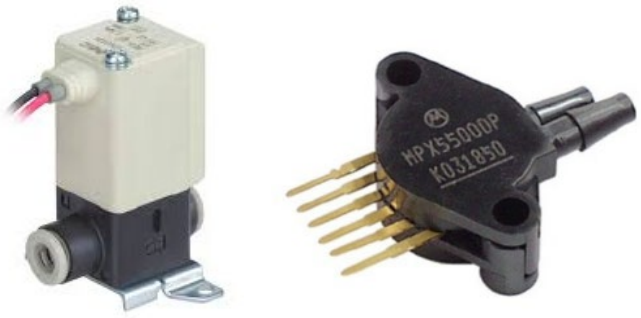

Figure 5.11 (a) Solenoid valve (SMC-VDW10EA) (b) Differential pressure sensor (MPX 5500DP).

To co-ordinate the pressure input to the solenoid actuation, a control must be established. With the help of a MyRIO from LabVIEW™, pressure data was acquired. The raw data from the pressure sensor was calibrated to zero at atmospheric pressure. The blocking force of the actuator was measured using a cantilever force sensor that has a measurement range of 0-50 N with an accuracy of 0.01N. The force sensor was calibrated using weights and made zero. A pressure with an increment of 5 kPa starting from 0 kPa was applied to the actuator, and the bending angle was measured. This process was repeated up to 80 kPa until the output of the actuator saturated. In the same manner, the force sensor was used to block the tip of the actuator, and the pressure was increased from 0 to 80 kPa. The resultant force for the input pressure was plotted in a .xlsx file. The output was also monitored live using LabVIEW, as shown in **Figure 5.12,** to stop the pressure during an emergency if the actuator becomes faulty. **Figure 5.13** shows the complete control and testing setup of the actuator.

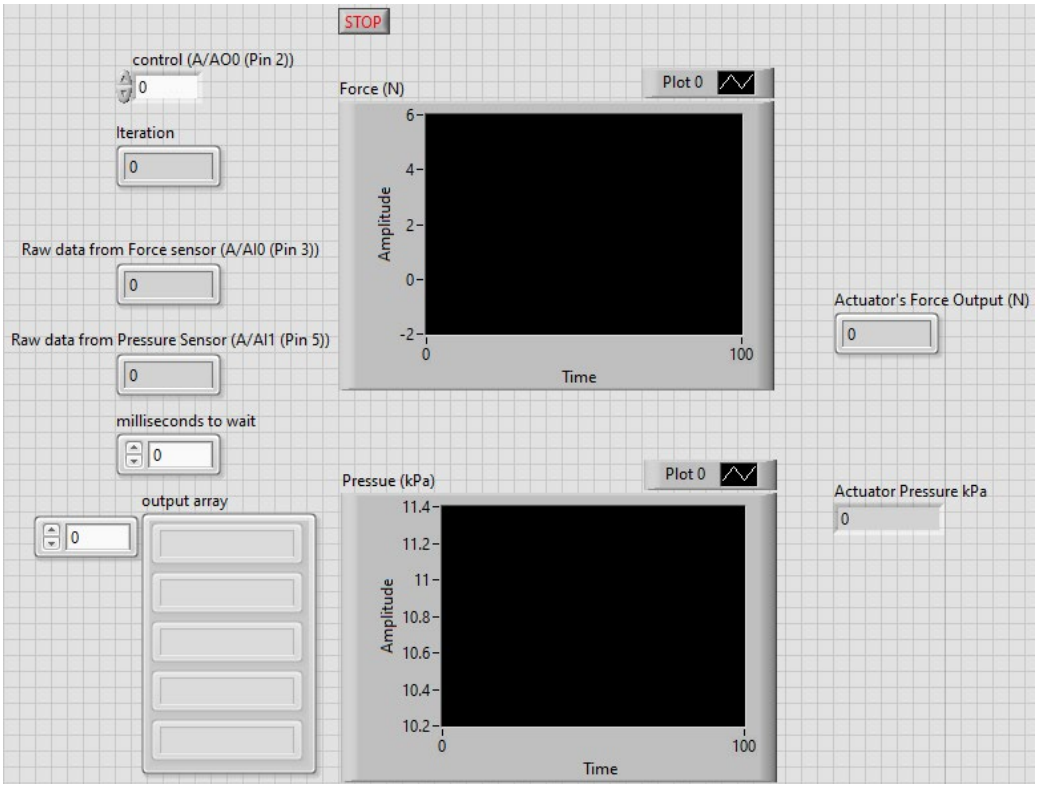

Figure 5.12 Input pressure and output force data acquisition using LabVIEW

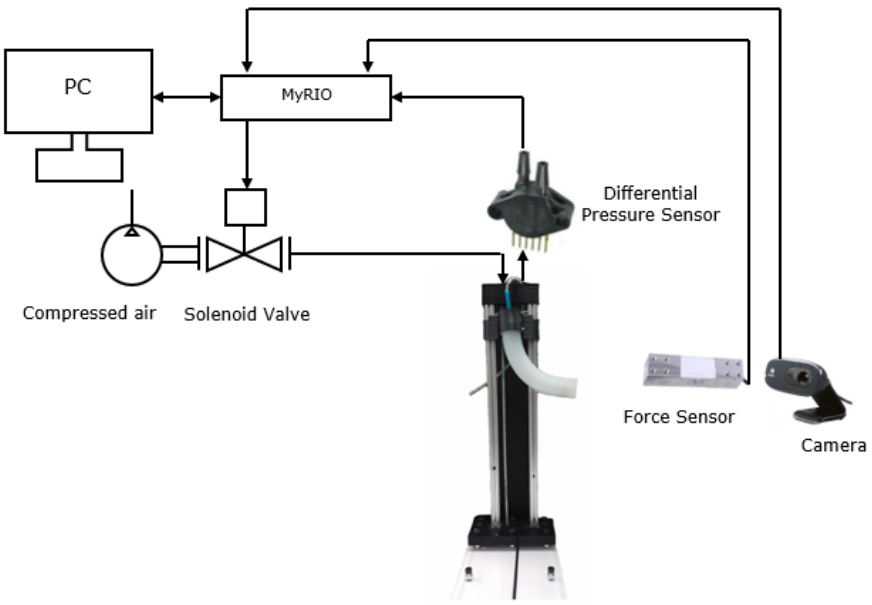

Figure 5.13 Schematic diagram of the experimental setup to measure blocking force and bending angle.

5.2.3.3 Testing observations

Mixing the elastomers may result in the formation of bubbles. If these bubbles are not removed properly, they will fail the actuator when pressurized, as shown in **Figure 5.14**.

Figure 5.14 Bubbles leading to actuator failure.

While forming the final layer of the actuator, a rubber stopper was attached to one end and then cured to form a blocked end. This prevents the stress from occurring at the tip of the actuator to prevent bulging or failure of the actuator, as shown in **Figure 5.15**.

Figure 5.15 Stress at the tip of the actuator resulting in bulging.

5.2.3.4 Preliminary results

SFR actuators made of low Young's modulus material were tested to determine bending angles and blocking forces for 10°/60° and 10°/70° braiding angle combinations with increasing input pressure. Results were compared to those of the benchmark bending actuator possessing high Young's modulus material. [74].

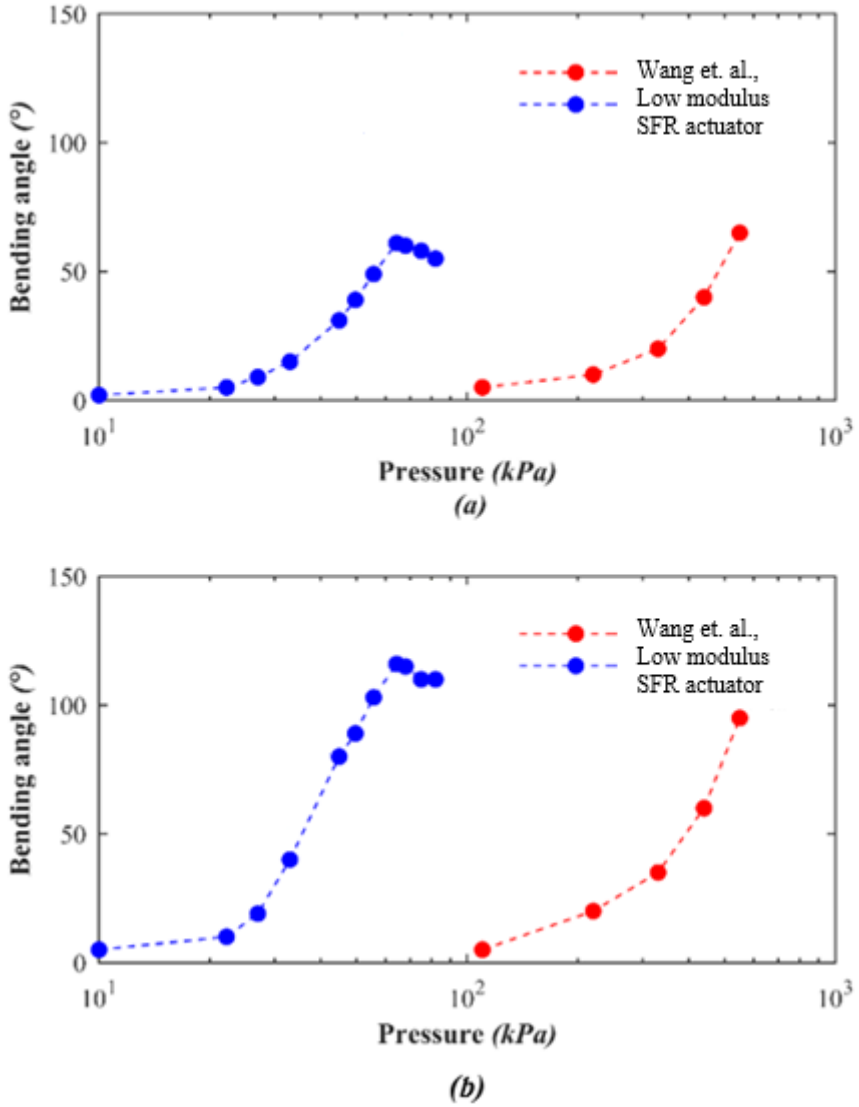

Figure 5.16 The bending angle for (a) 10°/60° (b) and 10°/70°. Braiding angle combination for SFR actuator against the benchmark actuator.

From **Figures 5.16 and 5.17**, it can be observed that actuators made from low-modulus material have significantly increased bending angles at much lower pressure levels as compared to the benchmark actuator. It is possible to achieve bending angles of 110° with pressure as low as 80kPa for a 10°/70° braiding combination actuator, whereas the benchmark actuator produces virtually no bending at such pressure [74].

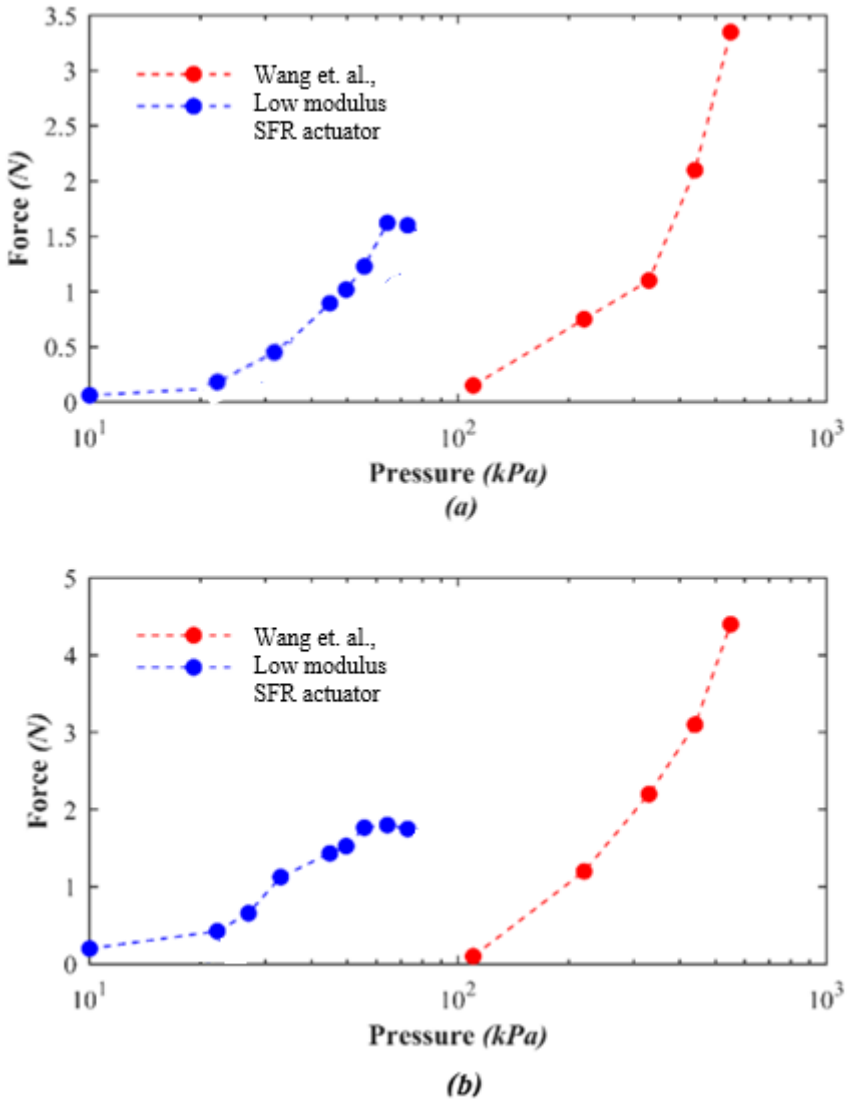

Figure 5.17 The blocking force for (a) 10°/60° and (b)10°/70°. Braiding angle combination for SFR actuator against the benchmark actuator.

The SFR actuator shows a continuous increase in blocking up to an input pressure of 60 kPa, whereas no significant force was generated by the benchmark actuator at that pressure. However, the blocking force stops increasing in the low-modulus SFR actuator after 60 kPa. This is due to the significant bulging at the joint between the two halves of the fibre braiding samples attached during the fabrication process. At pressures above 80kPa, delamination occurs and the bulging of SFR actuator maximises, as shown in **Figure 5.18**.

Figure 5.18 Bulging in SFR actuator at pressure above 80 kPa.

To resolve this, an improved fabrication technique has to be developed to eliminate the bulging at a higher pressure and improve the lifetime of the actuator while still achieving higher bending angles at relatively lower input pressures. This was made possible by using unique fabrication techniques, named continuous fibre-reinforcement technique (CFR), that can eliminate the problem faced in the SFR-based actuator, as explained in the following section.

5.2.4 Continuous fibre-reinforcement (CFR) varying angle bending actuator

This part of the chapter demonstrates a new fibre braiding process to prevent the breakage of actuators at the borderline by using CFR technique. This technique is explained in a series of

steps below. Firstly, an aluminium rod was taken, and holes were drilled every 1 mm using a mill, as shown in **Figure 5.19**. Next, 1mm guiding holes were inserted into the aluminium rod, as shown in **Figure 5.20.**

Figure 5.19 Drilling 1mm holes on the aluminium rod using a mill.

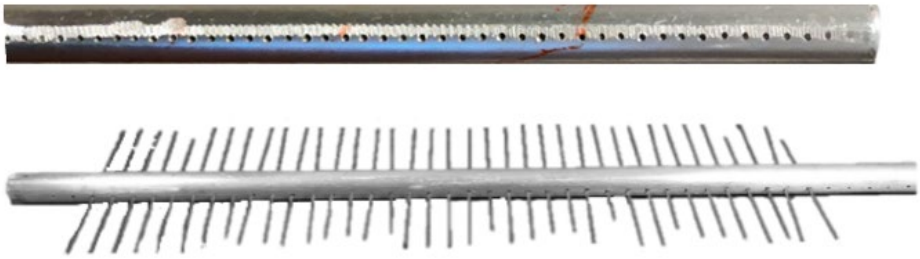

Figure 5.20 Aluminium rods with guiding pins for CFR actuator braiding.

Like the SFR actuator, the first layer of Ecoflex™ 00-30 is formed around the aluminium rod. Guiding pins of 1 mm diameter were inserted along the length of the rod. Then the fibre was wound on one half of the rod at one angle, and a loop was made around the guiding pin. The braiding was continued on the other half of the rod at another angle, creating a varying angle fibre on both sides of the actuator. Once the fibre wound around the guiding pins, the second layer of Ecoflex™ 00-30 was applied to hold the fibre in place and cured in the oven at 50°C for 2 hrs. The guiding pins were then removed, and the holes were sealed using Ecoflex™ 00-30, as shown in **Figure 5.21**.

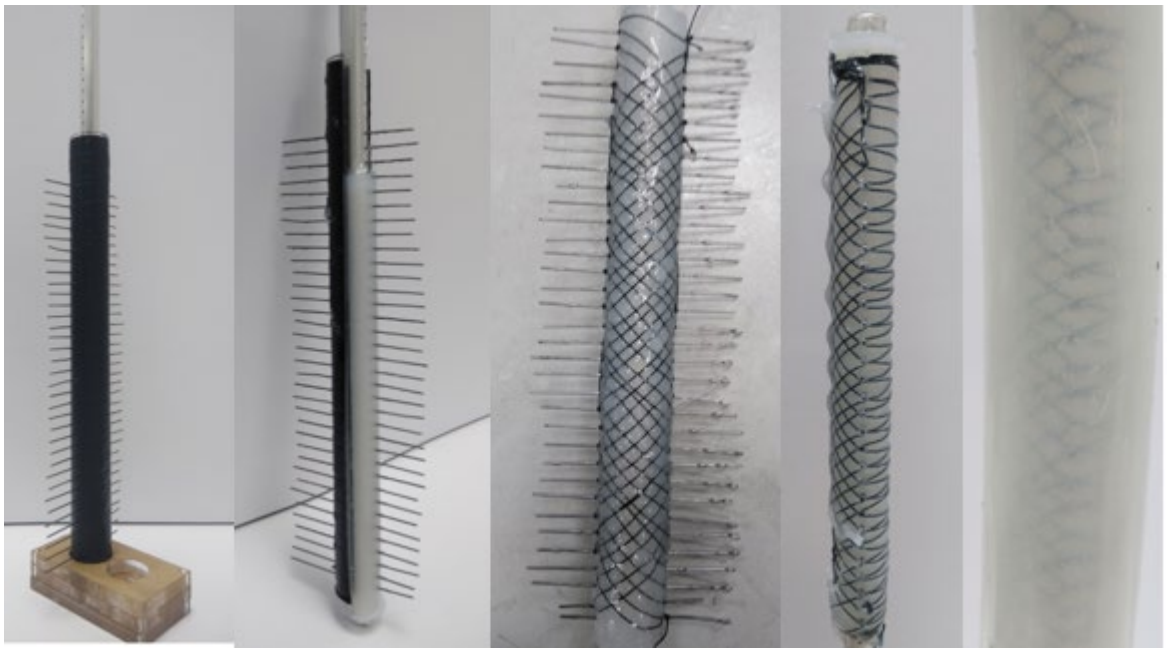

Figure 5.21 Fabrication of a CFR actuator.

For a secure leak-proof connection to an air compressor, a pneumatic pipefitting was fitted to the open end of the actuator, and Ecoflex™ 00-30 was applied to secure this fitting to the actuator and allowed to cure. To securely integrate the varying angle fibre-reinforced elastomer chamber to the top and bottom ends, the entire setup was placed into an acrylic cylindrical mould of 30 mm inner diameter, and Ecoflex™ 00-30 was poured to create a solid sealing layer

with a wall thickness of 10 mm. The final assembly was allowed to cure for 2 hours in an oven at 50° C.

5.3 Results and discussion

Tests were conducted on the bending actuators made from CFR techniques to determine bending angle and blocking forces at different input air pressure. The test results were compared against the low-modulus SFR actuators and the benchmark bending actuator presented by Wang et al. [74], [171], [173]. The bending angles and the blocking force responses for actuators fabricated by SFR and CFR techniques with 10°/60° and 10°/70° braiding angles were plotted against input pressure and compared with the benchmark bending actuator [74].

From **Figures 5.22 and 5.23**, it can be observed that actuators made by SFR, and CFR techniques have significantly increased bending angles at much lower pressure levels as compared to the benchmark actuator. Using CFR technique, bending angles as high as 145° were achieved with a very low input pressure of 80kPa, with barely less than 10 % achieved at similar operating pressures [74]. Furthermore, the bending angles of the CFR actuator design were much higher than that achieved using the SFR actuator fabrication technique at similar input pressure levels, with the actuators having a braiding angle of 10°/70° outperforming the bending characteristics compared to 10°/60°.

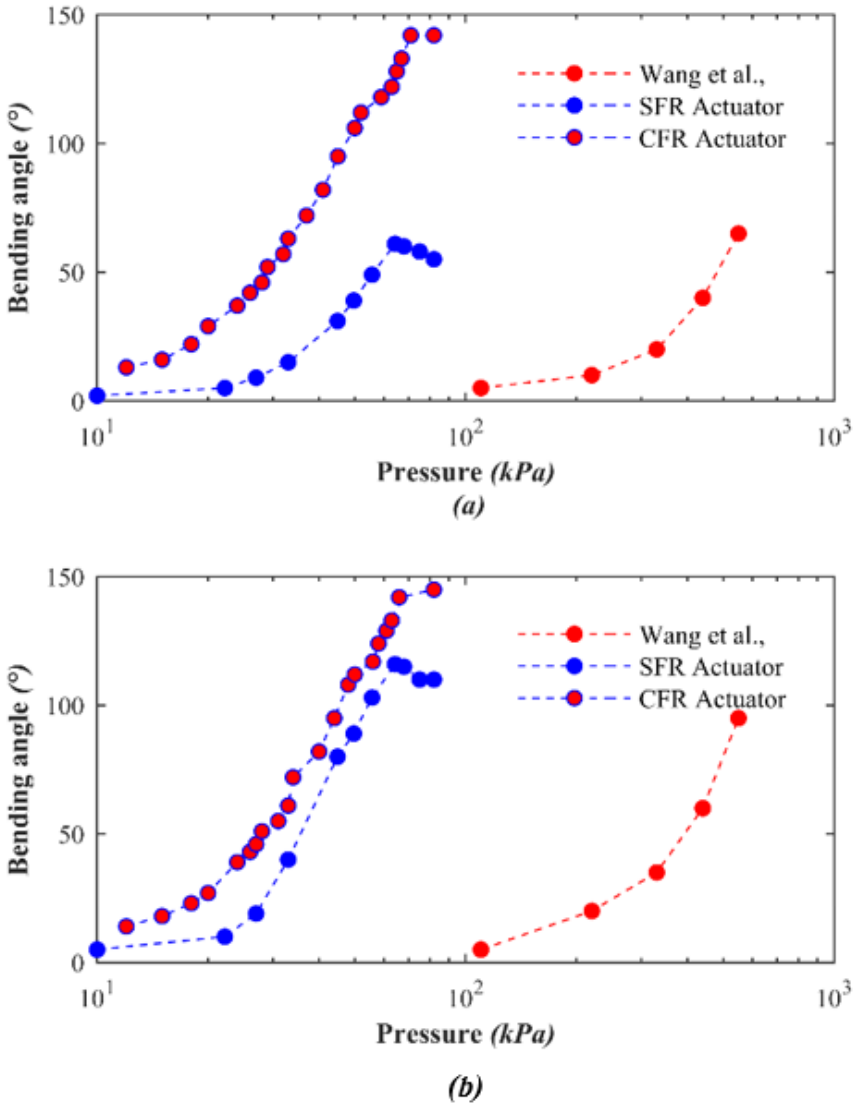

Figure 5.22 The bending angle for (a) 10°/60° (b) and 10°/70°. Braiding angle combination for both SFR and CFR actuators against the benchmark actuator.

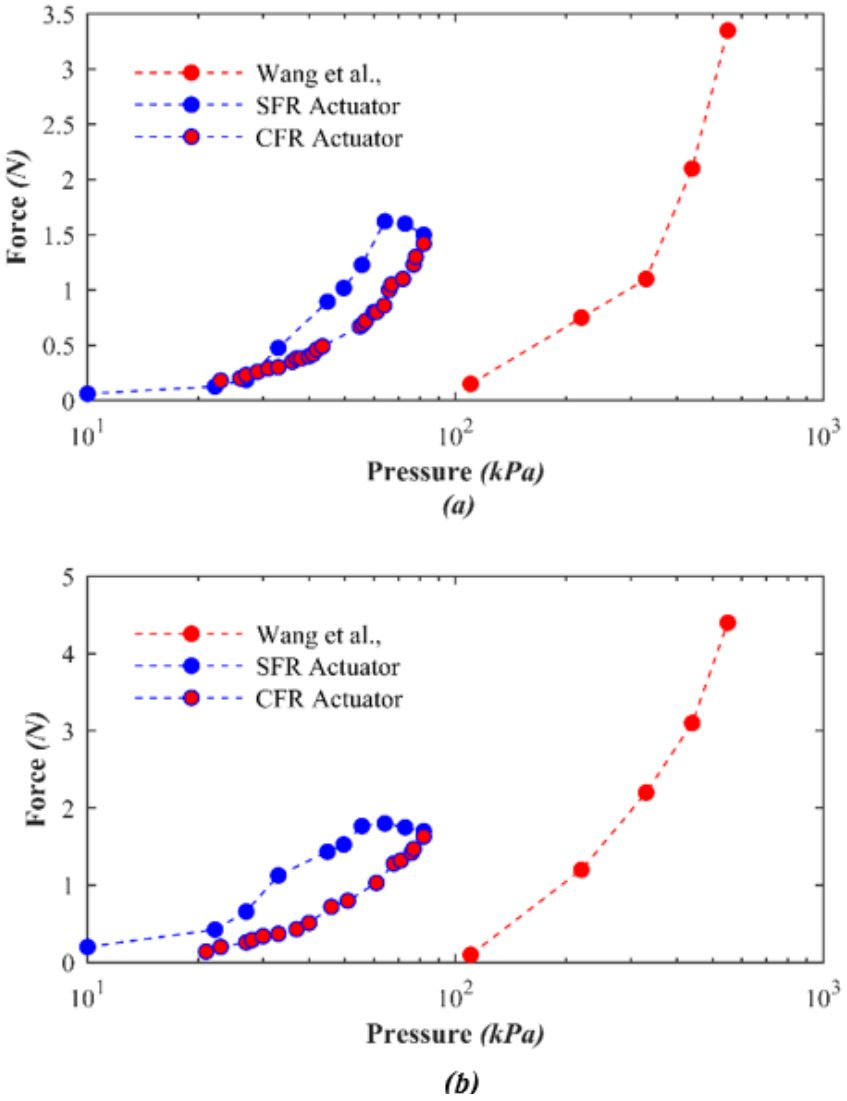

Figure 5.23 The blocking force for (a) 10°/60° and (b)10°/70°. Braiding angle combination for both SFR and CFR actuators against the benchmark actuator.

CFR suffers little bulging as it was constructed with a single continuous fibre. **Figure 5.22** shows the performance of the CFR actuator at various input pressures. Also, it is evident that the CFR actuator demonstrated a continuous increase in blocking force when the input pressure is increased. At 80 kPa, the blocking force of 1.5N is achieved, which is barely less than 30 % of the pressure used in the benchmark actuator [74].

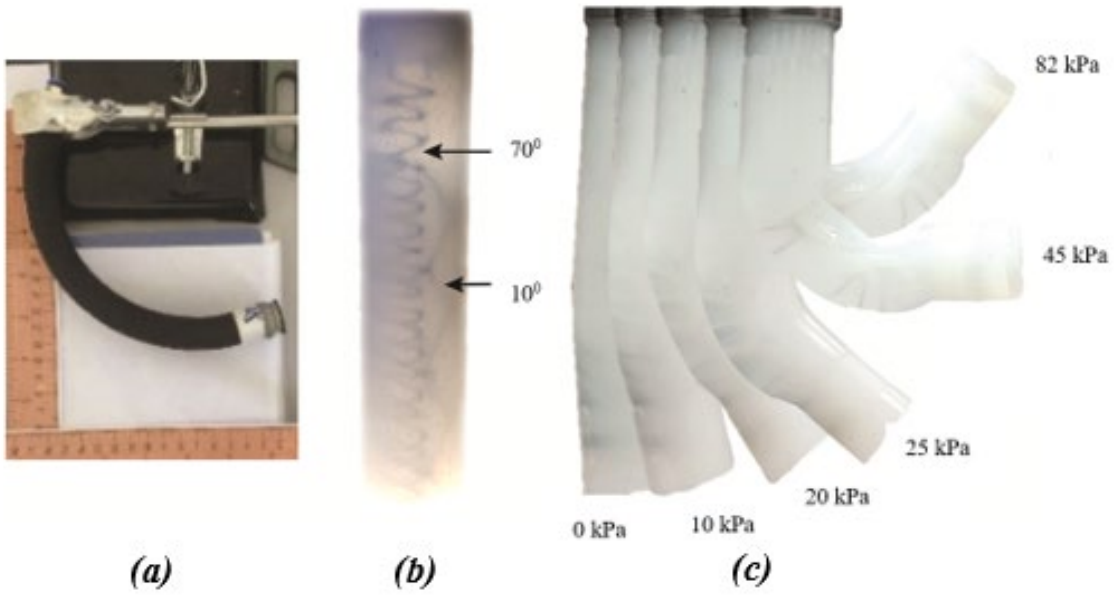

Figure 5.24 Experimental bending profile. (a) for 450kPa achieved by Wang et al., (b) The varying angle fibre-reinforced bending actuator, with fibres braided at 10°/70°, and (c) the CFR actuator at various input pressures.

5.4 Summary

The performance of fibre-reinforced soft bending actuators made from CFR techniques using Ecoflex™ 00-30 braided with different angles has been demonstrated here. The fabrication technique using Ecoflex™ 00-30 with CFR technique involved less complex fabrication compared to SFR.

The results have demonstrated that CFR actuators achieve high bending angles at low-pressure levels, with a linear bending rate of 1.77°/kPa. In comparison with the SFR actuator, the CFR actuator performs better due to its construction technique that significantly reduces delamination, as well as restricting the bulging that occurs in the SFR actuator.

By utilizing a varying angle fibre reinforced with low stiffness elastomeric material in bending actuator design and CFR fabrication technique, its ability to achieve higher bending angles than

those fabricated using the SFR technique was demonstrated. These actuators are highly suitable for applications demanding high bending angles with low input pressures. Experiments with different material properties are to be studied in the following chapter, and the results are to be compared with the previously determined numerical and FEA models.

Chapter 6

Experiments based on different elastomers and fluids

6.1 Introduction

The design of soft elastomeric actuators with appropriately reinforced fibres will result in a more controllable actuation and output force with low input pressure. In addition, by integrating these soft elastomeric actuators that can operate at a lower input pressure range, they can be easily powered by simple body movements that enhance the portability and minimize the complication in the design of a prosthetic arm. Simple, ready-to-wear, lightweight, and easy-to-handle devices are always desirable to users. Hence, developing a simpler and easier actuation method for elastomeric actuators would be greatly beneficial for grasping and gripping applications.

Here, this chapter presents the bending performance and blocking force output of elastomeric actuators made from different Young's modulus materials. Additionally, a syringe-powered bending actuator was studied to calculate the difference in pressure output from the syringe, when prefilled with different fluids like air and water.

6.2 Experimental section

6.2.1 Materials and preparation

This study uses actuators fabricated using CFR technique. Here, a 250 mm long hollow aluminium rod (10 mm ⌀) was coated with a thin layer of elastomeric material during fabrication. Later, fibres were braided over 60 mm long steel guiding pins (1 mm ⌀), which were cross-sectionally inserted into the aluminium rod. The commercially available 0.4 mm diameter Kast King Superpower braided fishing line with a breaking load of 227 N was used to create a braiding fibre in the actuator. Commercially available elastomers that offered different elastic moduli were chosen, including Ecoflex™ 00-30, Ecoflex™ 00-50, and Smooth

Sil™ 940. The Young's moduli of these three materials were experimentally determined using an Instron machine with a 30 kN load cell using the samples made based on ASTM D638 standard, as shown in **Figure 6.1**. The results are shown in **Table 6.1**.

Figure 6.1 ASTM D638 standard sample.

Table 6.1 Mechanical properties of different materials

Material	**Experimental Young's modulus (MPa)**
Ecoflex™ 00-30	0.15
Ecoflex™ 00-50	0.21
Smooth Sil™ 940	0.90

6.2.2 Fabrication of the fibre-reinforced elastomeric actuator

The fabrication started by coating a thin layer of one of the elastomer materials (Ecoflex™ 00-30, Ecoflex™ 00-50, or Smooth Sil™ 940) on an aluminium rod, as shown in **Figure 6.2a**. The assembly was degassed in a vacuum chamber to remove the extra bubbles formed during mixing. The mixing ratio and curing time were followed as per the procedure described for the elastomer. Once cured, the steel guiding pins were inserted every 2 mm along the length of the rod, as shown in **Figure 6.2b**. Two different braiding angles on either half were made by running the fibre around the guiding pins. 10°/80° was chosen as the braiding angle combination for the soft actuator because it produced the maximum bending displacement and blocking force [74]. The braiding started at 10° on one side of the rod and 80° on the other side

of the rod, and the braiding was repeated until the rod was completed, as shown in **Figure 6.2c**. As the next step, the elastomer mix was applied to the fibres to keep them intact, holding the braid in place. Once cured, the guiding pins were removed, and the holes created by the pins were sealed by using the elastomer **(Figure 6.2d)**.

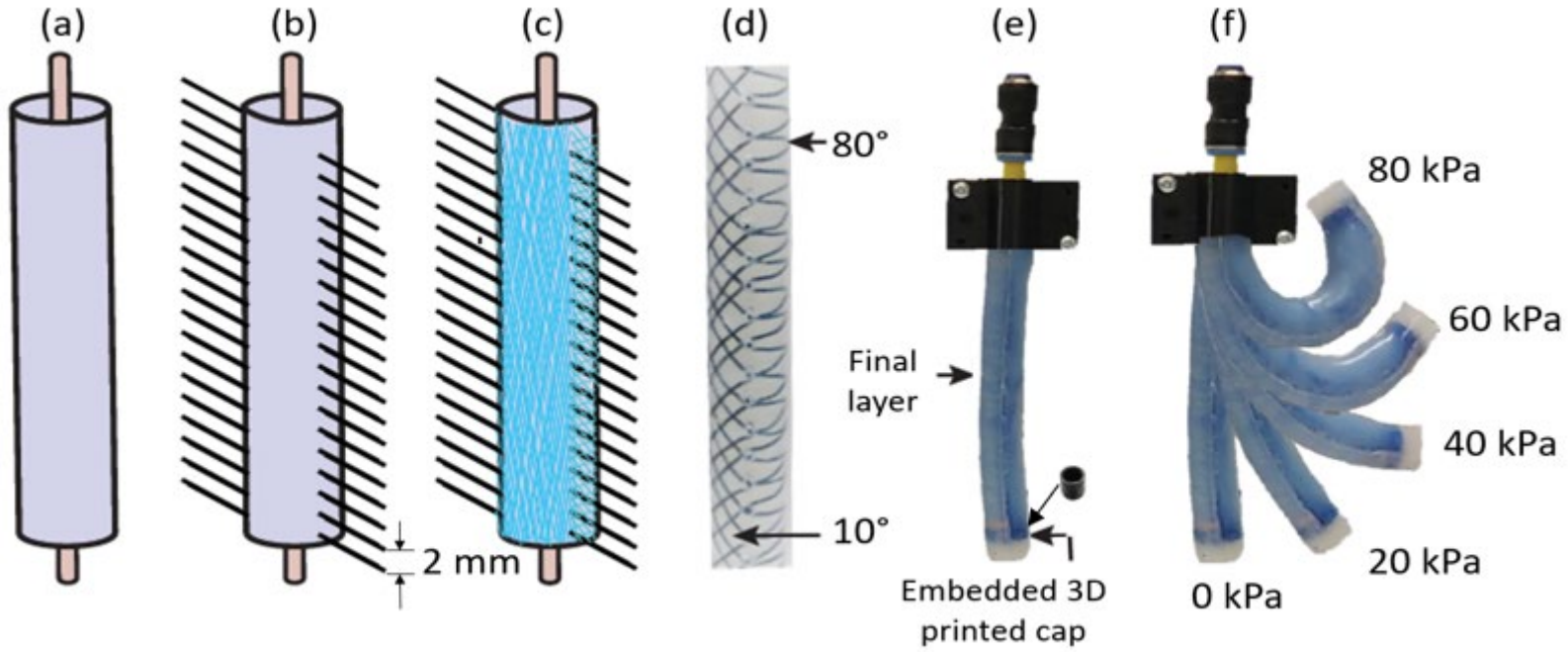

Figure 6.2 Schematic illustration of the fabrication process 10°/80° CFR actuator. (a) Pouring the elastomer mix into an acrylic mould with a supporting rod in the centre to form the first layer of elastomer, (b) inserting the guiding pins at a distance of 2 mm apart onto the cured elastomer, and (c) braiding the fibre at an angle of 10° on one side and 80° on the other side around the guiding pins; (d) photograph of the fibre-braided elastomer with the braiding angle combination of 10°/80°; (e) photograph of a complete actuator attached to actuation tubing with a final protective layer coated on the fibre-braided elastomer with an embedded cap at the tip; (f) bending profile of the actuator at various input pressures.

A 3D-printed end-cap was attached to the tip of the actuator to block one end of the actuator. A silicon pipe was fitted to the other end of the actuator using a Sil-poxy silicon adhesive to secure a leakproof pneumatic connection between the actuator and the power source (**Figure 6.2e**). To enhance the strength, the actuator was placed in a cylindrical acrylic mould of 20 mm diameter and filled with the elastomer to create an additional outer layer of elastomer. Pouring the elastomer mix from the top of the mould might trap the air bubbles inside them. To avoid this, an injection moulding device was designed (**Figure 6.3)**.

Figure 6.3 Injection moulding device to create a bubble-free actuator.

The handle at the end of the device is rotated, and the device will convert the rotational motion into translational motion. A syringe plunger set-up filled with elastomer mix was coupled to this device. This device helped to push the bubbles to the top of the mould and create a bubble-free actuator. **Figure 6.2f** shows the bending response of the fibre-reinforced soft elastomeric actuator at different pressures.

6.2.3 Testing set-up

6.2.3.1 Motion tracking

An optical signal processing method using a USB camera was used in motion tracking of the bending actuator. The images were acquired in real-time by the USB camera with the help of LabVIEW and myRIO. Configuring the image acquisition system is important to obtain quality

images with high contrast and to suppress distracting background features that complicate subsequent software processing. The logic scheme for the proposed tracking method is presented in the following flow chart (**Figure 6.4**).

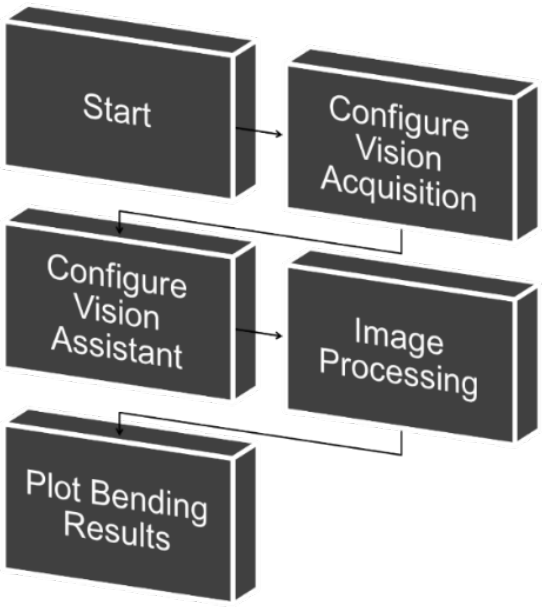

Figure 6.4 Bending angle measurement using vision acquisition.

Vision Acquisition Software, once installed, the main application can call the Vision Acquisition.vi subroutine, which can acquire, save and display the images from the camera connected to the computer in real-time. The configuration of this subroutine presumes to pass off some steps in which the acquisition method is selected finite or continuous, with in-line or post-processing the images. The configuration implies the selection of the parameters along the image: resolution (implies the refresh rate), brightness, contrast, and sharpness. These elements can be introduced into the main program as variables, so they can be modified in real-time. Vision Assistant.vi subroutine permits to process of the images acquired by the camera using a large variety of programming technologies. For measuring the vertical and horizontal motion, colour pattern matching technology is used. The application follows the movement of a colour

pattern (**Figure 6.5)**. The colour patterns indicated in red and black are detected as co-ordinates in 3d-space by the vision assistant, as shown in **Figure 6.6**.

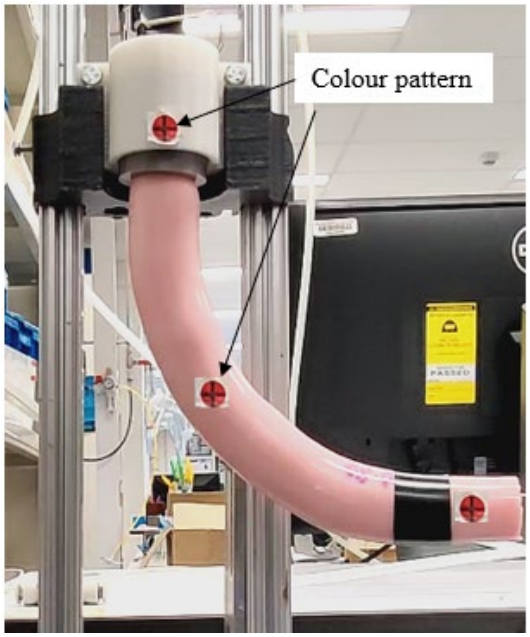

Figure 6.5 Actuator with colour pattern for co-ordinates tracking.

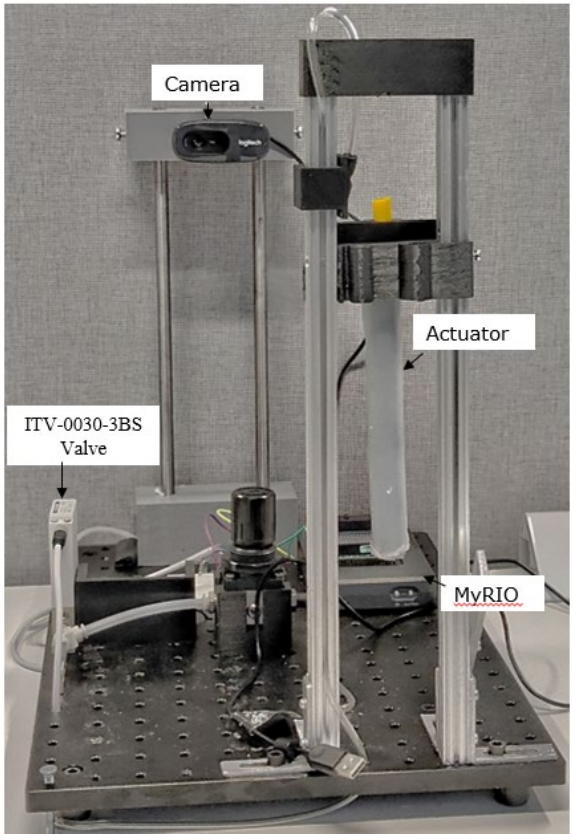

Figure 6.6 Camera in-position to acquire an image for co-ordinates detection.

Figure 6.7 shows the vision acquisition and vision assistant parameters used in acquiring the bending co-ordinates of the actuator. The refresh rate is essential because it will determine the reconstruction of the elements' trajectories. For an image with a continuity effect, a refresh rate with a minimum of 25 fps is necessary. The attributes which can be modified using this technology are the followings: the number of matches, minimum score, colour sensitivity, searching strategy, the possibility of searching rotated patterns, etc. The source code of the main application is presented in the appendix. The continuous acquisition with inline processing is permitted using a While loop.

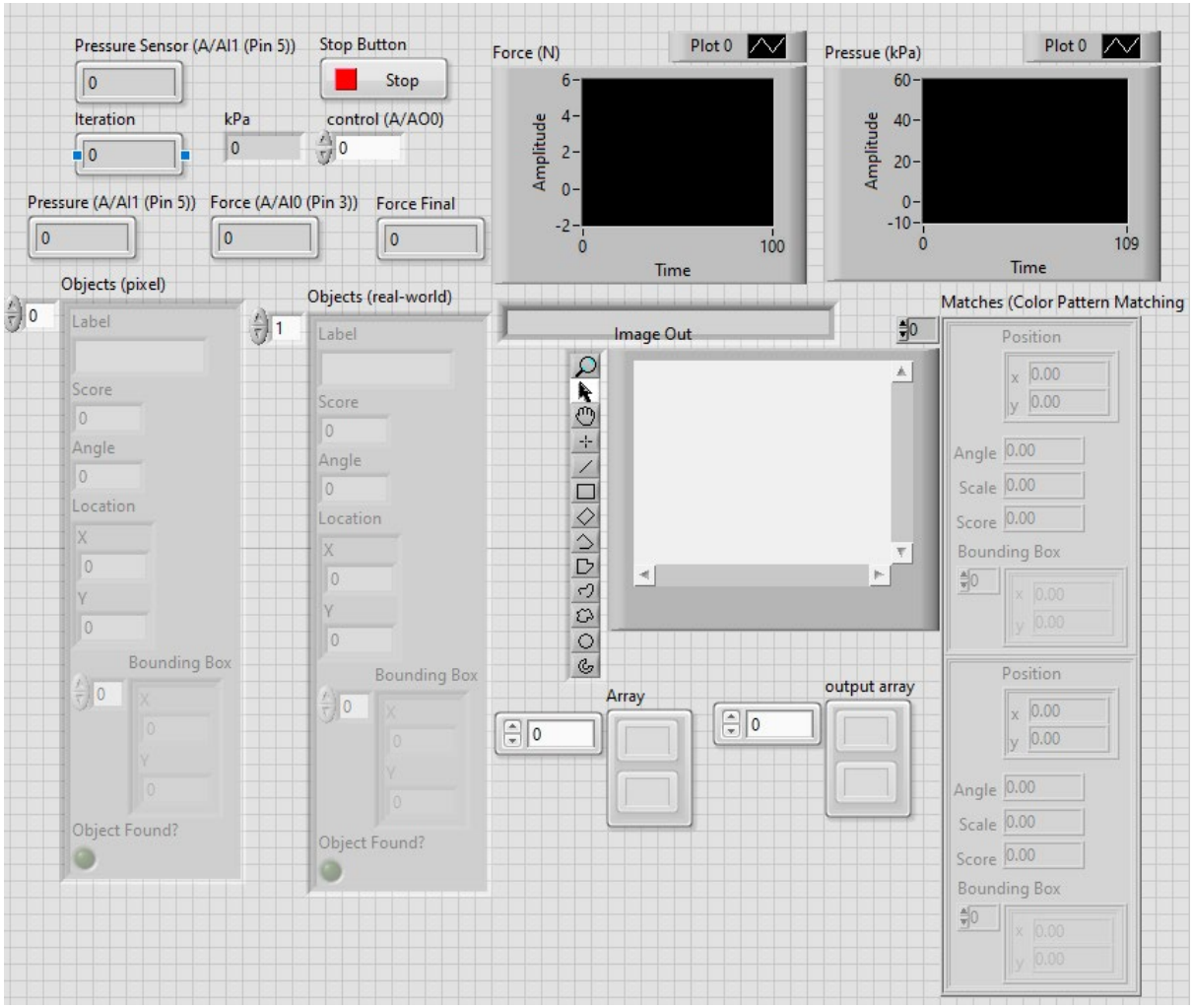

Figure 6.7 Vision acquisition using vision assistant in LabVIEW.

The information contains the templates, which must be optically tracked and flows into a cluster form. The coordinates of the centres of the markers form a vector which is written into an Excel file with the saving folder path and the file name, as shown in **Figure 6.8**. These recorded coordinates were used to obtain the bending angle relative to its equilibrium state (vertical position, 0°).

	A	B	C	D	F	G	H	I
1	Date	Time	Iteration	Pin	X0	Y0	X1	Y1
2	07/28/20	12:31:00 AM	169	199	96	48	197	471
3	07/28/20	12:31:01 AM	170	200	96	48	197	471
4	07/28/20	12:31:02 AM	171	199	96	48	197	471
5	07/28/20	12:31:03 AM	172	208	96	48	198	471
6	07/28/20	12:31:04 AM	173	215	96	48	199	470
7	07/28/20	12:31:05 AM	174	209	96	48	200	470
8	07/28/20	12:31:06 AM	175	209	96	48	200	470
9	07/28/20	12:31:07 AM	176	208	96	48	201	470
10	07/28/20	12:31:08 AM	177	210	96	48	201	470
11	07/28/20	12:31:09 AM	178	218	96	48	202	469
12	07/28/20	12:31:10 AM	179	218	96	48	204	468
13	07/28/20	12:31:11 AM	180	219	96	48	205	468
14	07/28/20	12:31:12 AM	181	217	96	48	208	467

Figure 6.8 Co-ordinates automatically registered in Excel file.

6.2.3.2 Bending and force testing setup

As the aim was to actuate the actuator using body movement, hence a plastic syringe was used instead of a compressed air supply to pressurize the fluid. Hence, a characterization of the amount of force and displacement required by the plunger to bend the actuator was conducted. The fabricated bending actuators had a 20 mm outer diameter with an 8 mm hollow inner core and a length of 150 mm. These actuators were clamped to a holder that allowed the actuator to hang in a vertical direction with the inlet at the top. The injection moulding set-up mentioned in the earlier section of this chapter was operated manually since it was only used for pumping the elastomer into the mould, which doesn't require any gradual increasing time frame.

Whereas it has to be automated when pumping air or water to record the actuator's bending or force performance. A linear motor was attached to the end of the injection moulding device to rotate the shaft which in turn pushes the syringe's plunger, as shown in **Figure 6.9**. The force measurement here was performed by using an aluminium alloy load cell from Top Sensor Technology Co., Ltd and controlled using a Phidget bridge, as shown in **Figure 6.10.**

Figure 6.9 Automatic shaft driving system.

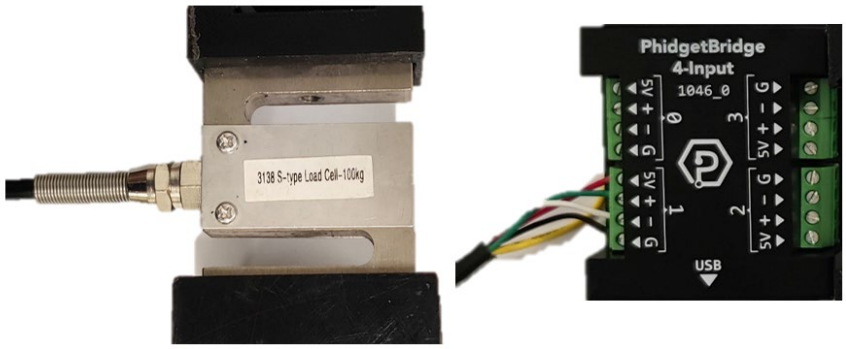

Figure 6.10 Force sensor and 4-input Phidget controller.

For all the experiments below, the pressure control voltage is transmitted through the myRIO 1900 (National Instruments, Texas) regulating proportional valve to inflate the actuator (ITV-0030-3BS, SMC, Noblesville, IN, USA), as shown in **Figure 6.11**.

Figure 6.11 ITV-0030-3BS pressure detection and fluidic control valve.

Characterizations were conducted with the system pre-filled with air or water as a working fluid. As the plunger was pushed, it pressurized the actuator, causing it to bend or curl upwards (**Figure 6.12a**). A camera was installed to track and record the bending of the actuator, and images were processed to obtain the bending angle relative to its equilibrium state (vertical position, 0°). In addition, a force sensor was attached to the plunger to measure the amount of force applied for actuation. This force, combined with the area of the plunger, could be converted into the pressure that was built up in the elastomeric actuators. For the measurement of the blocking force by the actuator, a second force sensor was attached to the rig close to the tip of the actuator (**Figure 6.12b**). Data acquired by these force sensors were read through myRIO using LabVIEW 2019 (National Instruments, Austin, TX, USA).

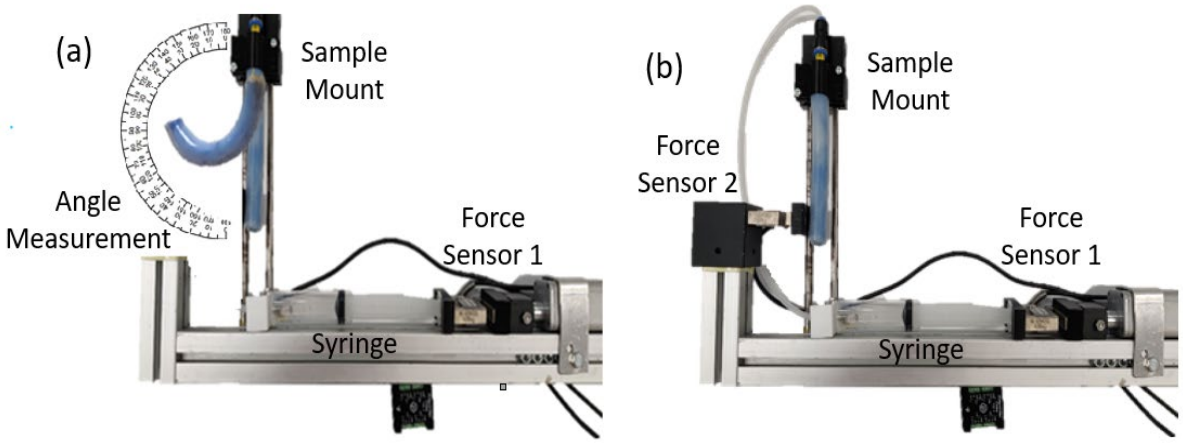

Figure 6.12 Testing setup for evaluating the performance of the fibre-reinforced actuators. (a) Photograph showing the bending of the actuator from rest (vertical position). The bending angle was then obtained objectively using goniometric measurements. (b) Photograph showing the blocking force analysis of the actuator, where the pressure was built up by pushing the plunger of the syringe.

6.3 Verification of bending characteristics

The bending angle vs pressure data obtained from numerical analysis, finite element model and through experiments for all three materials was compared against each other in **Figure 6.13**.

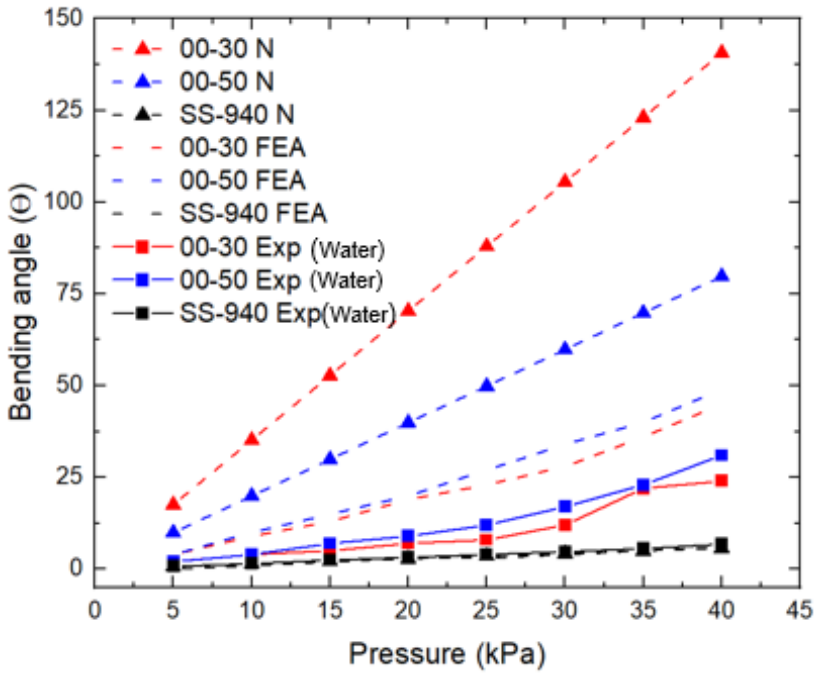

Figure 6.13 Bending angle comparison of numerical (N), simulation (FEA), and experiment results (Exp).

Figure 6.13 shows that the FEA results are closer to the experimental results that were determined numerically as the FEA does account for some radial strain. However, in real life

(experiment), the radial strain in the form of bulging is higher in Ecoflex 00-30 and 00-50 and leads to more departure between FEA and experimental results. The FEA and experimental results for Smooth-Sil 940 are a good match due to its higher modulus and negligible radial strain.

6.4 Results and discussion

6.4.1 Force characteristics

When air or water pressure is applied to this soft actuator, a force is generated along the inner curve of the actuator. The strain gauge measures the blocking force generated by the actuators made from Ecoflex™ 00-30, Ecoflex™ 00-50, and Smooth Sil™ 940. The force blocked by the actuators was measured as the pressure was increased up to 76 kPa, as shown in **Figure 6.14**. It was noted that there was a gradual increase in the force with input pressure at first, followed by a larger rate of increase. This was because the braided fibre was relaxed in the beginning and started to tighten when pressurized by extending slightly, causing radial stress. Once the stretching limit was exceeded, the fibres were inextensible, and the blocked force increased at a greater rate with pressure. At an air pressure of 76 kPa, the forces recorded by the Ecoflex™ 00-30, Ecoflex™ 00-50, and Smooth Sil™ 940 actuators were measured to be 0.719, 0.864, and 0.260 N, respectively (**Figure 6.14a**). Similarly, the actuators pressurized with water demonstrated an almost identical pattern and achieved maximum forces of 0.779, 0.827, and 0.280 N for the actuators made of Ecoflex™ 00-30, Ecoflex™ 00-50, and Smooth Sil™ 940, respectively (**Figure 6.14b**). Compared with Ecoflex™ 00-30 and Ecoflex™ 00-50, the Smooth Sil™ 940 actuator had a much lower blocking force when pressurized with air and water. These mechanical properties were consistent with its stiffness, as the Ecoflex™ 00-30 and Ecoflex™ 00-50 actuators, with their lower moduli, could be actuated at lower pressures, and, with its higher modulus, the Smooth Sil™ 940 actuator required a higher pressure for actuation, which resulted in a lower blocking force generated at the maximum tested pressure.

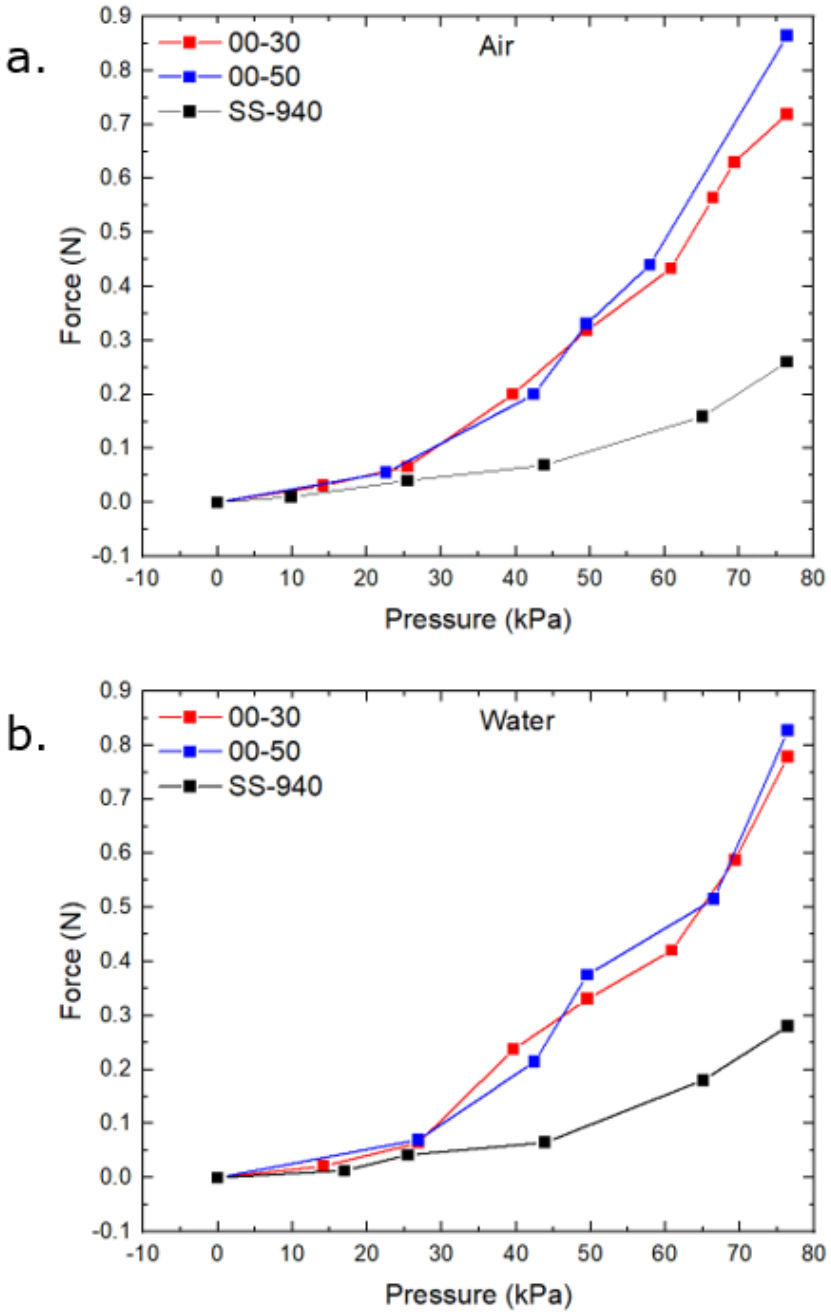

Figure 6.14 Blocking force measured at the tip of fibre-reinforced actuators made using Ecoflex™ 00−30, Ecoflex™ 00−50, and Smooth Sil 940 under the influence of (a) air and (b) water pressure in a vertical position (n = 3).

Overall, the forces produced in all three elastomers were proportional to the input pressures, and the forces achieved with air and water actuation were almost equivalent. In addition, these

results represent the fact that the bending and force performance of these soft actuators can be controlled with the pressure supplied. The relationship between the blocking force and input pressure can be further extended. Operating soft actuators at higher pressures affect their life span due to fatigue. However, these actuators were controlled with a fixed volume in a syringe, making them less likely to be overpowered, and they were tested for 500 cycles at a pressure of 100 kPa without failure. These soft actuators demonstrated blocking forces up to the ~1 N range, which is comparable to the range of existing elastomeric actuators [22], [179]. Two or more soft actuators can serve as a body-powered gripper that can be used to grasp objects when actuated.

6.4.2 Bending characteristics

As the motor pushed the plunger (**Figure 6.15**), the system filled with air or water, causing the actuator to bend in the direction where the fibre angle was 10°. This bending was the result of stress created on the inner walls of the actuator, where the higher angle in the braiding combination allowed more space to expand over a certain pressure, causing shrinkage on the side with the lower angle and resulting in curling when pressurized. When powered by air, both the Ecoflex™ 00-30 and Ecoflex™ 00-50 actuators quickly bent to 40° and 32° with 50 kPa, respectively, whereas the actuator made using Smooth Sil™ 940 managed to reach only 8°, as shown in **Figure 6.15a.**

When the working fluid was changed from air to water, the Ecoflex™ 00-30 and Ecoflex™ 00-50 actuators reached 50° and 40° with 50 kPa, whereas Smooth Sil™ 940 was slightly bent to 10° (**Figure 6.15b**). It could be seen that the amount of bending at any given pressure was affected by the elastomer Young's modulus. These bending properties are consistent with those observed by Yap et al. and Galloway et al., who evaluated the bending performance for different materials from Smooth-On Inc., PA, USA [22], [49].

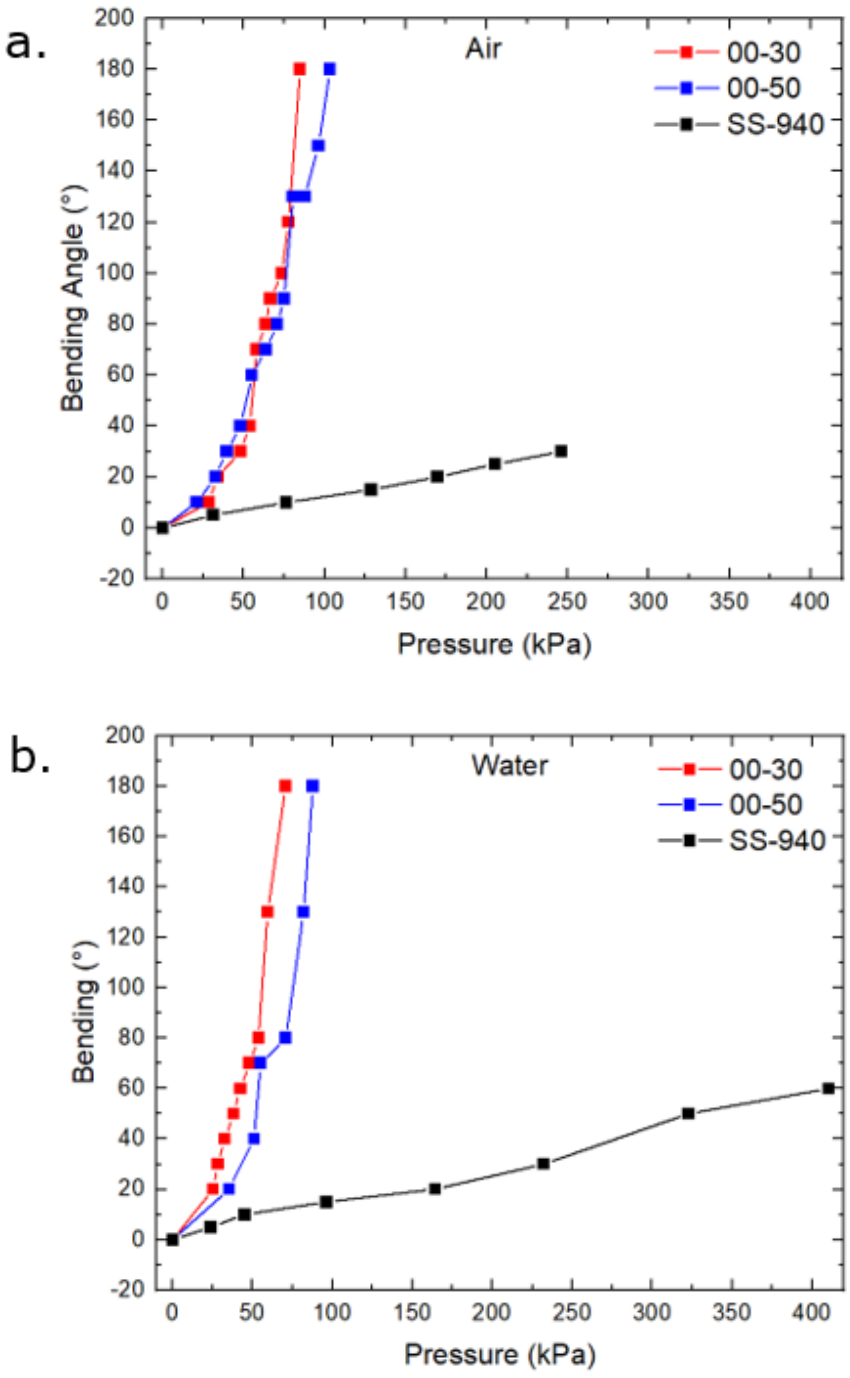

Figure 6.15 Bending behaviour of fibre-reinforced actuators made using Ecoflex™ 00−30, Ecoflex™ 00−50, and Smooth Sil™ 940 under the influence of (a) air and (b) water pressure by comparing actuators from the curled to the resting positions (vertical position).

6.4.3 Syringe plunger displacement versus pressure built up in the actuator

The plunger displacement of the syringe and the pressure built up in the actuator due to this displacement are two crucial parameters for it to be powered by the body. The pressure built up, P, is determined by force, F, applied to the plunger for the given syringe dimensions. As the syringe is pre-filled with air or water, the fluid will experience a fixed working area, A (area of the plunger, 7.1×10^{-4} m^2), and the pressure generated can be calculated using $P = F/A$ [180]–[182]. Although all actuators have the same geometry, actuators that are much stiffer allow less expansion, causing pressure to build up in the actuator, which also implies that it requires a high pressure to bend, which is very difficult to achieve when using shoulder movements.

To investigate this, the pressure built up was calculated with the help of a force sensor attached to the plunger. The built-up pressure increased almost linearly with increasing displacement in the plunger for the cases of the Ecoflex™ 00-30 and Ecoflex™ 00-50 actuators, whereas for the Smooth Sil™ 940 actuator, it quickly rose as the displacement increased for both the air- and water-filled syringes (**Figure 6.16**). When the plunger was pushed to displace 20 mm in the syringe with air, the pressure in all three actuators was approximately 20 kPa (**Figure 6.16a**). On the other hand, when using water, the pressure quickly jumped to approximately 50 kPa in the actuators made from Ecoflex™ 00-30 and Ecoflex™ 00-50 and to approximately 380 kPa in the actuators made from Smooth Sil™™ 940 (**Figure 6.16b**).

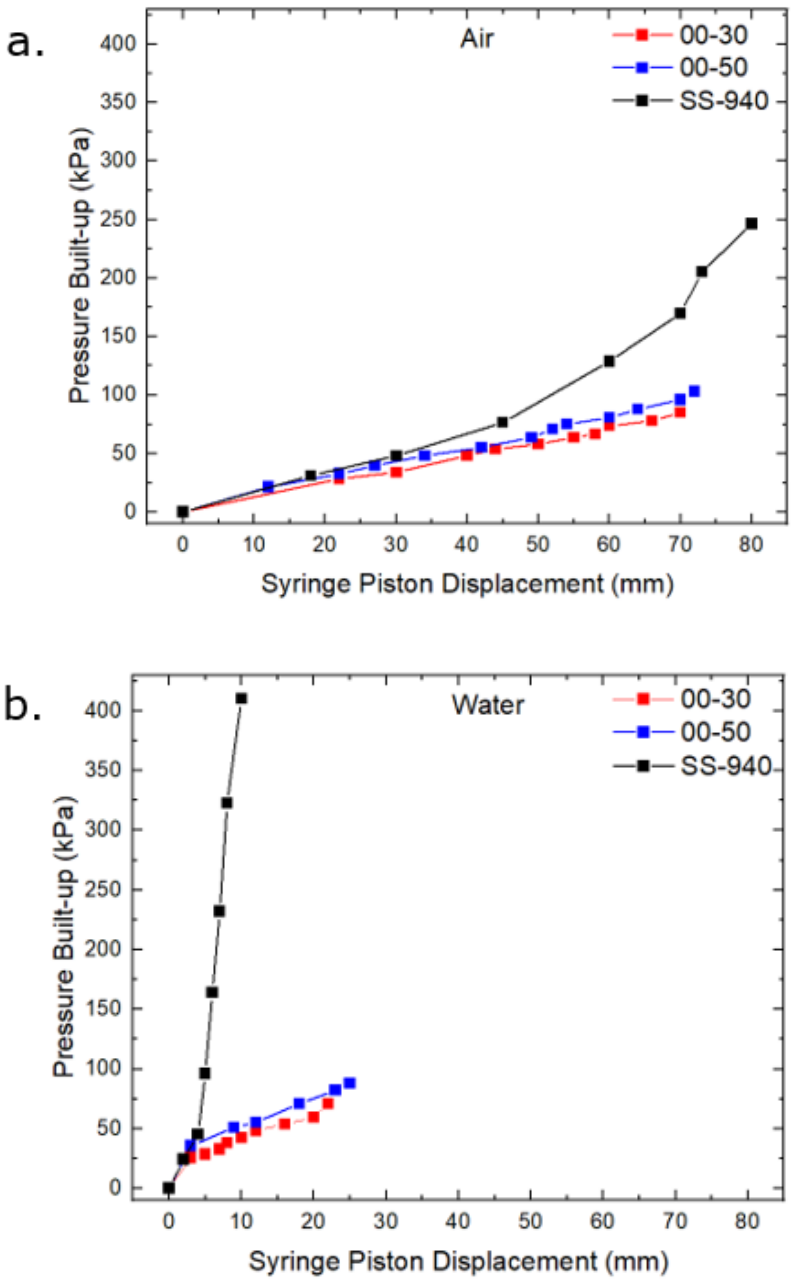

Figure 6.16 The pressure built up in the actuator against the syringe's plunger displacement for the Ecoflex™ 00-30, Ecoflex™ 00-50, and Smooth Sil™ 940 actuators were tested when filled with (a) air and (b) water.

Furthermore, it was observed that the displacement of the plunger needed to generate the same amount of pressure in the actuator was approximately three times lower when using water compared to air, as water is relatively incompressible [79] compared to air (**Figure 6.17**).

Hence, the use of water as a working fluid in bending actuators is suitable for body-powered actuator application, as a smaller body motion is required to generate the required pressure. Considering the bending angle, force, plunger displacement, and built-up pressure together, the actuators made from Ecoflex™ 00-30 and Ecoflex™ 00-50 had almost similar performance, but Ecoflex™ 00-50 had a slightly higher stiffness than Ecoflex™ 00-30, which limited the bending due to gravity when held horizontally. Therefore, Ecoflex™ 00-50 was chosen for body-powered application in the next chapter.

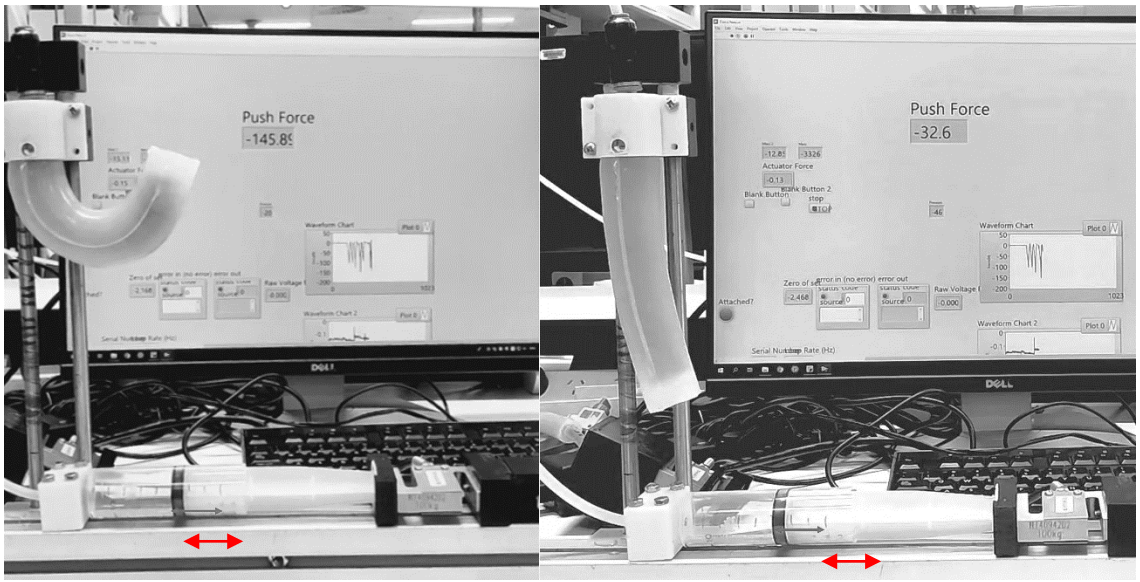

Figure 6.17 Bending output of water-powered and air-powered actuators for identical movement of the plunger.

6.5 Summary

This chapter discussed the effect of materials with different stiffness in bending. Also, it explained the difference in the effect of using air and water as powering fluids. The use of water as a working fluid in bending actuators is found to be suitable in the intended body-powered actuator application, as a smaller body motion is required to generate the required pressure. In this work, the shoulder's shrugging is considered as the body motion that actuates

the bending actuators. The actuators made from Ecoflex™ 00-30 and Ecoflex™ 00-50 showed more bending and higher blocking force compared to those of Smooth Sil™ 940. In addition, Ecoflex™ 00-50 had higher strength and could provide extra protection from bulging or failures at higher operating pressures and provide sufficient bending at low pressure with reasonable blocking force. Hence, Ecoflex™ 00-50 was chosen for these body-powered actuators as prosthetics.

Chapter 7

Application of the fibre-reinforced actuator as body-powered prosthetics

Instead of conventional actuators, which require an external pneumatic supply, using a simple assembly made from a syringe and drawbar mechanism, a body-powered prosthetic system can be realized. This application utilizes body movements as a source to generate hydraulic pressure to actuate these grippers. Hence, this will be standalone and truly portable.

Note: All experimental procedures in this study that involved human participants were subjected to ethical approval, which was endorsed by the University of Auckland Human Participants Ethics Committee (UoAHPEC- 023153).

As a first step, this chapter evaluates the shoulder shrugging distance and force generation capability of human shoulders by conducting a study on ten participants. Further, a design technique was employed to convert these shrugging movements into usable power for the actuators.

7.1 Experimental section

7.1.1 Evaluation of shrugging force

Ten (n = 10) healthy individual participants (two female and eight male) were recruited to convert their shoulder-shrugging movements to power the actuator. The participants were asked to shrug their shoulders, and the upward displacement was recorded, as shown in **Figure 7.1**.

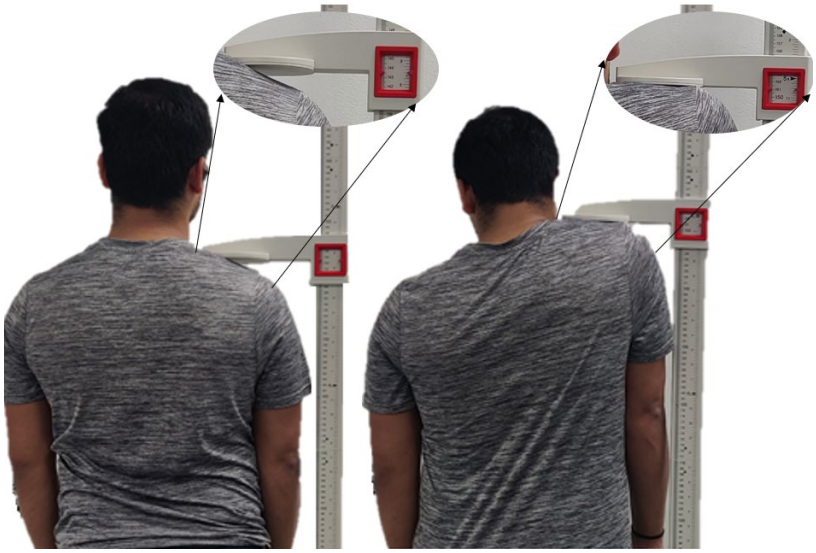

Figure 7.1 Shoulder elevation measurement.

The shoulder blade was pressed against a force sensor set-up, as shown in **Figure 7.2,** to determine the amount of force it could generate. With the upward displacement and the force generated by the shoulder, the maximum pressure generated to actuate the number of actuators could be determined.

Figure 7.2 Shoulder force measurement.

7.1.2 Preliminary experiment design for body power utilization

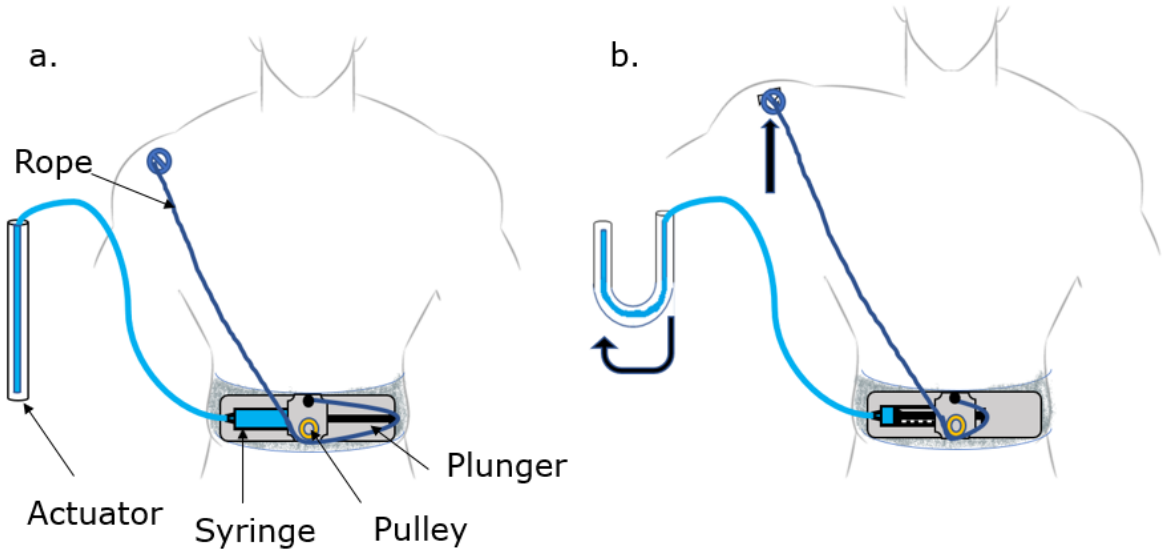

Figure 7.3 Shoulder-assisted actuation based on rope and pulley.

A pulley connected the syringe's plunger to the shoulder blade, as shown in **Figure 7.3**. As the shoulder flexes upwards, the rope pushes the plunger, causing the actuator to bend. However, it was found that the setup disturbed the user's sitting posture and that fixing the rope on the shoulder blade was difficult, causing discomfort and reduced efficiency.

7.1.3 Draw-bar spring mechanism for body power generation

A draw-bar spring mechanism was considered to be of potential use in transferring shoulder movement into fluidic power generation for actuators.

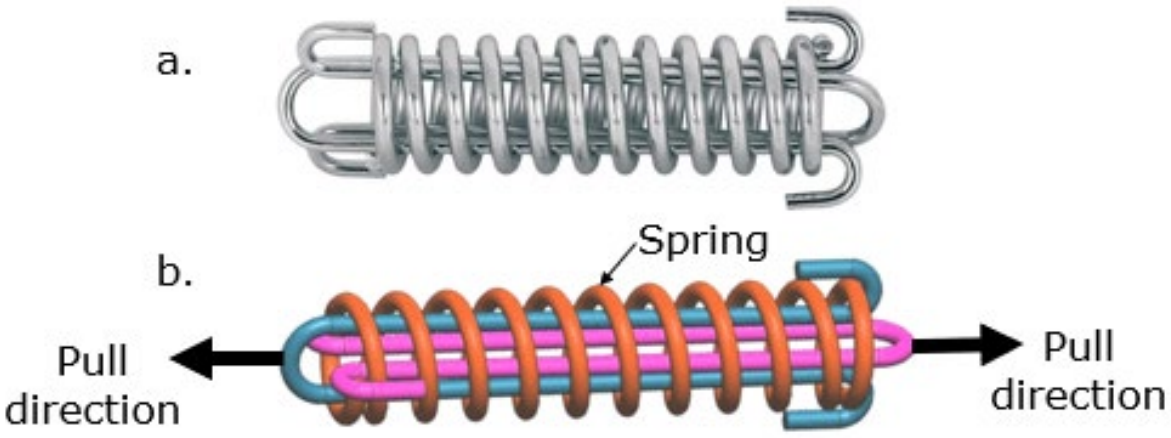

Figure 7.4 (a) Draw-bar spring (b) illustration of the working mechanism.

The spring works on the following mechanism. Two hooks, indicated in blue and pink, are pulled in the opposite direction (**Figure 7.4**). When this happens, a spring indicated in red colour squeezes its length.

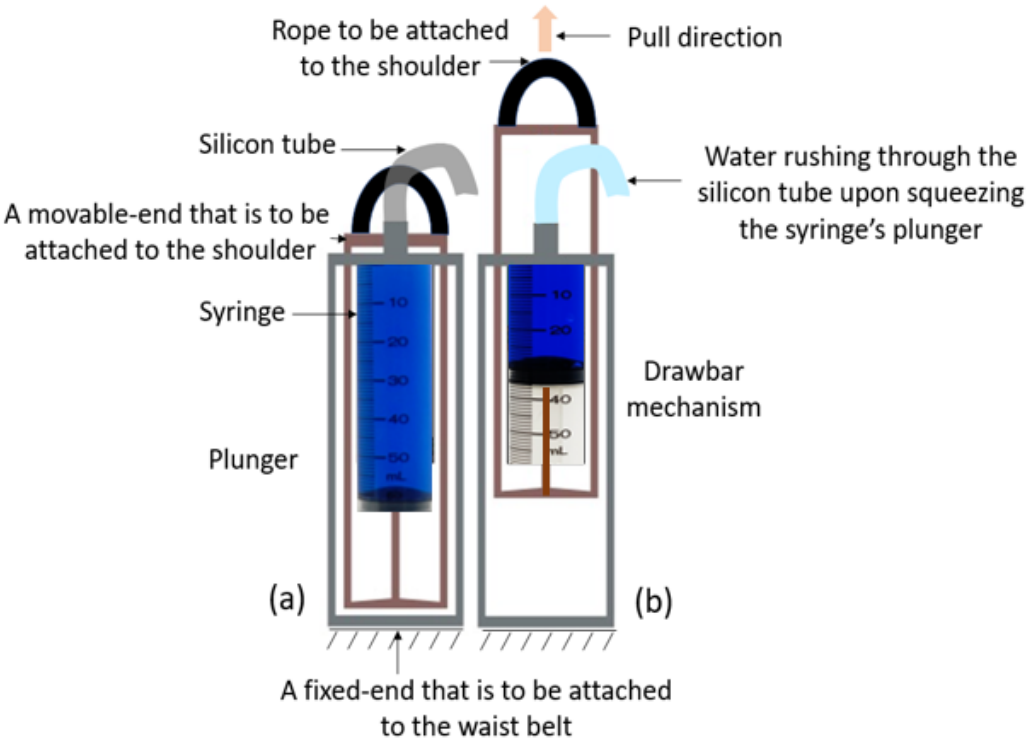

Figure 7.5 A schematic of the drawbar syringe setup for body-powered actuation. (a) initial syringe position before the pull and (b) squeezed syringe after the pull, to power the actuator.

This draw-bar spring mechanism was used in the syringe and plunger setup shown in **Figure 7.5**. The top end of this setup was strapped to the shoulder, and the bottom end was attached to a belt at the waist. The shrugged shoulder pulled the plunger upward, which squeezed the fluid inside the syringe, which powered the actuators. A body-powered transmission set-up with water as the working fluid was designed after determining the material and its actuation conditions, as shown in **Figure 7.6**.

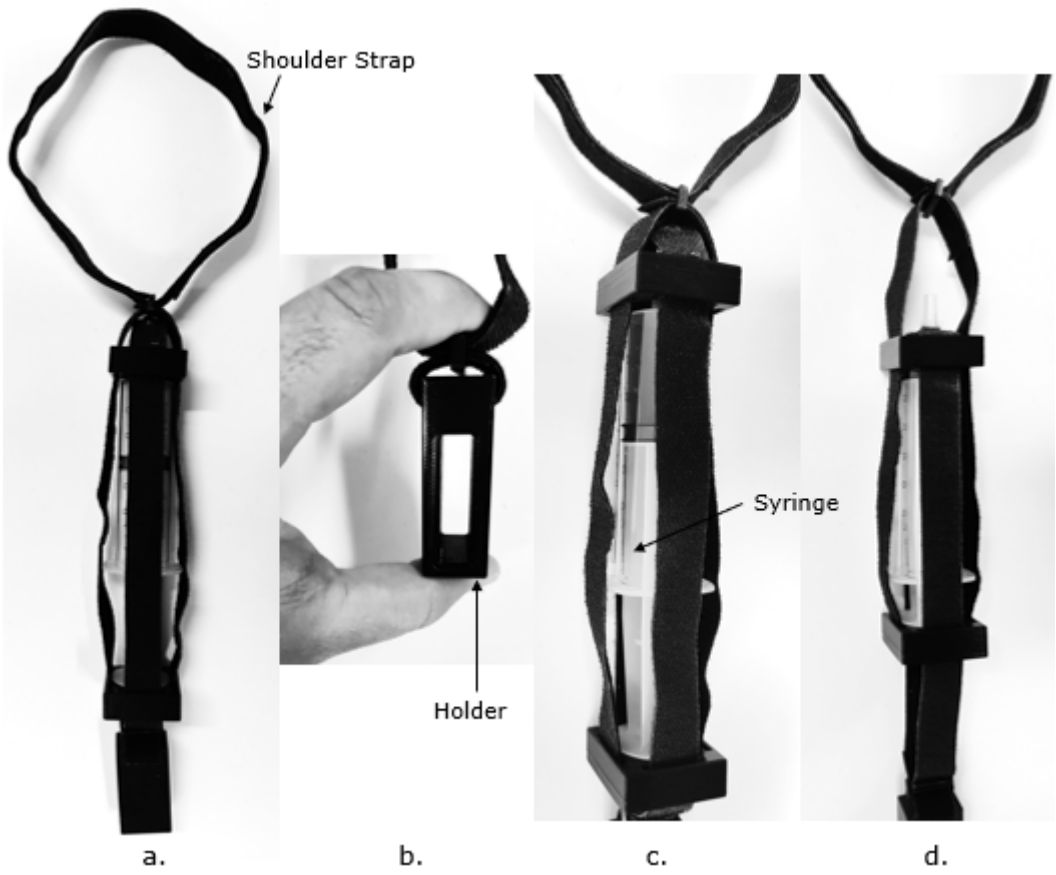

Figure 7.6 Body-power transmission set-up. (a) A syringe is enclosed in a draw bar setup. (b) A holder that buckles the set-up to the waist belt (c) Before shoulder movement (d) After shoulder movement.

7.2 Results and discussion

The test was conducted among ten healthy (two female and eight male) participants to determine the average upward displacement and force generated when shrugging the shoulder by using a measuring scale and a force sensor, respectively. The average shoulder elevation measured was 77 ± 29 mm. The average blocking force generated by shrugging the shoulder was 113 ± 55 N which is quite similar to the results obtained from dumbbell shrug experiments [183], which was equivalent to a pressure of 160 ± 78 kPa in the syringe with a plunger of 30 mm diameter and a total volume of 50 ml. As mentioned before in **Figure 6.6b**, bending the actuator to 120° requires approximately a pressure of 80 kPa, and to generate such pressure, the plunger had to move 25 mm (**Figure 6.7b**). Hence, based on the data collected from the ten human participants, the shrugging of the shoulder could displace the plunger by 48 mm, which was sufficient to actuate two actuators to bend 120° each using body power.

The body-power setup was made with the bottom end of the setup fixed to a belt at the waist to cause the syringe to stay in position when the shoulder was elevated, as the top end was strapped to the shoulder (**Figure 7.7a**). When the shoulder was elevated upwards, it pressurized the system and resulted in the bending of the actuators (**Figure 7.7b**). A photograph of the actual body-powered actuator being worn is shown in **Figure 7.7c**. Two actuators acting as fingers were connected to the syringe's outlet using a silicone tube. **Figure 7.7d, e** shows the fingers before and after actuation, respectively. **Figure 7.7f** shows the fingers grasping a water bottle with a weight of 500 g that was placed on a table; this was ten times more than the mass of the actuator itself, demonstrating a promising result for effective integration in soft robotic applications. In addition, two-actuator grippers were tested to assess the amount of force required to dislodge an item, which was found to be 5.8 N. The actuator is currently limited to grasping cylindrical objects. Future development of this device will include testing of actuators

of different lengths and a gripper that resembles a five-fingered human hand that can potentially grasp different objects irrespective of their shape and orientation.

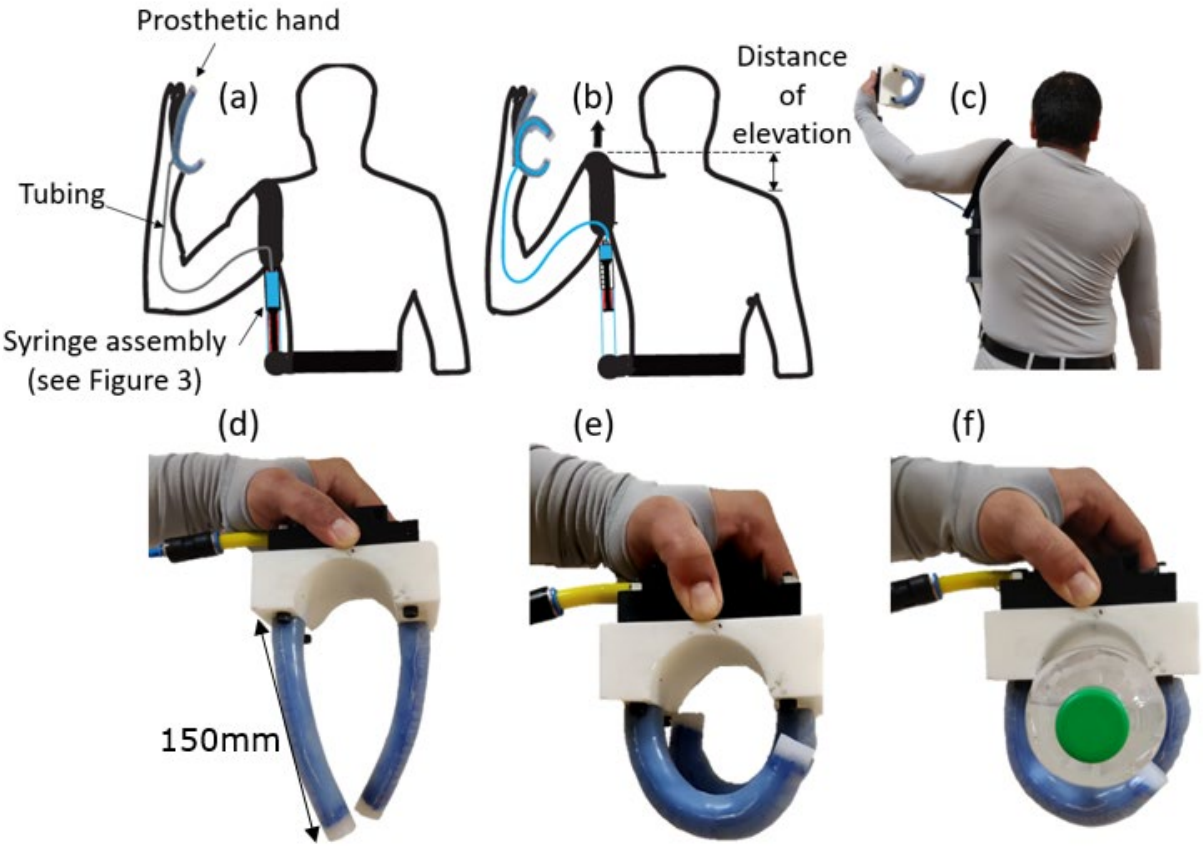

Figure 7.7 Body-powered actuator. (a) body-powered setup before actuation; (b) body-powered setup after actuation; (c) actuation test on participant; (d) gripper before actuation; (e) gripper after actuation; (f) grippers holding a 500 g water bottle.

7.3 Summary

The idea presented in this chapter represents a shift from the existing approach of using externally powered soft robots toward using body-powered robots. Prosthetics and wearable robots need to be portable, lightweight, and simple. Instead of using rigid linkages, as seen in traditional actuators powered by servo motors or chamber-based soft actuation techniques powered using external compressors, the proposed design is both soft and body powered; it

bends based on the variable stiffness created using a composite of an elastomer and fibres braided along the length of the actuator while utilizing shoulder elevation for power. Lastly, body-powered actuators for grasping using a shoulder-shrugging motion to grasp a water bottle with a mass of 500 g were successfully demonstrated. These actuators are highly suitable for applications that demand high bending angles with low input pressures.

Chapter 8

Conclusions and future work

8.1 Summary of contributions

This thesis presents a portable prostheses, especially those that are body-powered. A lightweight, flexible fibre-reinforced fluidic actuator was developed to replace rigid linkages and traditional actuators. A hypothesis was put forth to manufacture and operate variable stiffness fibre-reinforced soft fluidic actuators using body movements. Bending concept demonstration and the evolution of soft elastomeric actuator designs involving multiple fabrication techniques and shoulder movement utilization has successfully provided a conclusive validation of the hypothesis that ultimately resulted in this thesis.

8.2 Conclusions

8.2.1 Validation of bending based on variable stiffness of the actuator

It was hypothesized that an actuator possessing materials of two different stiffnesses on each half of the structure would undergo bending upon internal pressurization. A mathematical model was derived to explain this possibility of bending by assuming it as a closed thick wall cylinder made from two variable stiffness materials. Also, it explained a process in which fibres braided at different angles could be used to program the stiffness of the material. These stiffness values were experimentally tested and applied to the mathematical model to calculate the bending undergone by a cylinder. Additionally, these variable stiffness values obtained from testing were used to validate the possibility of bending using an FEA model. However, experiments have shown that the actuators bend, but not exactly in an arc and that they expand radially when powered, which causes the experimental results to differ from simulations. These validations set a path to manufacture a fibre-reinforced soft bending actuator for use in body-powered prostheses applications.

8.2.2 Design and manufacturing

An established split fibre-reinforcement braiding technique has been tested using low-stiffness elastomer materials, and the results have been observed in chapter 5. At higher pressures, this technique creates more stress along the length of the actuator, where the two differently braided materials bind together. This stress makes the SFR actuators prone to radial bulging and reduces their lifetime. In the process of eliminating the weak joint, the fibres were wound continuously using the CFR technique and, at the same time, created two different braiding angles on each half of the actuator. The results have demonstrated that CFR actuators achieve high bending angles at low-pressure levels, with a linear bending rate of 1.77°/kPa. The CFR actuator performs better than the SFR actuator due to its construction technique that reduces the bulging problem, potentially increasing the lifetime and repeatability of the actuator. The CFR fabrication technique is much simpler than the SFR technique, and the low operating pressure makes them a suitable candidate for body-powered applications.

8.2.3 Effect of the material property on actuator performance

The effect of Young's modulus on the materials towards actuator performance has been studied by utilizing Ecoflex™ 00-30, 00-50, and Smooth Sil-940 in the continuous fibre-reinforcement (CFR) technique in chapter 6. These three materials possess different Young's moduli, and their bending and force characteristics were studied and compared against each other. It was observed that low-stiffness materials tend to exhibit more bending compared to high-stiffness materials. Ecoflex™ 00-30 has low stiffness compared to Ecoflex™ 00-50; however, an actuator made from Ecoflex™ 00-50 was chosen for this application since there is no significant difference between their performances with the chosen actuator possessing resistance against the additional bending due to gravity when held horizontally.

8.2.4 Fluidic power

The difference in the effects of using air and water as powering fluids was studied. An experimental set-up containing a syringe-plunger set up was used to study their performance. It was observed that an identical movement of the syringe's plunger containing water was able to generate comparatively higher bending than air. Hence the use of water as a working fluid in bending actuators is found to be suitable in the intended body-powered actuator application, as a smaller body motion is required to generate the required pressure.

8.2.5 Application

In this work, the shoulder's shrugging action of the body was considered to power the soft actuators. The distance elevation and force generation capability of the human shoulders have been analysed through a study conducted among ten human participants of mixed height and weight. It was observed that a shoulder shrugging action with the combination of continuous fibre-reinforcement technique, low-powered actuator, and water-powered fluidic actuation could produce a highly efficient body-powered gripping device.

8.3 Future work

While this thesis has shown promising proof-of-concept results using a unique fibre braiding technique to establish seamless bending in low-stiffness material actuators and their usage in a portable body-powered prosthetic application, there is much more work that can be done to establish this as a commercial product. Areas of potential future work are discussed in this section.

8.3.1 Manufacturing of CFR actuators

In CFR actuators, elastomeric materials were used instead of neoprene rubber, reducing the difficulties associated with melting rubber and the need for a high-temperature oven. However, the winding process involved here in the CFR technique is tedious as well. This can be

improved by designing an automatic fibre winding machine similar to the one utilized in chapter 5 of this thesis to speed up the manufacturing process. The actuator in chapters 5 and 6 was made of 180 mm and 150 mm, respectively, with a diameter of 30 mm and 20 mm. The length and diameter of these actuators can further be reduced to study their force and bending generation capabilities, enabling them to be used in a wide variety of wearable and prosthetic applications. A bi-directional bending actuator can be created by splitting the internal chamber into two, adding additional capabilities to these soft bending actuators.

8.3.2 Modelling and characterization

Numerical and FEA models have been developed in chapters 3 and 4 of this thesis to demonstrate the bending of the fibre-reinforced soft bending actuator. The FEA model used the material properties measured from the fibre braided samples tested using the Universal Testing Machine. These results serve as a preliminary source to verify the bending in fibre-reinforced soft bending actuators. However, in the future, a more sophisticated FEA model can be created by designing the more complex CFR fibre braiding as an individual part and embedding it inside the elastomeric material. This will help to achieve more accurate results and a realistic comparison of the FEA model actuator with that of the manufactured practical actuator. This will also allow a way to test more different materials using the FEA model without requiring the testing of fibre-reinforced samples in a Universal Testing Machine.

8.3.3 Testing and verification

The actuator was tested for 500 cycles at a pressure of 100 KPa without failure, and the actuator was able to repeat the same bending characteristics over the testing period. The testing can further be continued to study the repeatability performance and lifetime of the actuator before failure. The performance of soft-elastomeric actuators is considered non-linear. Hence, they cannot be used in environments that demand a precise outcome. In this scenario, closed-loop control is vital to achieving the desired performance. Additionally, sensing technologies can

be embedded into these actuators at the fabrication stage, which could facilitate a controlled output. Once the actuator performance is evaluated, a suitable controller (PID or adaptive control) will be identified to facilitate feedback control.

8.3.4 Application of actuators in a five-fingered prosthetic hand

The current prototype only demonstrates the feasibility of implementing a soft pneumatic bending actuator onto a two-fingered prosthetic system with the ability to grasp an object of 500g weight, as demonstrated in chapter 7. This work can be further extended by implementing a five-finger prosthetic hand or five-fingered assistive device that will be more like a human hand (as shown in **Figure 8.1**) and improve the object handling process of the user [184] and also can assist in rehab therapy.

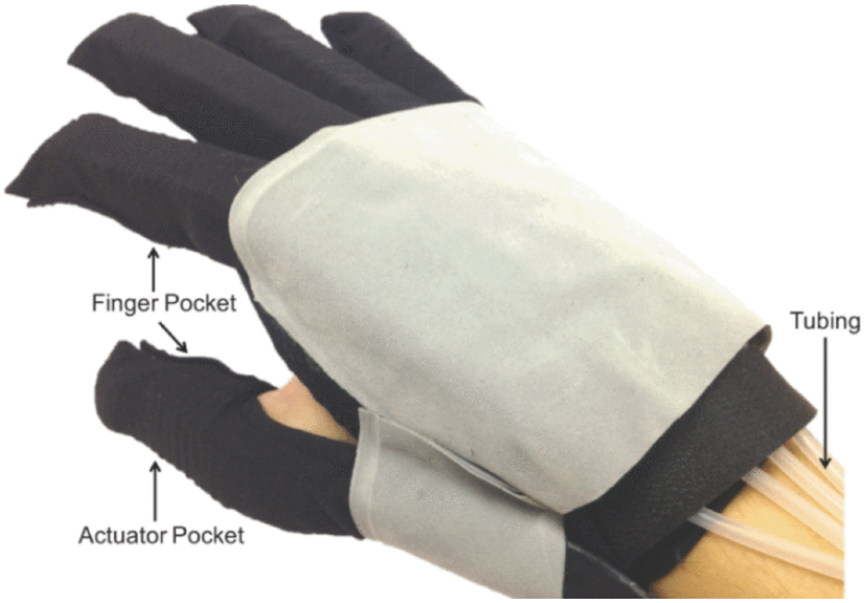

Figure 8.1 A soft robotic glove prototype.

Moving on from the development of the actuator and body-powered prosthetic system presented in this thesis, clinical trials will be the next critical milestone. The shoulder

movements of ten healthy subjects were studied here and it can further be extended to patients with disability and study their response to generate shoulder elevation and force to determine the feasibility and comfort of implementing this application in them. Additionally, future work is also planned to study the long-term efficacy and longitudinal outcomes of a body-powered prosthesis in patients.

List of publications

Parts of this thesis have been published in the following journals and conferences.

Journals

- **Kandasamy, S.**; Teo, M.; Ravichandran, N.; McDaid, A.; Jayaraman, K.; Aw, K. **Body-Powered and Portable Soft Hydraulic Actuators as Prosthetic Hands**. Robotics **2022**, *11*, 71. https://doi.org/10.3390/robotics11040071

- **Kandasamy, S.**; Teo, M.; McDaid, A.; Jayaraman, K. **A Review: Soft actuators for use in wearable devices and body-powered prosthesis**. Int. J. Biomechatronics and Biomedical Robotics, **2023**, (pp 17-31). https://doi.org/10.1504/IJBBR.2022.128678

Conferences

- **Kandasamy, S.**, Devaraj, H., Stuart, L., McDaid, A., & Aw, K. C. **A Novel Varying Angle Fibre-Reinforced Elastomer as a Soft Pneumatic Bending Actuator**. In Proceedings of the 2019 3rd International Conference on Automation, Control and Robots (pp. 50-54). https://doi.org/10.1145/3365265.3365272

References

[1] M. Wnuk *et al.*, "Challenges in Robotic Soft Tissue Manipulation—Problem Identification Based on an Interdisciplinary Case Study of a Teleoperated Drawing Robot in Practice," *Mechatronics Mach. Vis. Pract. 4*, pp. 245–262, 2021, doi: 10.1007/978-3-030-43703-9_20.

[2] S. Coyle, C. Majidi, P. LeDuc, and K. J. Hsia, "Bio-inspired soft robotics: Material selection, actuation, and design," *Extrem. Mech. Lett.*, vol. 22, pp. 51–59, Jul. 2018, doi: 10.1016/j.eml.2018.05.003.

[3] A. lakhan, M. A. Mohammed, D. A. Ibrahim, and K. H. Abdulkareem, "Bio-inspired robotics enabled schemes in blockchain-fog-cloud assisted IoMT environment," *J. King Saud Univ. - Comput. Inf. Sci.*, Nov. 2021, doi: 10.1016/J.JKSUCI.2021.11.009.

[4] H. Jin, E. Dong, M. Xu, C. Liu, G. Alici, and Y. Jie, "Soft and smart modular structures actuated by shape memory alloy (SMA) wires as tentacles of soft robots," *Smart Mater. Struct.*, vol. 25, no. 8, p. 085026, Jul. 2016, doi: 10.1088/0964-1726/25/8/085026.

[5] D. Rus and M. T. Tolley, "Design, fabrication and control of soft robots," *Nat. 2015 5217553*, vol. 521, no. 7553, pp. 467–475, May 2015, doi: 10.1038/nature14543.

[6] H. R. Lim, H. S. Kim, R. Qazi, Y. T. Kwon, J. W. Jeong, and W. H. Yeo, "Advanced Soft Materials, Sensor Integrations, and Applications of Wearable Flexible Hybrid Electronics in Healthcare, Energy, and Environment," *Adv. Mater.*, vol. 32, no. 15, p. 1901924, Apr. 2020, doi: 10.1002/ADMA.201901924.

[7] M. I. Caravantes-Cortes, E. Roldan-Valadez, R. D. Zwojewski-Martinez, S. Y. Salazar-Ruiz, and A. A. Carballo-Zarate, "Breast Prosthesis Syndrome: Pathophysiology and Management Algorithm," *Aesthetic Plast. Surg.*, vol. 44, no. 5, pp. 1423–1437, Oct. 2020, doi: 10.1007/S00266-020-01663-9/FIGURES/7.

[8] A. Pal, V. Restrepo, D. Goswami, and R. V. Martinez, “Exploiting Mechanical Instabilities in Soft Robotics: Control, Sensing, and Actuation,” *Adv. Mater.*, vol. 33, no. 19, p. 2006939, May 2021, doi: 10.1002/ADMA.202006939.

[9] N. Ebrahimi *et al.*, “Magnetic Actuation Methods in Bio/Soft Robotics,” *Adv. Funct. Mater.*, vol. 31, no. 11, p. 2005137, Mar. 2021, doi: 10.1002/ADFM.202005137.

[10] S. G. Fitzgerald, G. W. Delaney, and D. Howard, “A Review of Jamming Actuation in Soft Robotics,” *Actuators 2020, Vol. 9, Page 104*, vol. 9, no. 4, p. 104, Oct. 2020, doi: 10.3390/ACT9040104.

[11] R. K. Katzschmann, A. De Maille, D. L. Dorhout, and D. Rus, “Cyclic hydraulic actuation for soft robotic devices,” *IEEE Int. Conf. Intell. Robot. Syst.*, vol. 2016-Novem, pp. 3048–3055, Nov. 2016, doi: 10.1109/IROS.2016.7759472.

[12] J. H. Youn *et al.*, “Dielectric Elastomer Actuator for Soft Robotics Applications and Challenges,” *Appl. Sci. 2020, Vol. 10, Page 640*, vol. 10, no. 2, p. 640, Jan. 2020, doi: 10.3390/APP10020640.

[13] T. Wang, Y. Zhang, Y. Zhu, and S. Zhu, “A computationally efficient dynamical model of fluidic soft actuators and its experimental verification,” *Mechatronics*, vol. 58, pp. 1–8, Apr. 2019, doi: 10.1016/J.MECHATRONICS.2018.11.012.

[14] J. Shintake, H. Shea, and D. Floreano, “Biomimetic underwater robots based on dielectric elastomer actuators,” *IEEE Int. Conf. Intell. Robot. Syst.*, vol. 2016-November, pp. 4957–4962, Nov. 2016, doi: 10.1109/IROS.2016.7759728.

[15] P. Polygerinos *et al.*, “Soft Robotics: Review of Fluid-Driven Intrinsically Soft Devices; Manufacturing, Sensing, Control, and Applications in Human-Robot Interaction,” *Adv. Eng. Mater.*, vol. 19, no. 12, Dec. 2017, doi: 10.1002/ADEM.201700016.

[16] C. P. Chou and B. Hannaford, “Measurement and modeling of McKibben pneumatic artificial muscles,” *IEEE Trans. Robot. Autom.*, vol. 12, no. 1, pp. 90–102, 1996, doi: 10.1109/70.481753.

[17] H. K. Yap, J. H. Lim, F. Nasrallah, F. Z. Low, J. C. H. Goh, and R. C. H. Yeow, “MRC-glove: A fMRI compatible soft robotic glove for hand rehabilitation application,” *IEEE Int. Conf. Rehabil. Robot.*, vol. 2015-Septe, no. 65, pp. 735–740, 2015, doi: 10.1109/ICORR.2015.7281289.

[18] F. Connolly, C. J. Walsh, and K. Bertoldi, “Automatic design of fiber-reinforced soft actuators for trajectory matching,” *Proc. Natl. Acad. Sci.*, vol. 114, no. 1, pp. 51–56, Jan. 2017, doi: 10.1073/pnas.1615140114.

[19] Y. Tang, M. Li, T. Wang, X. Dong, W. Hu, and M. Sitti, “Wireless Miniature Magnetic Phase-Change Soft Actuators,” *Adv. Mater.*, p. 2204185, Sep. 2022, doi: 10.1002/ADMA.202204185.

[20] H. K. Yap, H. Y. Ng, and C.-H. H. Yeow, “High-Force Soft Printable Pneumatics for Soft Robotic Applications,” *Soft Robot.*, vol. 3, no. 3, pp. 144–158, Sep. 2016, doi: 10.1089/soro.2016.0030.

[21] P. H. Nguyen and W. Zhang, “Design and Computational Modeling of Fabric Soft Pneumatic Actuators for Wearable Assistive Devices,” *Sci. Reports 2020 101*, vol. 10, no. 1, pp. 1–13, Jun. 2020, doi: 10.1038/s41598-020-65003-2.

[22] K. C. Galloway, P. Polygerinos, C. J. Walsh, and R. J. Wood, “Mechanically programmable bend radius for fiber-reinforced soft actuators,” in *2013 16th International Conference on Advanced Robotics (ICAR)*, IEEE, Nov. 2013, pp. 1–6. doi: 10.1109/ICAR.2013.6766586.

[23] S. Chen, Y. Pang, Y. Cao, X. Tan, and C. Cao, “Soft Robotic Manipulation System Capable of Stiffness Variation and Dexterous Operation for Safe Human–Machine Interactions,” *Adv. Mater. Technol.*, vol. 6, no. 5, p. 2100084, May 2021, doi: 10.1002/ADMT.202100084.

[24] A. A. Stokes, R. F. Shepherd, S. A. Morin, F. Ilievski, and G. M. Whitesides, “A Hybrid Combining Hard and Soft Robots,” *Soft Robot.*, vol. 1, no. 1, pp. 70–74, Mar. 2014, doi: 10.1089/soro.2013.0002.

[25] N. Gariya and P. Kumar, “A review on soft materials utilized for the manufacturing of soft robots,” *Mater. Today Proc.*, vol. 46, pp. 11177–11181, Jan. 2021, doi: 10.1016/J.MATPR.2021.02.380.

[26] S. Kim, C. Laschi, and B. Trimmer, *Soft robotics: A bioinspired evolution in robotics*, vol. 31, no. 5. Elsevier Current Trends, 2013, pp. 287–294. doi: 10.1016/J.TIBTECH.2013.03.002.

[27] D. W. Nicholson, N. W. Nelson, B. Lin, and A. Farinella, “Finite Element Analysis of Hyperelastic Components,” *Appl. Mech. Rev.*, vol. 51, no. 5, pp. 303–320, May 1998, doi: 10.1115/1.3099007.

[28] Z. Cui *et al.*, “Haptically Quantifying Young’s Modulus of Soft Materials Using a Self-Locked Stretchable Strain Sensor,” *Adv. Mater.*, vol. 34, no. 25, p. 2104078, Jun. 2022, doi: 10.1002/ADMA.202104078.

[29] J. L. Sparks *et al.*, “Use of silicone materials to simulate tissue biomechanics as related to deep tissue injury,” *Adv. Skin Wound Care*, vol. 28, no. 2, pp. 59–68, 2015, doi: 10.1097/01.ASW.0000460127.47415.6E.

[30] J. Vaicekauskaite, P. Mazurek, S. Vudayagiri, and A. L. Skov, “Mapping the mechanical

and electrical properties of commercial silicone elastomer formulations for stretchable transducers," *J. Mater. Chem. C*, vol. 8, no. 4, pp. 1273–1279, Jan. 2020, doi: 10.1039/C9TC05072H.

[31] J. Vaicekauskaite, P. Mazurek, S. Vudayagiri, A. Ladegaard Skov Justina Vaicekauskaite, and A. Ladegaard Skov, "Silicone elastomer map: design the ideal elastomer," *https://doi.org/10.1117/12.2515305*, vol. 10966, no. 13, pp. 297–305, Mar. 2019, doi: 10.1117/12.2515305.

[32] I. De Falco, C. Culmone, A. Menciassi, J. Dankelman, and J. J. van den Dobbelsteen, "A variable stiffness mechanism for steerable percutaneous instruments: integration in a needle," *Med. Biol. Eng. Comput.*, vol. 56, no. 12, pp. 2185–2199, Dec. 2018, doi: 10.1007/S11517-018-1847-7/FIGURES/15.

[33] B. Wang and A. Facchetti, "Mechanically Flexible Conductors for Stretchable and Wearable E-Skin and E-Textile Devices," *Adv. Mater.*, vol. 31, no. 28, p. 1901408, Jul. 2019, doi: 10.1002/ADMA.201901408.

[34] C. Majidi, "Soft-Matter Engineering for Soft Robotics," *Adv. Mater. Technol.*, vol. 4, no. 2, p. 1800477, Feb. 2019, doi: 10.1002/ADMT.201800477.

[35] N. Elango and A. A. M. Faudzi, "A review article: investigations on soft materials for soft robot manipulations," *Int. J. Adv. Manuf. Technol. 2015 805*, vol. 80, no. 5, pp. 1027–1037, Apr. 2015, doi: 10.1007/S00170-015-7085-3.

[36] X. Jing, S. Chen, C. Zhang, and F. Xie, "Increasing Bending Performance of Soft Actuator by Silicon Rubbers of Multiple Hardness," *Mach. 2022, Vol. 10, Page 272*, vol. 10, no. 4, p. 272, Apr. 2022, doi: 10.3390/MACHINES10040272.

[37] M. Bustamante-Torres, D. Romero-Fierro, B. Arcentales-Vera, S. Pardo, and E. Bucio,

"Interaction between Filler and Polymeric Matrix in Nanocomposites: Magnetic Approach and Applications," *Polym. 2021, Vol. 13, Page 2998*, vol. 13, no. 17, p. 2998, Sep. 2021, doi: 10.3390/POLYM13172998.

[38] P. Polygerinos, Z. Wang, K. Galloway, B. Overvelde, and R. Wood, "Soft Elastomeric Actuators with Fiber Reinforcement," *Mater. Res. Soc.*, p. 2, 2013.

[39] R. V. Ramanujan and L. L. Lao, "The mechanical behavior of smart magnet–hydrogel composites," *Smart Mater. Struct.*, vol. 15, no. 4, p. 952, Jun. 2006, doi: 10.1088/0964-1726/15/4/008.

[40] A. Charalambides, S. Bergbreiter, A. Charalambides, and S. Bergbreiter, "Rapid Manufacturing of Mechanoreceptive Skins for Slip Detection in Robotic Grasping," *Adv. Mater. Technol.*, vol. 2, no. 1, p. 1600188, Jan. 2017, doi: 10.1002/ADMT.201600188.

[41] S. Park *et al.*, "Silicones for Stretchable and Durable Soft Devices: Beyond Sylgard-184," *ACS Appl. Mater. Interfaces*, vol. 10, no. 13, pp. 11261–11268, Apr. 2018, doi: 10.1021/ACSAMI.7B18394/ASSET/IMAGES/LARGE/AM-2017-18394K_0006.JPEG.

[42] J.-Y. Sun *et al.*, "Ionic skin," *Adv. Mater.*, vol. 26, no. 45, pp. 7608–7614, Dec. 2014, doi: 10.1002/ADMA.201403441.

[43] M. D. Bartlett, A. Fassler, N. Kazem, E. J. Markvicka, P. Mandal, and C. Majidi, "Liquid Metals: Stretchable, High-k Dielectric Elastomers through Liquid-Metal Inclusions (Adv. Mater. 19/2016)," *Adv. Mater.*, vol. 28, no. 19, pp. 3791–3791, May 2016, doi: 10.1002/ADMA.201670133.

[44] Y. Chen, J. Zhang, and Y. Gong, "Utilizing Anisotropic Fabrics Composites for High-

Strength Soft Manipulator Integrating Soft Gripper," *IEEE Access*, vol. 7, pp. 127416–127426, 2019, doi: 10.1109/ACCESS.2019.2940499.

[45] C. Thalman, T. Hertzell, H. L.-2020 3rd I. International, and undefined 2020, "Toward a soft robotic ankle-foot orthosis (sr-afo) exosuit for human locomotion: Preliminary results in late stance plantarflexion assistance," *ieeexplore.ieee.org*, Accessed: Sep. 20, 2022. [Online]. Available: https://ieeexplore.ieee.org/abstract/document/9116050/

[46] F. Z. Low, R. C. H. Yeow, H. K. Yap, and J. H. Lim, "Study on the use of soft ankle-foot exoskeleton for alternative mechanical prophylaxis of deep vein thrombosis," *IEEE Int. Conf. Rehabil. Robot.*, vol. 2015-September, pp. 589–593, Sep. 2015, doi: 10.1109/ICORR.2015.7281264.

[47] R. Ezzibdeh, P. Arora, and D. F. Amanatullah, "Utilization of a pneumatic exoskeleton after total knee arthroplasty," *Arthroplast. Today*, vol. 5, no. 3, pp. 314–315, Sep. 2019, doi: 10.1016/J.ARTD.2019.02.008.

[48] J. Fang *et al.*, "Novel Accordion-Inspired Foldable Pneumatic Actuators for Knee Assistive Devices," *Soft Robot.*, vol. 7, no. 1, pp. 95–108, Feb. 2020, doi: 10.1089/SORO.2018.0155/ASSET/IMAGES/LARGE/SORO.2018.0155_FIGURE10.JPEG.

[49] H. K. Yap, J. H. Lim, F. Nasrallah, J. Cho Hong Goh, and C. H. Yeow, "Characterisation and evaluation of soft elastomeric actuators for hand assistive and rehabilitation applications," *J. Med. Eng. Technol.*, vol. 40, no. 4, pp. 199–209, 2016, doi: 10.3109/03091902.2016.1161853.

[50] P. H. Nguyen, I. I. B. Mohd, K. Duford, X. Bao, and W. Zhang, "Design, fabrication, and characterization of a helical twisting, contracting, and bending fabric soft continuum actuator," *2021 IEEE 4th Int. Conf. Soft Robot. RoboSoft 2021*, pp. 567–570, Apr. 2021,

doi: 10.1109/ROBOSOFT51838.2021.9479350.

[51] T. Abe, S. Koizumi, H. Nabae, G. Endo, and K. Suzumori, “Muscle textile to implement soft suit to shift balancing posture of the body,” *2018 IEEE Int. Conf. Soft Robot. RoboSoft 2018*, pp. 572–578, Jul. 2018, doi: 10.1109/ROBOSOFT.2018.8405387.

[52] L. J. Romasanta, M. A. Lopez-Manchado, and R. Verdejo, “Increasing the performance of dielectric elastomer actuators: A review from the materials perspective,” *Prog. Polym. Sci.*, vol. 51, pp. 188–211, Dec. 2015, doi: 10.1016/J.PROGPOLYMSCI.2015.08.002.

[53] H. Shigemune *et al.*, “Dielectric Elastomer Actuators with Carbon Nanotube Electrodes Painted with a Soft Brush,” *Actuators 2018, Vol. 7, Page 51*, vol. 7, no. 3, p. 51, Aug. 2018, doi: 10.3390/ACT7030051.

[54] H. F. Schlaak, M. Jungmann, M. Matysek, and P. Lotz, “Novel multilayer electrostatic solid state actuators with elastic dielectric (Invited Paper),” *Smart Struct. Mater. 2005 Electroact. Polym. Actuators Devices*, vol. 5759, p. 121, May 2005, doi: 10.1117/12.604468.

[55] C. Keplinger, T. Li, R. Baumgartner, Z. Suo, and S. Bauer, “Harnessing snap-through instability in soft dielectrics to achieve giant voltage-triggered deformation,” *Soft Matter*, vol. 8, no. 2, pp. 285–288, Dec. 2011, doi: 10.1039/C1SM06736B.

[56] J. Kunze *et al.*, “Design and fabrication of silicone-based dielectric elastomer rolled actuators for soft robotic applications,” *https://doi.org/10.1117/12.2558444*, vol. 11375, pp. 287–294, Apr. 2020, doi: 10.1117/12.2558444.

[57] C. Rendl *et al.*, “FlexSense,” pp. 129–138, Oct. 2014, doi: 10.1145/2642918.2647405.

[58] G. Rizzello *et al.*, “Closed loop control of dielectric elastomer actuators based on self-

sensing displacement feedback," *iopscience.iop.org*, 2017, doi: 10.1088/0964-1726/25/3/035034.

[59] U. Gupta, L. Qin, Y. Wang, … H. G.-S. M. and, and undefined 2019, "Soft robots based on dielectric elastomer actuators: A review," *iopscience.iop.org*, Accessed: Sep. 20, 2022. [Online]. Available: https://iopscience.iop.org/article/10.1088/1361-665X/ab3a77/meta

[60] Y. Bar-Cohen and I. A. Anderson, "Electroactive polymer (EAP) actuators—background review," *Mech. Soft Mater. 2019 11*, vol. 1, no. 1, pp. 1–14, Mar. 2019, doi: 10.1007/S42558-019-0005-1.

[61] M. Yamada, Y. Murakami, T. Kawashima, and M. Nagao, "Electrical breakdown of dielectric elastomer and its lamination effect," *2014 IEEE Conf. Electr. Insul. Dielectr. Phenomena, CEIDP 2014*, pp. 126–129, Dec. 2014, doi: 10.1109/CEIDP.2014.6995795.

[62] S. Lenz, B. Holz, S. Hau, and S. Seelecke, "Development of a high voltage source for dielectric elastomer actuators (DEA)," *ACTUATOR 2018 - 16th Int. Conf. Exhib. New Actuators Drive Syst. Conf. Proc.*, no. June, pp. 196–199, 2018.

[63] Y. Wang, T. Sugino, Y. Wang, and T. Sugino, "Ionic Polymer Actuators: Principle, Fabrication and Applications," *Actuators*, Mar. 2018, doi: 10.5772/INTECHOPEN.75085.

[64] L. Chang *et al.*, "Ionic Electroactive Polymers Used in Bionic Robots: A Review," *J. Bionic Eng. 2018 155*, vol. 15, no. 5, pp. 765–782, Sep. 2018, doi: 10.1007/S42235-018-0065-1.

[65] E. Roels *et al.*, "Processing of Self-Healing Polymers for Soft Robotics," *Adv. Mater.*,

vol. 34, no. 1, p. 2104798, Jan. 2022, doi: 10.1002/ADMA.202104798.

[66] M. Luqman, A. Anis, H. M. Shaikh, S. M. Al-Zahrani, and M. A. Alam, “Development of a Soft Robotic Bending Actuator Based on a Novel Sulfonated Polyvinyl Chloride–Phosphotungstic Acid Ionic Polymer–Metal Composite (IPMC) Membrane,” *Membr. 2022, Vol. 12, Page 651*, vol. 12, no. 7, p. 651, Jun. 2022, doi: 10.3390/MEMBRANES12070651.

[67] H.-J. Chung, A. M. Parsons, and L. Zheng, “Magnetically Controlled Soft Robotics Utilizing Elastomers and Gels in Actuation: A Review,” *Adv. Intell. Syst.*, vol. 3, no. 3, p. 2000186, Mar. 2021, doi: 10.1002/AISY.202000186.

[68] H. Zhang *et al.*, “Smart gripper based on electric-triggered superhydrophobic polyurethane arrays coated bucky gel composite membrane for reversible capture/release of both solid and liquid,” *Chem. Eng. J.*, vol. 417, p. 128072, Aug. 2021, doi: 10.1016/J.CEJ.2020.128072.

[69] T. Huang *et al.*, “A Lightweight Flexible Semi-Cylindrical Valve for Seamless Integration in Soft Robots Based on the Giant Electrorheological Fluid,” *SSRN Electron. J.*, Jul. 2022, doi: 10.2139/SSRN.4164529.

[70] Y. Liang *et al.*, “Efficient Electrorheological Technology for Materials, Energy, and Mechanical Engineering: From Mechanisms to Applications,” *Engineering*, May 2022, doi: 10.1016/J.ENG.2022.01.014.

[71] E. M. Sierra and J. L. Ordoñez-Avila, “Mathematical Modeling of a Multi-Chamber Pneumatic Soft Actuator,” *Actuators 2022, Vol. 11, Page 221*, vol. 11, no. 8, p. 221, Aug. 2022, doi: 10.3390/ACT11080221.

[72] Y. Luo *et al.*, “Digital Fabrication of Pneumatic Actuators with Integrated Sensing by

Machine Knitting; Digital Fabrication of Pneumatic Actuators with Integrated Sensing by Machine Knitting," *CHI Conf. Hum. Factors Comput. Syst.*, 2022, doi: 10.1145/3491102.

[73] F. Connolly, P. Polygerinos, C. J. Walsh, and K. Bertoldi, "Mechanical Programming of Soft Actuators by Varying Fiber Angle," *Soft Robot.*, vol. 2, no. 1, pp. 26–32, Mar. 2015, doi: 10.1089/soro.2015.0001.

[74] B. Wang, K. C. Aw, M. Biglari-Abhari, and A. McDaid, "Design and fabrication of a fiber-reinforced pneumatic bending actuator," in *2016 IEEE International Conference on Advanced Intelligent Mechatronics (AIM)*, IEEE, Jul. 2016, pp. 83–88. doi: 10.1109/AIM.2016.7576747.

[75] P. Polygerinos, Z. Wang, K. C. Galloway, R. J. Wood, and C. J. Walsh, "Soft robotic glove for combined assistance and at-home rehabilitation," *Rob. Auton. Syst.*, vol. 73, pp. 135–143, Nov. 2015, doi: 10.1016/j.robot.2014.08.014.

[76] B. Jamil and Y. Choi, "Modified Stiffness-Based Soft Optical Waveguide Integrated Pneumatic Artificial Muscle (PAM) Actuators for Contraction and Force Sensing," *IEEE/ASME Trans. Mechatronics*, vol. 26, no. 6, pp. 3243–3253, Dec. 2021, doi: 10.1109/TMECH.2021.3056563.

[77] Y. Yang, Z. He, G. Lin, H. Wang, and P. Jiao, "Large deformation mechanics of the thrust performances generated by combustion-enabled soft actuators," *Int. J. Mech. Sci.*, vol. 229, p. 107513, Sep. 2022, doi: 10.1016/J.IJMECSCI.2022.107513.

[78] J. Kim, K. Luo, and Z. Suo, "A Chemical Pump that Generates High-Pressure Gas by Transmitting Liquid Fuel against Pressure Gradient," *Adv. Intell. Syst.*, vol. 4, no. 5, p. 2100246, May 2022, doi: 10.1002/AISY.202100246.

[79] G. Chen, X. Yang, X. Zhang, and H. Hu, “Water hydraulic soft actuators for underwater autonomous robotic systems,” *Appl. Ocean Res.*, vol. 109, p. 102551, Apr. 2021, doi: 10.1016/J.APOR.2021.102551.

[80] H. Yuk, S. Lin, C. Ma, M. Takaffoli, N. X. Fang, and X. Zhao, “Hydraulic hydrogel actuators and robots optically and sonically camouflaged in water,” *Nat. Commun. 2017 81*, vol. 8, no. 1, pp. 1–12, Feb. 2017, doi: 10.1038/ncomms14230.

[81] S. Nie, L. Huo, H. Ji, Y. Lan, and Z. Wu, “Bending deformation characteristics of high-pressure soft actuator driven by water-hydraulics for underwater manipulator,” *Sensors Actuators A Phys.*, vol. 344, p. 113736, Sep. 2022, doi: 10.1016/J.SNA.2022.113736.

[82] Y. Yang, Y. Chen, Y. Li, Z. Wang, and Y. Li, “Novel Variable-Stiffness Robotic Fingers with Built-In Position Feedback,” *Soft Robot.*, vol. 4, no. 4, pp. 338–352, Dec. 2017, doi: 10.1089/SORO.2016.0060/SUPPL_FILE/SUPP_VIDEO1.ZIP.

[83] P. Glick, S. A. Suresh, D. Ruffatto, M. Cutkosky, M. T. Tolley, and A. Parness, “A Soft Robotic Gripper with Gecko-Inspired Adhesive,” *IEEE Robot. Autom. Lett.*, vol. 3, no. 2, pp. 903–910, Apr. 2018, doi: 10.1109/LRA.2018.2792688.

[84] N. Bira *et al.*, “Investigation on a soft grasping gripper based on dielectric elastomer actuators,” *Smart Mater. Struct.*, vol. 28, no. 3, p. 035009, Feb. 2019, doi: 10.1088/1361-665X/AAF767.

[85] M. Luo *et al.*, “A Single-Chamber Pneumatic Soft Bending Actuator with Increased Stroke-Range by Local Electric Guidance,” *IEEE Trans. Ind. Electron.*, vol. 68, no. 9, pp. 8455–8463, Sep. 2021, doi: 10.1109/TIE.2020.3013544.

[86] Y. Li *et al.*, “Design of Isometric and Isotonic Soft Hand for Rehabilitation Combining with Noninvasive Brain Machine Interface,” *2018 15th Int. Conf. Ubiquitous Robot. UR*

2018, pp. 749–754, 2018, doi: 10.1109/URAI.2018.8441816.

[87] Y. Kim and Y. Cha, "Soft Pneumatic Gripper With a Tendon-Driven Soft Origami Pump," *Front. Bioeng. Biotechnol.*, vol. 8, p. 461, May 2020, doi: 10.3389/FBIOE.2020.00461/BIBTEX.

[88] M. A. Bell, B. Gorissen, K. Bertoldi, J. C. Weaver, and R. J. Wood, "A Modular and Self-Contained Fluidic Engine for Soft Actuators," *Adv. Intell. Syst.*, vol. 4, no. 1, p. 2100094, Jan. 2022, doi: 10.1002/AISY.202100094.

[89] A. Pagoli, F. Chapelle, J. A. Corrales, Y. Mezouar, and Y. Lapusta, "A Soft Robotic Gripper with an Active Palm and Reconfigurable Fingers for Fully Dexterous In-Hand Manipulation ∗," *IEEE Robot. Autom. Lett.*, vol. 6, no. 4, pp. 7706–7713, Oct. 2021, doi: 10.1109/LRA.2021.3098803.

[90] A. Pagoli, F. Chapelle, J. A. Corrales-Ramon, Y. Mezouar, and Y. Lapusta, "Design and Optimization of a Dextrous Robotic Finger: Incorporating a Sliding, Rotating, and Soft-Bending Mechanism while Maximizing Dexterity and Minimizing Dimensions," *IEEE Robot. Autom. Mag.*, vol. 27, no. 4, pp. 56–64, Dec. 2020, doi: 10.1109/MRA.2020.3024283.

[91] J. Guo, K. Elgeneidy, C. Xiang, N. Lohse, L. Justham, and J. Rossiter, "Soft pneumatic grippers embedded with stretchable electroadhesion," *Smart Mater. Struct.*, vol. 27, no. 5, p. 055006, Mar. 2018, doi: 10.1088/1361-665X/AAB579.

[92] Y. S. Narang, J. J. Vlassak, R. D. Howe, Y. S. Narang, J. J. Vlassak, and R. D. Howe, "Mechanically Versatile Soft Machines through Laminar Jamming," *Adv. Funct. Mater.*, vol. 28, no. 17, p. 1707136, Apr. 2018, doi: 10.1002/ADFM.201707136.

[93] Y. Yang, Y. Zhang, Z. Kan, J. Zeng, and M. Y. Wang, "Hybrid Jamming for Bioinspired

Soft Robotic Fingers," *Soft Robot.*, vol. 7, no. 3, pp. 292–308, Jun. 2020, doi: 10.1089/SORO.2019.0093/ASSET/IMAGES/LARGE/SORO.2019.0093_FIGURE15.JPEG.

[94] Y. Chen, Y. Li, Y. Li, and Y. Wang, "Stiffening of soft robotic actuators-Jamming approaches," *2017 IEEE Int. Conf. Real-Time Comput. Robot. RCAR 2017*, vol. 2017-July, pp. 17–21, Mar. 2018, doi: 10.1109/RCAR.2017.8311829.

[95] I. De Falco, M. Cianchetti, and A. Menciassi, "A soft multi-module manipulator with variable stiffness for minimally invasive surgery," *Bioinspir. Biomim.*, vol. 12, no. 5, p. 056008, Sep. 2017, doi: 10.1088/1748-3190/AA7CCD.

[96] M. Yu, W. Yang, Y. Yu, X. Cheng, and Z. Jiao, "A Crawling Soft Robot Driven by Pneumatic Foldable Actuators Based on Miura-Ori," *Actuators 2020, Vol. 9, Page 26*, vol. 9, no. 2, p. 26, Apr. 2020, doi: 10.3390/ACT9020026.

[97] A. Jemima, C. Raghavendran, and H. Chetan, "SOFT ROBOTICS: A Bio-Inspired Revolution," *Proc. B-HTC 2020 - 1st IEEE Bangalore Humanit. Technol. Conf.*, Oct. 2020, doi: 10.1109/B-HTC50970.2020.9297869.

[98] J. Liu, Z. Ma, Y. Wang, and S. Zuo, "Reconfigurable Self-Sensing Pneumatic Artificial Muscle with Locking Ability Based on Modular Multi-Chamber Soft Actuator," *IEEE Robot. Autom. Lett.*, vol. 7, no. 4, pp. 8635–8642, Oct. 2022, doi: 10.1109/LRA.2022.3189154.

[99] G. Gu, D. Wang, L. Ge, and X. Zhu, "Analytical Modeling and Design of Generalized Pneu-Net Soft Actuators with Three-Dimensional Deformations," *Soft Robot.*, vol. 8, no. 4, pp. 462–477, Aug. 2021, doi: 10.1089/SORO.2020.0039/ASSET/IMAGES/LARGE/SORO.2020.0039_FIGURE12.JPEG.

[100] G. Miron, B. Bédard, and J. S. Plante, “Sleeved Bending Actuators for Soft Grippers: A Durable Solution for High Force-to-Weight Applications,” *Actuators 2018, Vol. 7, Page 40*, vol. 7, no. 3, p. 40, Jul. 2018, doi: 10.3390/ACT7030040.

[101] T. Wang, L. Ge, and G. Gu, “Programmable design of soft pneu-net actuators with oblique chambers can generate coupled bending and twisting motions,” *Sensors Actuators A Phys.*, vol. 271, pp. 131–138, Mar. 2018, doi: 10.1016/J.SNA.2018.01.018.

[102] M. Tiboni and C. Amici, “Soft Gloves: A Review on Recent Developments in Actuation, Sensing, Control and Applications,” *Actuators 2022, Vol. 11, Page 232*, vol. 11, no. 8, p. 232, Aug. 2022, doi: 10.3390/ACT11080232.

[103] N. Guo *et al.*, “Simulation analysis for optimal design of pneumatic bellow actuators for soft-robotic glove,” *Biocybern. Biomed. Eng.*, vol. 40, no. 4, pp. 1359–1368, Oct. 2020, doi: 10.1016/J.BBE.2020.08.002.

[104] C. Thalman and P. Artemiadis, “A review of soft wearable robots that provide active assistance: Trends, common actuation methods, fabrication, and applications,” *Wearable Technol.*, vol. 1, p. e3, 2020, Accessed: Sep. 26, 2022. [Online]. Available: https://doi.org/10.1017/wtc.2020.4

[105] Y. L. Park, J. Santos, K. G. Galloway, E. C. Goldfield, and R. J. Wood, “A soft wearable robotic device for active knee motions using flat pneumatic artificial muscles,” *Proc. - IEEE Int. Conf. Robot. Autom.*, pp. 4805–4810, Sep. 2014, doi: 10.1109/ICRA.2014.6907562.

[106] S. Liu *et al.*, “Otariidae-Inspired Soft-Robotic Supernumerary Flippers by Fabric Kirigami and Origami,” *IEEE/ASME Trans. Mechatronics*, vol. 26, no. 5, pp. 2747–2757, Oct. 2021, doi: 10.1109/TMECH.2020.3045476.

[107] S. Chen *et al.*, “Topology Optimization of Skeleton-Reinforced Soft Pneumatic Actuators for Desired Motions,” *IEEE/ASME Trans. Mechatronics*, vol. 26, no. 4, pp. 1745–1753, Aug. 2021, doi: 10.1109/TMECH.2021.3071394.

[108] Y. Sun, H. Feng, I. R. Manchester, R. C. H. Yeow, and P. Qi, “Static Modeling of the Fiber-Reinforced Soft Pneumatic Actuators Including Inner Compression: Bending in Free Space, Block Force, and Deflection upon Block Force,” *Soft Robot.*, vol. 9, no. 3, pp. 451–472, Jun. 2022, doi: 10.1089/SORO.2020.0081/ASSET/IMAGES/LARGE/SORO.2020.0081_FIGURE10.JPEG.

[109] A. Baranwal and P. K. Agnihotri, “Harnessing fiber induced anisotropy in design and fabrication of soft actuator with simultaneous bending and twisting actuations,” *Compos. Sci. Technol.*, vol. 230, p. 109724, Nov. 2022, doi: 10.1016/J.COMPSCITECH.2022.109724.

[110] P. Rothemund, S. Kirkman, and C. Keplinger, “Dynamics of electrohydraulic soft actuators,” *Proc. Natl. Acad. Sci. U. S. A.*, vol. 117, no. 28, pp. 16207–16213, Jul. 2020, doi: 10.1073/PNAS.2006596117/SUPPL_FILE/PNAS.2006596117.SM03.AVI.

[111] S. Liu, J. Jiao, F. Meng, T. Mei, X. Sun, and W. Kong, “Modelling of a soft actuator with a semicircular cross section under gravity and external load,” *IEEE Trans. Ind. Electron.*, 2022, doi: 10.1109/TIE.2022.3183334.

[112] Y. Sun, Y. S. Song, and J. Paik, “Characterization of silicone rubber based soft pneumatic actuators,” *IEEE Int. Conf. Intell. Robot. Syst.*, pp. 4446–4453, 2013, doi: 10.1109/IROS.2013.6696995.

[113] M. Memarian, R. Gorbet, and D. Kulic, “Modelling and experimental analysis of a novel design for soft pneumatic artificial muscles,” *IEEE Int. Conf. Intell. Robot. Syst.*, vol.

2015-Decem, pp. 1718–1724, Dec. 2015, doi: 10.1109/IROS.2015.7353599.

[114] B. Mosadegh *et al.*, "Pneumatic networks for soft robotics that actuate rapidly," *Adv. Funct. Mater.*, vol. 24, no. 15, pp. 2163–2170, Apr. 2014, doi: 10.1002/adfm.201303288.

[115] R. V. Martinez, C. R. Fish, X. Chen, and G. M. Whitesides, "Elastomeric Origami: Programmable Paper-Elastomer Composites as Pneumatic Actuators," *Adv. Funct. Mater.*, vol. 22, no. 7, pp. 1376–1384, Apr. 2012, doi: 10.1002/ADFM.201102978.

[116] P. Tran *et al.*, "FLEXotendon Glove-III: Voice-Controlled Soft Robotic Hand Exoskeleton With Novel Fabrication Method and Admittance Grasping Control," *IEEE/ASME Trans. Mechatronics*, 2022, doi: 10.1109/TMECH.2022.3148032.

[117] Y. Dong *et al.*, "Untethered small-scale magnetic soft robot with programmable magnetization and integrated multifunctional modules," *Sci. Adv.*, vol. 8, no. 25, p. 8932, Jun. 2022, doi: 10.1126/SCIADV.ABN8932/SUPPL_FILE/SCIADV.ABN8932_MOVIES_S1_TO_S7.ZIP.

[118] R. F. Shepherd *et al.*, "Multigait soft robot.," *Proc. Natl. Acad. Sci. U. S. A.*, vol. 108, no. 51, pp. 20400–3, Dec. 2011, doi: 10.1073/pnas.1116564108.

[119] Z. Chen, A. Zou, Z. Qin, X. Han, T. Li, and S. Liu, "Modeling and Fabrication of Soft Actuators Based on Fiber-Reinforced Elastomeric Enclosures," *Actuators 2021, Vol. 10, Page 127*, vol. 10, no. 6, p. 127, Jun. 2021, doi: 10.3390/ACT10060127.

[120] P. Polygerinos, K. C. Galloway, E. Savage, M. Herman, K. O. Donnell, and C. J. Walsh, "Soft robotic glove for hand rehabilitation and task specific training," in *2015 IEEE International Conference on Robotics and Automation (ICRA)*, IEEE, May 2015, pp.

2913–2919. doi: 10.1109/ICRA.2015.7139597.

[121] G. Bao *et al.*, “Soft Robotics: Academic Insights and Perspectives Through Bibliometric Analysis.,” *Soft Robot.*, vol. 5, no. 3, pp. 229–241, Jun. 2018, doi: 10.1089/soro.2017.0135.

[122] M. Cianchetti *et al.*, “Soft Robotics Technologies to Address Shortcomings in Today’s Minimally Invasive Surgery: The STIFF-FLOP Approach,” *Soft Robot.*, vol. 1, no. 2, pp. 122–131, 2014, doi: 10.1089/soro.2014.0001.

[123] M. Fani and A. Ghanbary, “Clinical and Laboratory Assessments of the Scapula: A Review Article,” 2022, Accessed: Sep. 28, 2022. [Online]. Available: https://jpsr.mums.ac.ir/article_19753.html

[124] J. Kim, J. Kim, Y. Jung, D. Lee, and J. Bae, “A Passive Upper Limb Exoskeleton With Tilted and Offset Shoulder Joints for Assisting Overhead Tasks,” *IEEE/ASME Trans. Mechatronics*, 2022, doi: 10.1109/TMECH.2022.3169617.

[125] S. Sridar *et al.*, “Soft Robotic Shoulder Assist Device: Towards Prevention of Shoulder Overuse Syndrome in Wheelchair Users,” *Front. Biomed. Devices, BIOMED - 2018 Des. Med. Devices Conf. DMD 2018*, Jun. 2018, doi: 10.1115/DMD2018-6808.

[126] S. Magnetti Gisolo, G. G. Muscolo, M. Paterna, C. De Benedictis, and C. Ferraresi, “Feasibility study of a passive pneumatic exoskeleton for upper limbs based on a mckibben artificial muscle,” *Mech. Mach. Sci.*, vol. 102, pp. 208–217, 2021, doi: 10.1007/978-3-030-75259-0_23/FIGURES/6.

[127] Y. Huang, Y. Chen, X. Zhang, H. Zhang, C. Song, and J. Ota, “A Novel Cable-Driven 7-DOF Anthropomorphic Manipulator,” *IEEE/ASME Trans. Mechatronics*, vol. 26, no. 4, pp. 2174–2185, Aug. 2021, doi: 10.1109/TMECH.2020.3033309.

[128] C. Fu, Z. Xia, C. Hurren, A. Nilghaz, and X. Wang, “Textiles in soft robots: Current progress and future trends,” *Biosens. Bioelectron.*, vol. 196, p. 113690, Jan. 2022, doi: 10.1016/J.BIOS.2021.113690.

[129] I. Sahin, J. Dube, C. Mucchiani, K. Karydis, and E. Kokkoni, “A Bidirectional Fabric-based Pneumatic Actuator for the Infant Shoulder: Design and Comparative Kinematic Analysis,” Jun. 2022, doi: 10.48550/arxiv.2206.10773.

[130] A. Z. Rao and M. A. Hasan, “Evaluation of a Chair-Mounted Passive Trunk Orthosis: A Pilot Study on Able-Bodied Subjects,” *Sensors 2021, Vol. 21, Page 8366*, vol. 21, no. 24, p. 8366, Dec. 2021, doi: 10.3390/S21248366.

[131] J. won Lee and G. Kim, “Design and Control of a Lifting Assist Device for Preventing Lower Back Injuries in Industrial Athletes,” *Int. J. Precis. Eng. Manuf.*, vol. 20, no. 10, pp. 1825–1838, Oct. 2019, doi: 10.1007/S12541-019-00183-0/FIGURES/15.

[132] P. M. Kuber and E. Rashedi, “Towards Reducing Risk of Injury in Nursing: Design and Analysis of a New Passive Exoskeleton for Torso Twist Assist,” *https://doi.org/10.1177/2327857921101141*, vol. 10, no. 1, pp. 217–222, Jul. 2021, doi: 10.1177/2327857921101141.

[133] M. Gorsic, Y. Song, A. P. Johnson, B. Dai, and D. Novak, “Simultaneously varying back stiffness and trunk compression in a passive trunk exoskeleton during different activities: A pilot study,” *Proc. Annu. Int. Conf. IEEE Eng. Med. Biol. Soc. EMBS*, pp. 4886–4890, 2021, doi: 10.1109/EMBC46164.2021.9630081.

[134] C. Ophaswongse, “Design of Wheelchair Robot for Active Postural Support (WRAPS) for Users with Trunk Impairments,” 2021.

[135] N. Lotti *et al.*, “Myoelectric or Force Control? A Comparative Study on a Soft Arm

Exosuit," *IEEE Trans. Robot.*, vol. 38, no. 3, pp. 1363–1379, Jun. 2022, doi: 10.1109/TRO.2021.3137748.

[136] M. A. Laribi, M. Ceccarelli, J. Sandoval, M. Bottin, and G. Rosati, "Experimental Validation of Light Cable-Driven Elbow-Assisting Device L-CADEL Design," *J. Bionic Eng. 2021 192*, vol. 19, no. 2, pp. 416–428, Jan. 2022, doi: 10.1007/S42235-021-00133-5.

[137] J. Nassour and F. Hamker, "Enfolded textile actuator for soft wearable robots," *2019 IEEE Int. Conf. Cyborg Bionic Syst. CBS 2019*, pp. 60–65, Sep. 2019, doi: 10.1109/CBS46900.2019.9114425.

[138] C. M. Thalman, Q. P. Lam, P. H. Nguyen, S. Sridar, and P. Polygerinos, "A Novel Soft Elbow Exosuit to Supplement Bicep Lifting Capacity," *IEEE Int. Conf. Intell. Robot. Syst.*, pp. 6965–6971, Dec. 2018, doi: 10.1109/IROS.2018.8594403.

[139] T. A. Burkhart and D. M. Andrews, "The Effectiveness of Wrist Guards for Reducing Wrist and Elbow Accelerations Resulting from Simulated Forward Falls," *J. Appl. Biomech.*, vol. 26, no. 3, pp. 281–289, Aug. 2010, doi: 10.1123/JAB.26.3.281.

[140] D. Chiaradia, L. Tiseni, M. Xiloyannis, M. Solazzi, L. Masia, and A. Frisoli, "An Assistive Soft Wrist Exosuit for Flexion Movements With an Ergonomic Reinforced Glove," *Front. Robot. AI*, vol. 7, p. 182, Jan. 2021, doi: 10.3389/FROBT.2020.595862/BIBTEX.

[141] Y. Liu, Y. Chen, H. Li, and J. Dong, "Design an Augmentation Exoskeleton to Enhance Lifting Strength," *ASME Int. Mech. Eng. Congr. Expo. Proc.*, vol. 6, Feb. 2021, doi: 10.1115/IMECE2020-24658.

[142] W. Machold, O. Kwasny, … P. E.-J. of T., and undefined 2002, "Reduction of severe

wrist injuries in snowboarding by an optimized wrist protection device: a prospective randomized trial," *journals.lww.com*, Accessed: Oct. 11, 2022. [Online]. Available: https://journals.lww.com/jtrauma/Fulltext/2002/03000/Letters_To_the_Editor.16.aspx

[143] T. Aghil, S. Rahul, S. Buvan Kumaar, Y. Vijay, S. Tharun Kumar, and B. Sidhharth, "A Futuristic Approach for Stroke Rehabilitation Using Smart Gloves," *J. Phys. Conf. Ser.*, vol. 2115, no. 1, p. 012025, Nov. 2021, doi: 10.1088/1742-6596/2115/1/012025.

[144] F. Aggogeri, T. Mikolajczyk, and J. O'Kane, "Robotics for rehabilitation of hand movement in stroke survivors," *https://doi.org/10.1177/1687814019841921*, vol. 11, no. 4, pp. 1–14, Apr. 2019, doi: 10.1177/1687814019841921.

[145] R. Moya-Jiménez, T. Magal-Royo, D. Ponce, M. Flores, and M. Caiza, "Hand Exoskeleton Design for the Rehabilitation of Patients with Rheumatoid Arthritis," *Commun. Comput. Inf. Sci.*, vol. 1307, pp. 12–21, 2020, doi: 10.1007/978-3-030-62833-8_2/FIGURES/2.

[146] M. Sarac, M. Solazzi, and A. Frisoli, "Design Requirements of Generic Hand Exoskeletons and Survey of Hand Exoskeletons for Rehabilitation, Assistive, or Haptic Use," *IEEE Trans. Haptics*, vol. 12, no. 4, pp. 400–413, Oct. 2019, doi: 10.1109/TOH.2019.2924881.

[147] H. Al-Fahaam, S. Davis, S. Nefti-Meziani, and T. Theodoridis, "Novel soft bending actuator-based power augmentation hand exoskeleton controlled by human intention," *Intell. Serv. Robot.*, vol. 11, no. 3, pp. 247–268, Jul. 2018, doi: 10.1007/S11370-018-0250-4/FIGURES/25.

[148] T. M. Schnieders and R. T. Stone, "A Current Review of Human Factors and Ergonomic Intervention With Exoskeletons," *https://services.igi-global.com/resolvedoi/resolve.aspx?doi=10.4018/978-1-7998-3432-8.ch002*, pp. 12–

34, Jan. 1AD, doi: 10.4018/978-1-7998-3432-8.CH002.

[149] M.-L. Olar, M. Leba, and M. Risteiu, “Exoskeleton - wearable devices. Literature review; Exoskeleton - wearable devices. Literature review”, doi: 10.1051/matecconf/202134205005.

[150] S. Lee *et al.*, “Autonomous multi-joint soft exosuit with augmentation-power-based control parameter tuning reduces energy cost of loaded walking,” *J. Neuroeng. Rehabil.*, vol. 15, no. 1, pp. 1–9, Jul. 2018, doi: 10.1186/S12984-018-0410-Y/FIGURES/7.

[151] H. Xiong and X. Diao, “A review of cable-driven rehabilitation devices,” *https://doi.org/10.1080/17483107.2019.1629110*, vol. 15, no. 8, pp. 885–897, Nov. 2019, doi: 10.1080/17483107.2019.1629110.

[152] Y. Li and M. Hashimoto, “PVC gel soft actuator-based wearable assist wear for hip joint support during walking,” *Smart Mater. Struct.*, vol. 26, no. 12, p. 125003, Oct. 2017, doi: 10.1088/1361-665X/AA9315.

[153] A. L. Kulasekera, R. B. Arumathanthri, D. S. Chathuranga, T. D. Lalitharatne, and R. C. Gopura, “A Low-Profile Vacuum Actuator: Towards a Sit-to-Stand Assist Exosuit,” *2020 3rd IEEE Int. Conf. Soft Robot. RoboSoft 2020*, pp. 110–115, May 2020, doi: 10.1109/ROBOSOFT48309.2020.9115999.

[154] W. Zhang, “Soft Wearable Robotics for Ankle and Lower Body Gait Rehabilitation: Design, Modeling, and Implementation of Fabric-Based Actuators to Assist Human,” 2021.

[155] S. H. Lee *et al.*, “Wearable hip-assist robot modulates cortical activation during gait in stroke patients: a functional near-infrared spectroscopy study,” *J. Neuroeng. Rehabil.*, vol. 17, no. 1, pp. 1–8, Dec. 2020, doi: 10.1186/S12984-020-00777-0/FIGURES/3.

[156] C. Di Natali *et al.*, "Design and Evaluation of a Soft Assistive Lower Limb Exoskeleton," *Robotica*, vol. 37, no. 12, pp. 2014–2034, Dec. 2019, doi: 10.1017/S0263574719000067.

[157] A. McDaid, K. Kora, S. Xie, J. Lutz, and M. Battley, "Human-inspired robotic exoskeleton (HuREx) for lower limb rehabilitation," *2013 IEEE Int. Conf. Mechatronics Autom. IEEE ICMA 2013*, pp. 19–24, 2013, doi: 10.1109/ICMA.2013.6617887.

[158] J. R. J. Greenfield, H. F. Hwang, C. Davies, and A. J. McDaid, "Soft-stop knee brace for rehabilitation from ligament injuries: Design and pilot trial," *IEEE Int. Conf. Rehabil. Robot.*, pp. 352–357, Aug. 2017, doi: 10.1109/ICORR.2017.8009272.

[159] J. Park, J. Choi, S. J. Kim, K. H. Seo, and J. Kim, "Design of an Inflatable Wrinkle Actuator with Fast Inflation/Deflation Responses for Wearable Suits," *IEEE Robot. Autom. Lett.*, vol. 5, no. 3, pp. 3804–3810, Jul. 2020, doi: 10.1109/LRA.2020.2976299.

[160] J. Arnold and H. Lee, "Variable Impedance Control for pHRI: Impact on Stability, Agility, and Human Effort in Controlling a Wearable Ankle Robot," *IEEE Robot. Autom. Lett.*, vol. 6, no. 2, pp. 2429–2436, Apr. 2021, doi: 10.1109/LRA.2021.3062015.

[161] T. H. Chang *et al.*, "A Wearable Ankle Exercise Device for Deep Vein Thrombosis Prevention Using Thin McKibben Muscles," *Proc. IEEE RAS EMBS Int. Conf. Biomed. Robot. Biomechatronics*, vol. 2020-November, pp. 42–47, Nov. 2020, doi: 10.1109/BIOROB49111.2020.9224295.

[162] S. P. M. Babu, A. Sadeghi, A. Mondini, and B. Mazzolai, "Soft sucker shoe for anti-slippage application," *2018 IEEE Int. Conf. Soft Robot. RoboSoft 2018*, pp. 491–496, Jul. 2018, doi: 10.1109/ROBOSOFT.2018.8405374.

[163] L. Gerez, J. Chen, and M. Liarokapis, "On the Development of Adaptive, Tendon-

Driven, Wearable Exo-Gloves for Grasping Capabilities Enhancement," *IEEE Robot. Autom. Lett.*, vol. 4, no. 2, pp. 422–429, Jan. 2019, doi: 10.1109/LRA.2019.2890853Y.

[164] E. Scheme and K. Englehart, "Electromyogram pattern recognition for control of powered upper-limb prostheses: State of the art and challenges for clinical use," *J. Rehabil. Res. Dev.*, vol. 48, no. 6, pp. 643–660, 2011, doi: 10.1682/JRRD.2010.09.0177.

[165] N. El-Atab *et al.*, "Soft Actuators for Soft Robotic Applications: A Review," *Adv. Intell. Syst.*, vol. 2, no. 10, p. 2000128, Oct. 2020, doi: 10.1002/AISY.202000128.

[166] M. Li, A. Pal, A. Aghakhani, A. Pena-Francesch, and M. Sitti, "Soft actuators for real-world applications," *Nat. Rev. Mater. 2021 73*, vol. 7, no. 3, pp. 235–249, Nov. 2021, doi: 10.1038/s41578-021-00389-7.

[167] M. Pan *et al.*, "Soft Actuators and Robotic Devices for Rehabilitation and Assistance," *Adv. Intell. Syst.*, vol. 4, no. 4, p. 2100140, Apr. 2022, doi: 10.1002/AISY.202100140.

[168] P. Boyraz, G. Runge, and A. Raatz, "An overview of novel actuators for soft robotics," *High-Throughput*, vol. 7, no. 3, Sep. 2018, doi: 10.3390/ACT7030048.

[169] N. K. Persson, J. G. Martinez, Y. Zhong, A. Maziz, and E. W. H. Jager, "Actuating Textiles: Next Generation of Smart Textiles," *Adv. Mater. Technol.*, vol. 3, no. 10, p. 1700397, Oct. 2018, doi: 10.1002/ADMT.201700397.

[170] "Artificial Life Approach to Interactive Architecture - ProQuest." https://www.proquest.com/docview/2675222970?pq-origsite=gscholar&fromopenview=true (accessed Jul. 19, 2023).

[171] B. Wang, A. McDaid, T. Giffney, M. Biglari-Abhari, and K. C. Aw, "Design, modelling and simulation of soft grippers using new bimorph pneumatic bending actuators," *Cogent Eng.*, vol. 4, no. 1, p. 1285482, Jan. 2017, doi:

10.1080/23311916.2017.1285482.

[172] B. Wang, A. Mcdaid, M. Biglari-Abhari, and K. C. Aw, “Design and development of a glove for post-stroke hand rehabilitation,” *IEEE/ASME Int. Conf. Adv. Intell. Mechatronics, AIM*, pp. 1047–1051, Aug. 2017, doi: 10.1109/AIM.2017.8014157.

[173] B. Wang, A. McDaid, M. Biglari-Abhari, T. Giffney, and K. Aw, “A bimorph pneumatic bending actuator by control of fiber braiding angle,” *Sensors Actuators A Phys.*, vol. 257, pp. 173–184, Apr. 2017, doi: 10.1016/j.sna.2017.02.003.

[174] D. Steck, J. Qu, S. B. Kordmahale, D. Tscharnuter, A. Muliana, and J. Kameoka, “Mechanical Responses of Ecoflex Silicone Rubber: Compressible and Incompressible Behaviors”, doi: 10.1002/app.47025.

[175] P. Polygerinos *et al.*, “Modeling of Soft Fiber-Reinforced Bending Actuators,” *IEEE Trans. Robot.*, vol. 31, no. 3, pp. 778–789, Jun. 2015, doi: 10.1109/TRO.2015.2428504.

[176] J. Bishop-Moser and S. Kota, “Design and Modeling of Generalized Fiber-Reinforced Pneumatic Soft Actuators,” *IEEE Trans. Robot.*, vol. 31, no. 3, pp. 536–545, Jun. 2015, doi: 10.1109/TRO.2015.2409452.

[177] Y. Sun *et al.*, “Stiffness Customization and Patterning for Property Modulation of Silicone-Based Soft Pneumatic Actuators,” *Soft Robot.*, 2017, doi: 10.1089/soro.2016.0047.

[178] Z. Wang, P. Polygerinos, J. T. B. Overvelde, K. C. Galloway, K. Bertoldi, and C. J. Walsh, “Interaction Forces of Soft Fiber Reinforced Bending Actuators,” *IEEE/ASME Trans. Mechatronics*, vol. 22, no. 2, pp. 717–727, Apr. 2017, doi: 10.1109/TMECH.2016.2638468.

[179] P. Polygerinos *et al.*, “Towards a soft pneumatic glove for hand rehabilitation,” *IEEE*

Int. Conf. Intell. Robot. Syst., pp. 1512–1517, 2013, doi: 10.1109/IROS.2013.6696549.

[180] J. C. Veilleux and J. E. Shepherd, "Pressure and stress transients in autoinjector devices," *Drug Deliv. Transl. Res.*, vol. 8, no. 5, pp. 1238–1253, 2018, doi: 10.1007/s13346-018-0568-7.

[181] D. P. Jackson and P. W. Laws, "Syringe thermodynamics: The many uses of a glass syringe," *Am. J. Phys.*, vol. 74, no. 2, pp. 94–101, 2006, doi: 10.1119/1.2162547.

[182] A. Allmendinger and S. Fischer, "Tissue Resistance during Large-Volume Injections in Subcutaneous Tissue of Minipigs," *Pharm. Res.*, vol. 37, no. 10, pp. 1–9, 2020, doi: 10.1007/s11095-020-02906-9.

[183] "https://strengthlevel.com/strength-standards/dumbbell-shrug/kg."

[184] H. K. Yap, B. W. K. Ang, J. H. Lim, J. C. H. Goh, and C. H. Yeow, "A fabric-regulated soft robotic glove with user intent detection using EMG and RFID for hand assistive application," *Proc. - IEEE Int. Conf. Robot. Autom.*, vol. 2016-June, pp. 3537–3542, Jun. 2016, doi: 10.1109/ICRA.2016.7487535.

Appendix 1 Stepper motor control for automatic fibre braiding machine

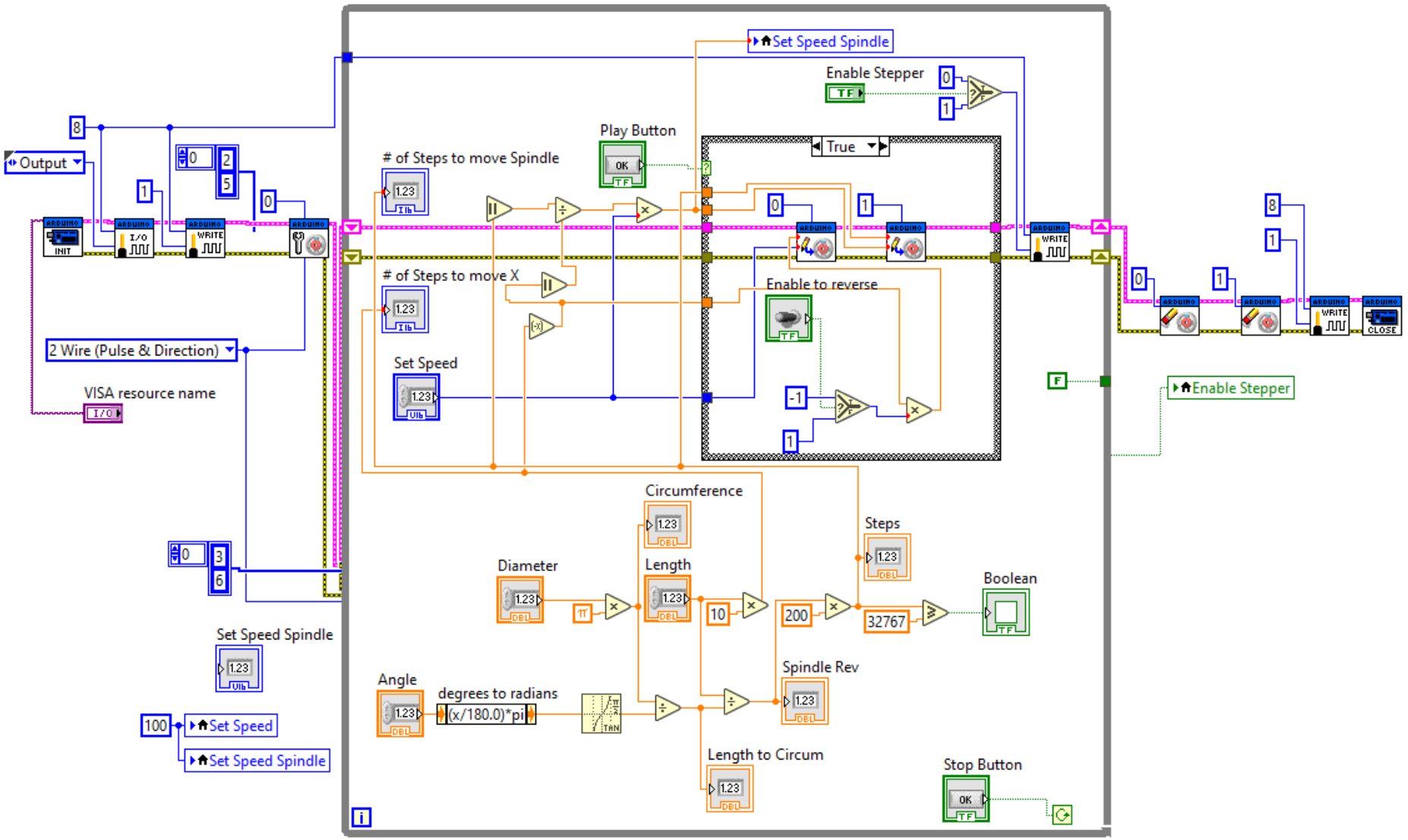

Appendix 2 Input pressure and output force data acquisition using LabVIEW